Radiation from accelerated particles in shocks and reconnections

Ken Nishikawa

National Space Science & Technology Center/UAH

Collaborators:

B. Zhang (*Univ. Nevada, Las Vegas*)
E. J. Choi (*KAIST*)
K. W. Min (*KAIST*)
J. Niemiec (*Institute of Nuclear Physics PAN*)
M. Medvedev (*Univ. of Kansas*)
P. Hardee (*Univ. of Alabama, Tuscaloosa*)
Y. Mizuno (*Nationa; Tsing Hua University, Taiwan*)
Å. Nordlund (*Neils Bohr Institute*)
J. Frederiksen (*Neils Bohr Institute*)
H. Sol (*Meudon Observatory*)
M. Pohl (*U-Potsdam/DESY*)
D. H. Hartmann (*Clemson Univ.*)

Chirps, Mergers and Explosions:
The Final Moments of Coalescing Compact Binaries,
KITP, Santa Barbara, July 16 – October 12, 2012

2704 BATSE Gamma-Ray Bursts

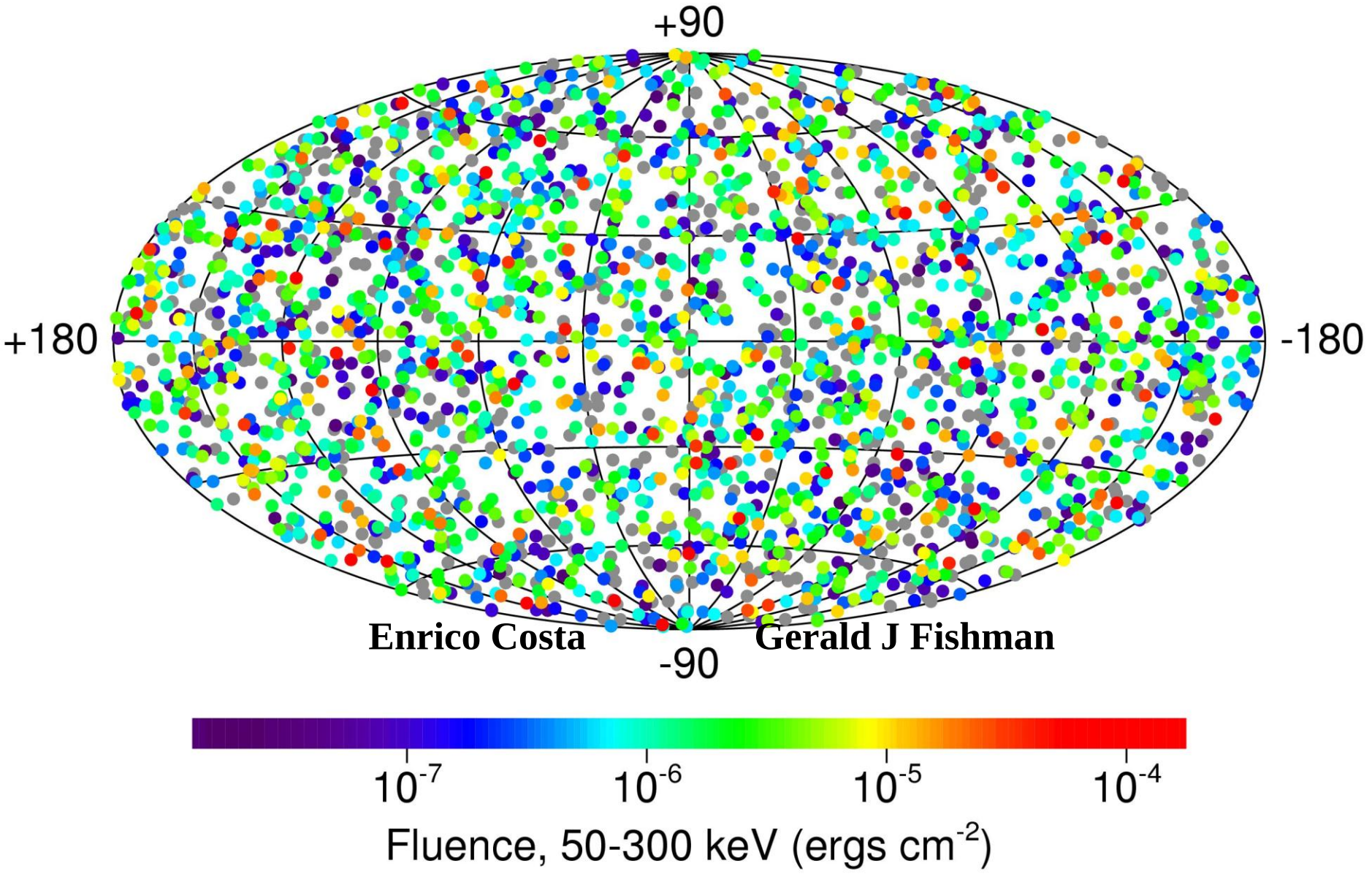

Gerald Jerry Fishman received Shaw Prize for GRBs are cosmic origin (Sept 28,2011)

Outline of talk

- **Introduction and Weibel instability**
- **Recent 3-D particle simulations of relativistic jets**
  * **$e^{\pm}$pair jet into $e^{\pm}$pair, γ= 15 and electron-ion (m_i/m_e = 20) into electron-ion γ= 15 shock structures**
- **Radiation from two electrons**
- **New initial results of radiation from jet electrons which are traced in the simulations self-consistently**
- **Future plans of our simulations of relativistic jets**

Terminal Hotspots

Kino & Takahara 04

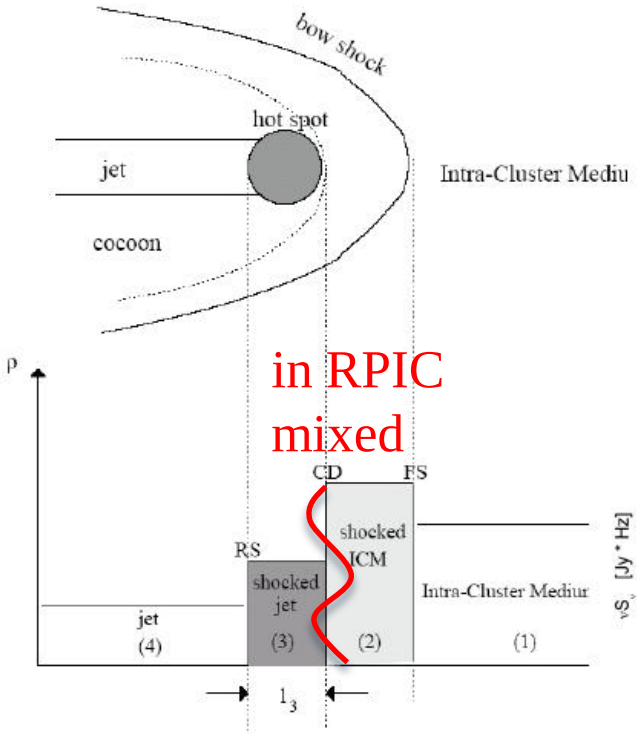

Hotspots in powerful radio sources are understood as the terminal regions of relativistic jets, where bulk kinetic power transported by the outflows from the active centers is converted at a strong shock (formed due to the interaction of the jet with the ambient gaseous medium) to the internal energy of the jet plasma.

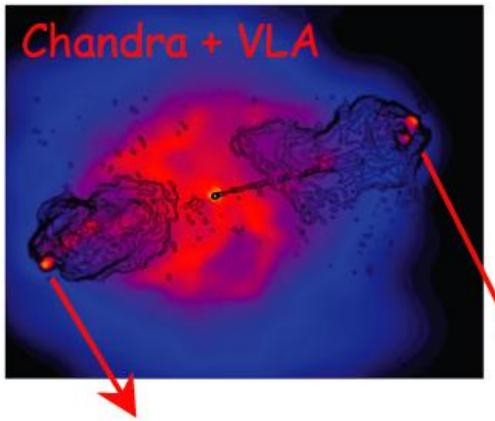

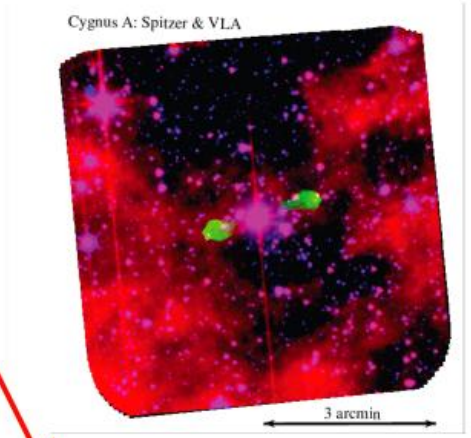

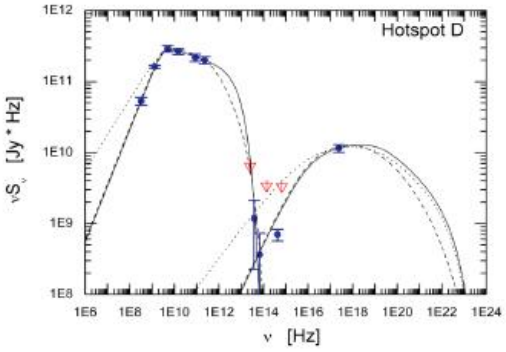

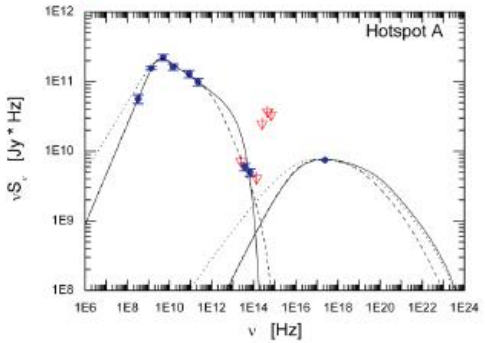

Hotspots of exceptionally bright radio galaxy Cygnus A (d_L = 250 Mpc) can be resolved at different frequencies (VLA, Spitzer, Chandra), enabling us to understand how (mildly) relativistic shocks work (**LS+ 07**).

from the talk by L. Stawarz

Schematic GRB from a massive stellar progenitor

(Meszaros, Science 2001)

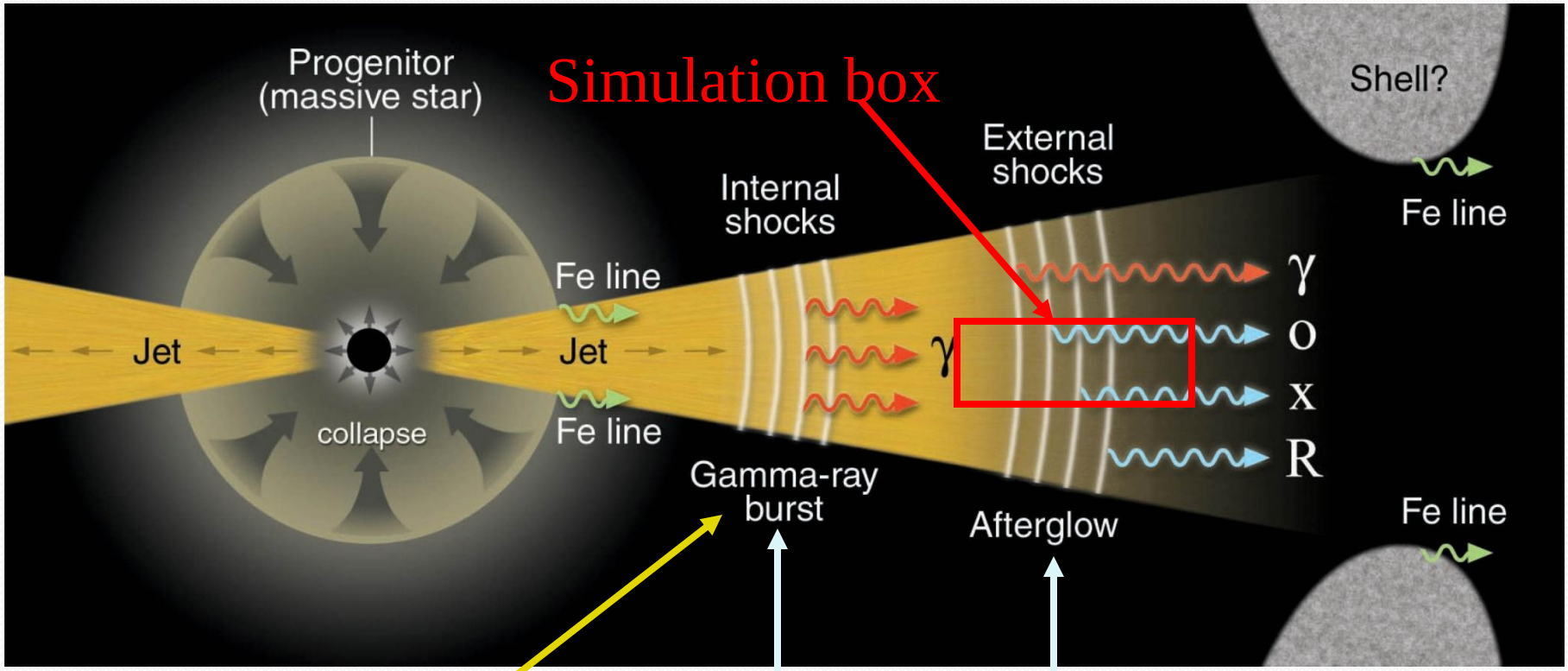

Prompt emission

Polarization ?

Accelerated particles emit waves at shocks

3-D simulation

with MPI code

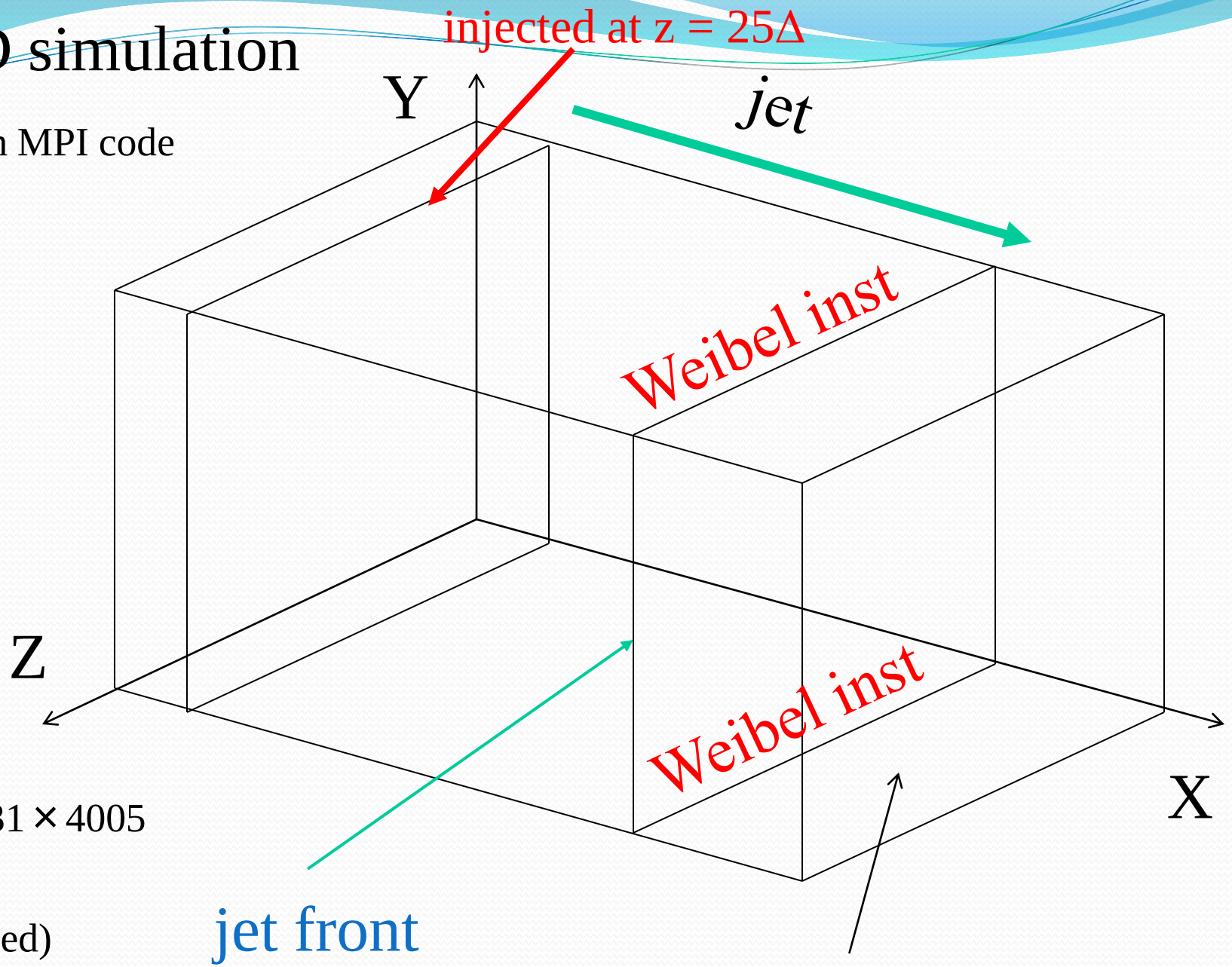

131 × 131 × 4005 grids

(not scaled)

1.2 billion particles

Collisionless shock

Electric and magnetic fields created self-consistently by particle dynamics randomize particles

(Buneman 1993)

$$\partial B / \partial t = -\nabla \times E$$

$$\partial E / \partial t = \nabla \times B - J$$

$$dm_0 \gamma v / dt = q(E + v \times B)$$

$$\partial r / \partial t + \nabla \cdot J = 0$$

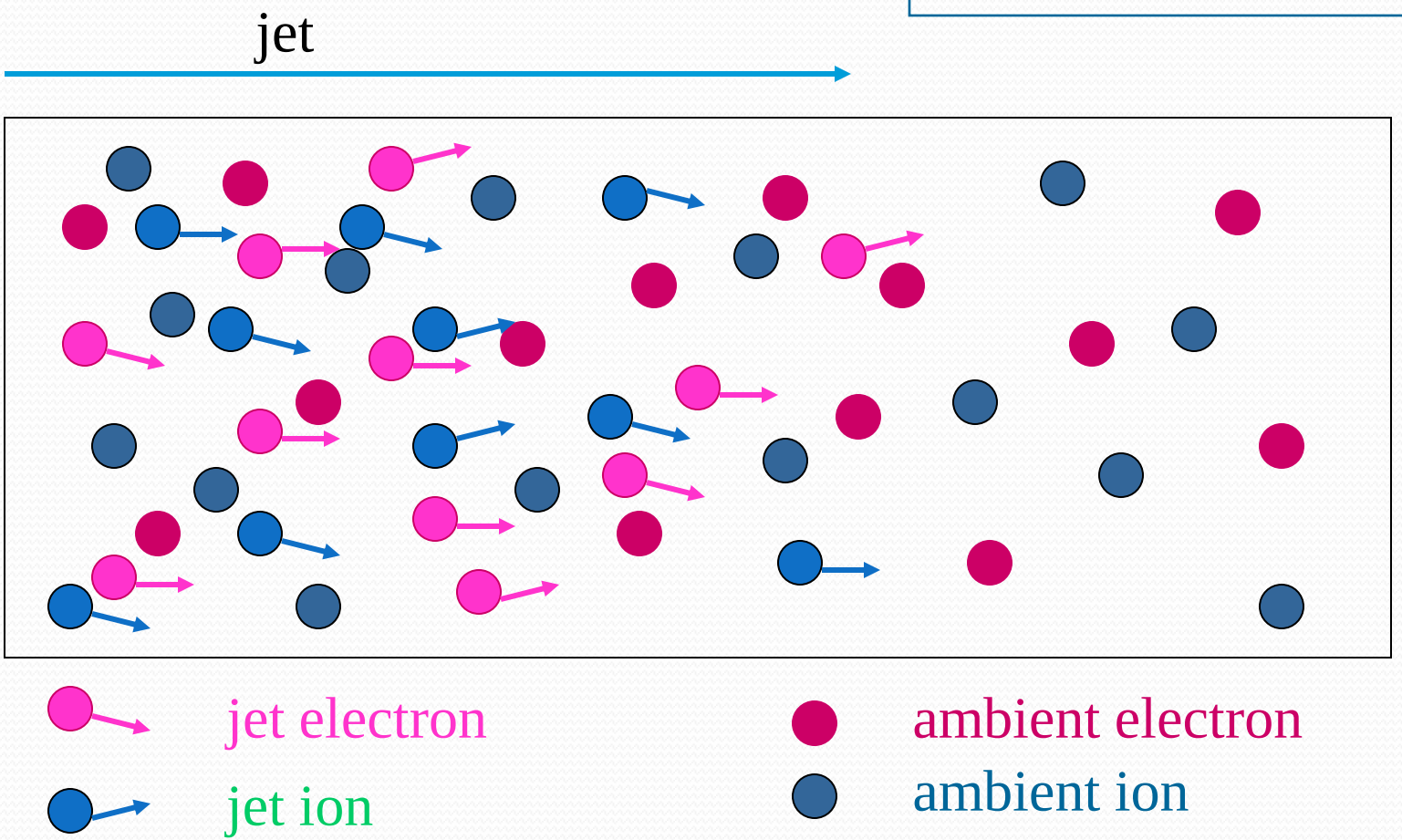

Weibel instability

current filamentation

Time:

$\tau = \gamma_{sh}^{1/2}/\omega_{pe} \approx 21.5$

Length:

$\lambda = \gamma_{th}^{1/2} c/\omega_{pe} \approx 9.6\Delta$

jet

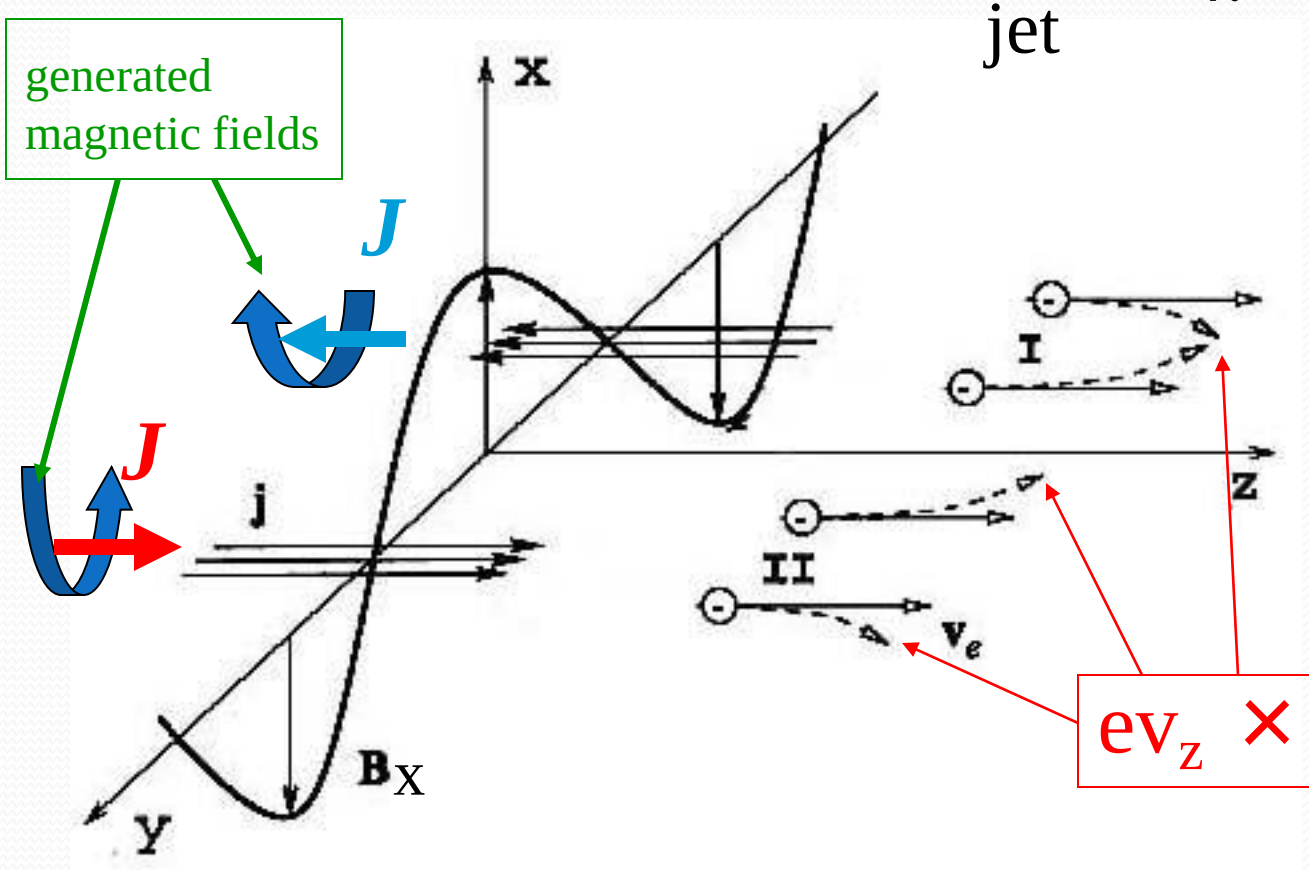

$ev_z \times B_x$ (electrons)

(Medvedev & Loeb, 1999, ApJ)

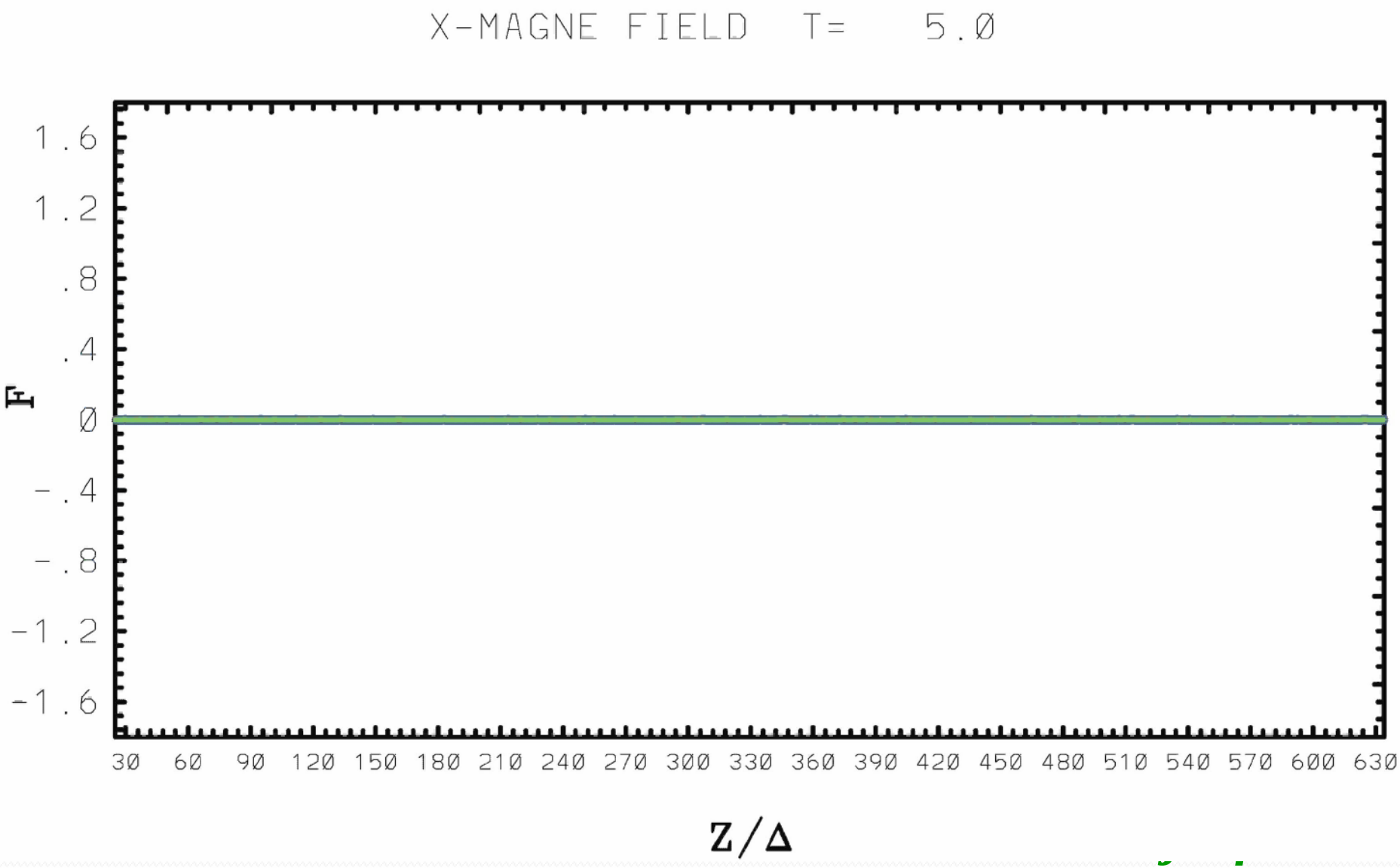

Weibel instability

(Nishikawa et al. 2005)

Ion Weibel instability

ion current

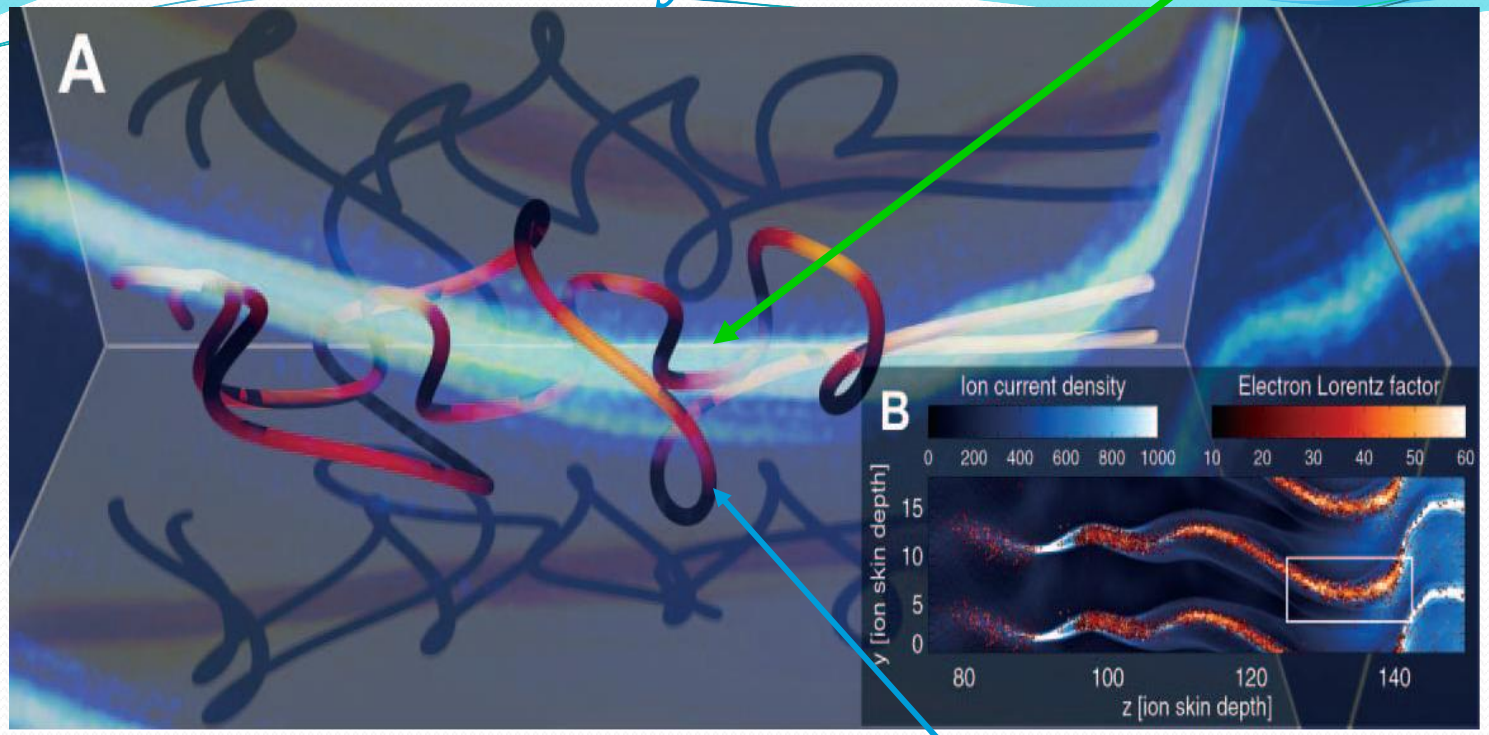

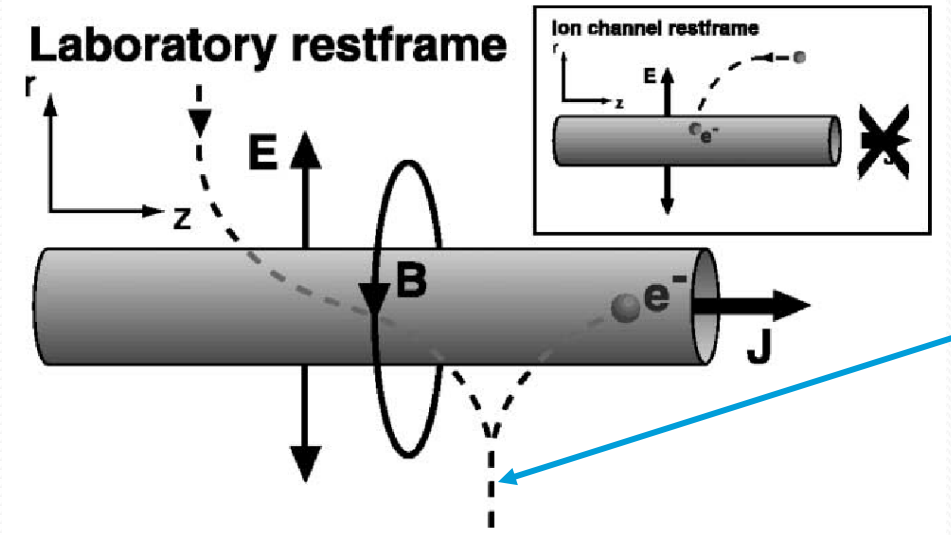

***E* × *B* acceleration**

electron trajectory

(Hededal et al 2004)

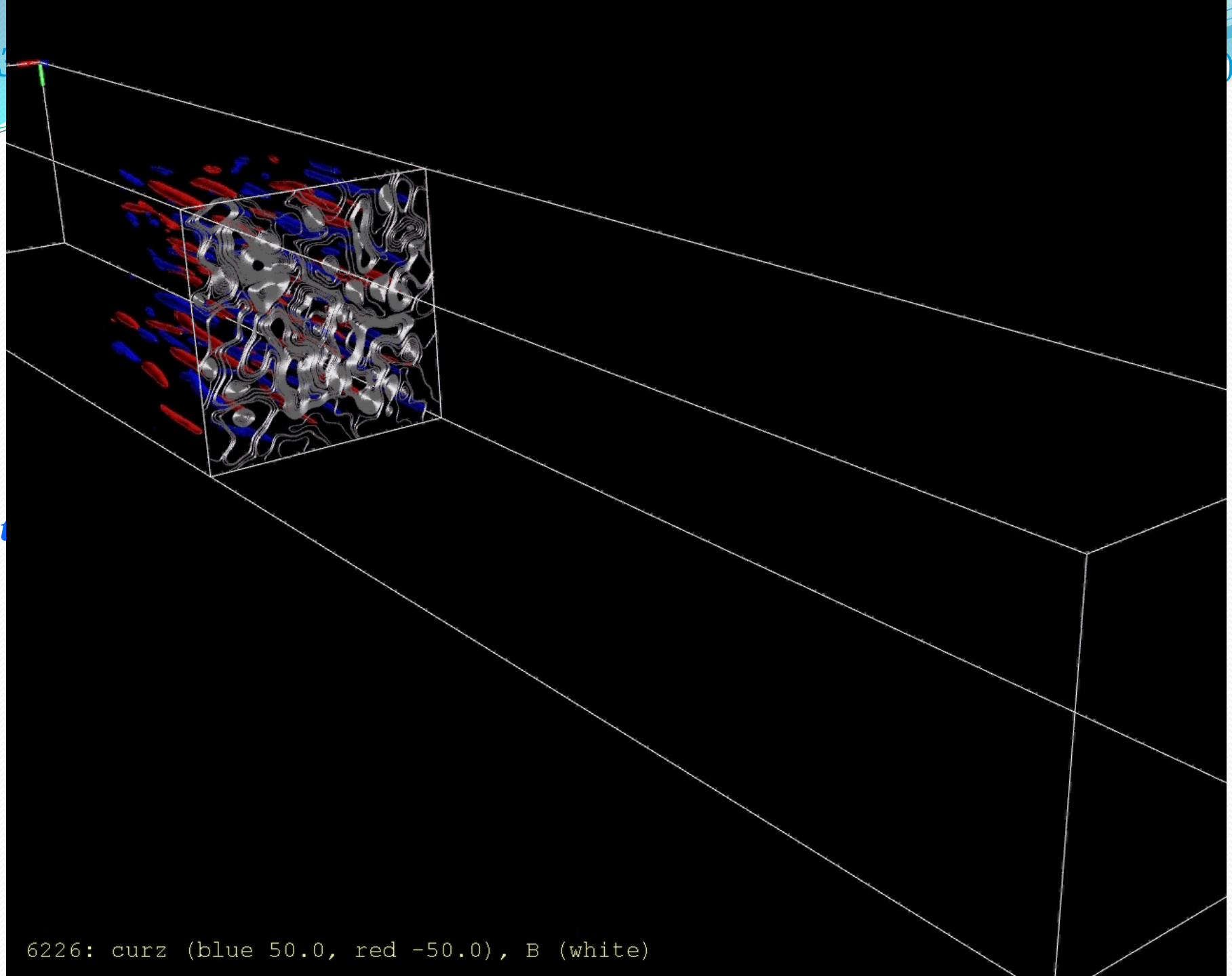
6226: curz (blue 50.0, red -50.0), B (white)

Fermi acceleration (self-consistent with turbulent magnetic field)

$\omega_{pe}t = 8400$

density

ε_B

Av.density

Av. ε_B

electron

x-v_x

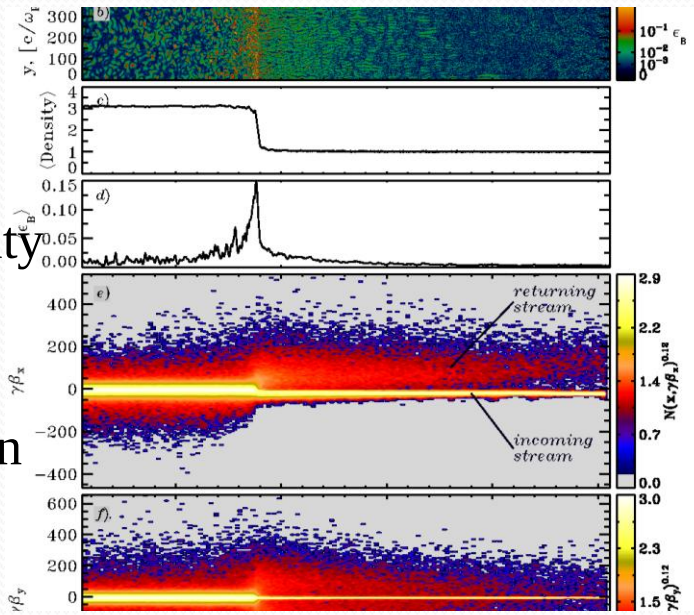

Fermi acceleration has been done with self-consistent magnetic fields (Spitkovsky, ApJ, 2008)

particle spectrum at $\omega_{pe}t = 10^4$

particle trajectories

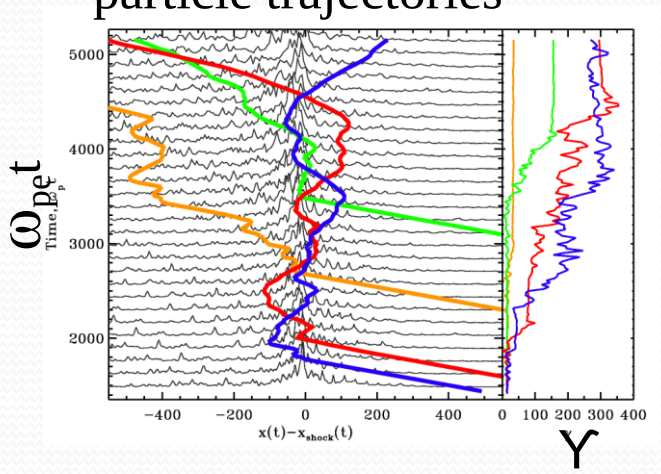

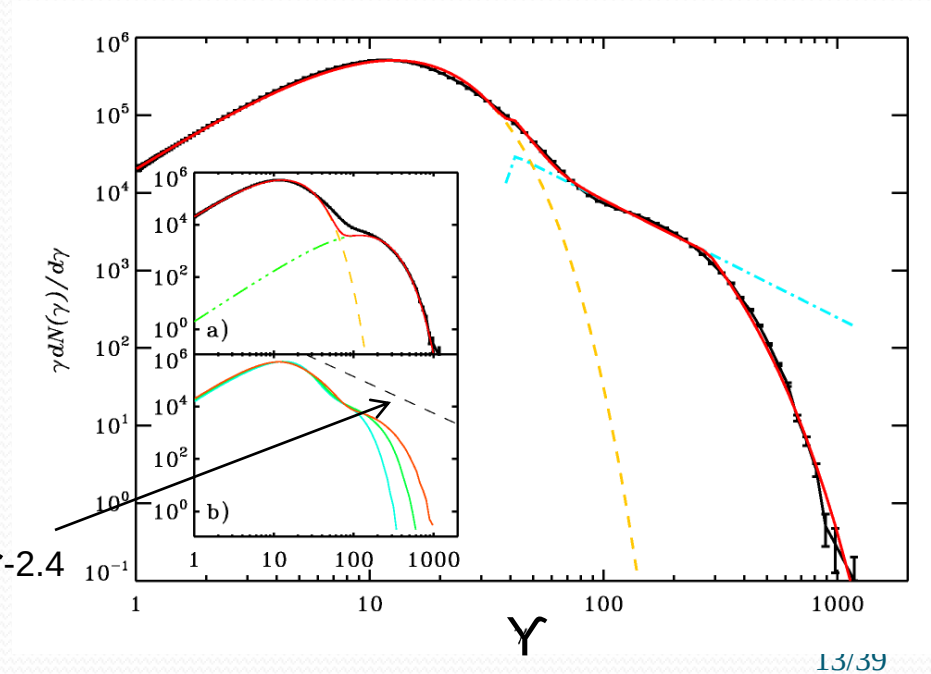

Shock velocity and bulk velocity

contact discontinuity

trailing shock
(reverse shock)

leading shock
(forward shock)

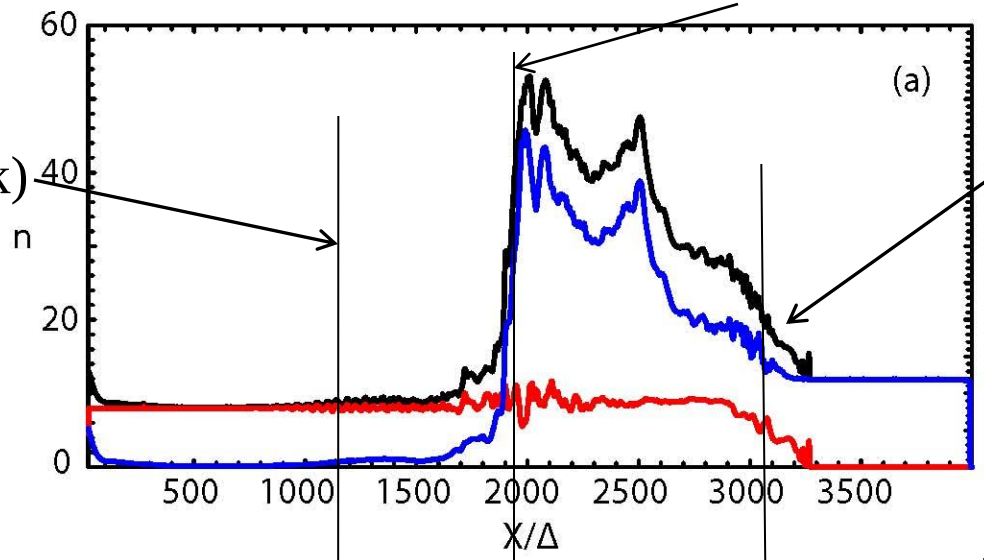

jet electrons

Fermi acceleration ?

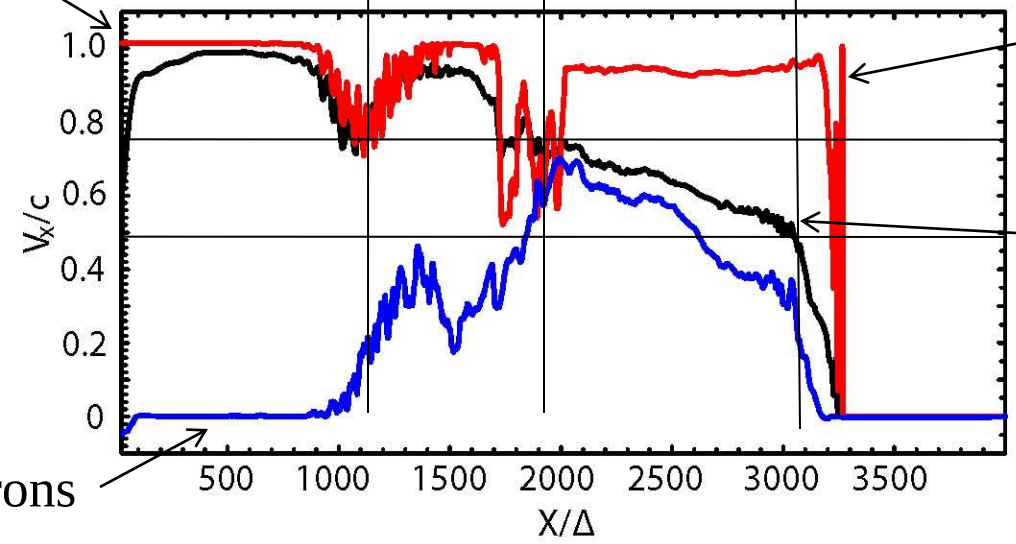

total electrons

ambient electrons

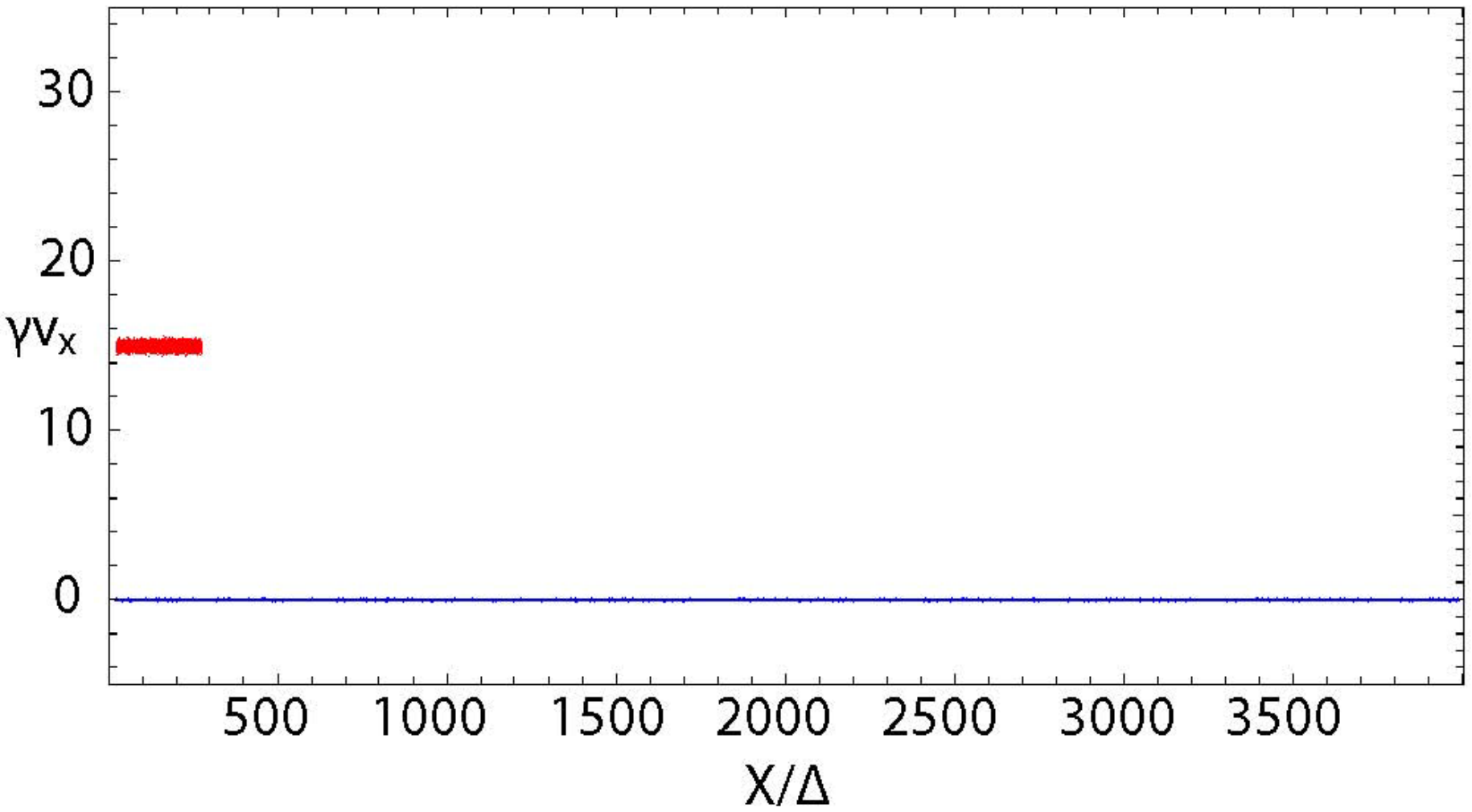

(Nishikawa et al. ApJ, 698, L10, 2009)

Sho hock

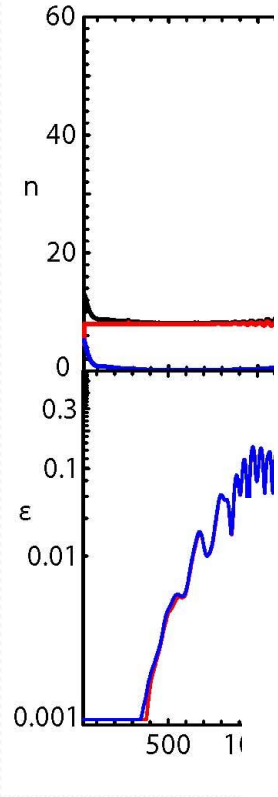

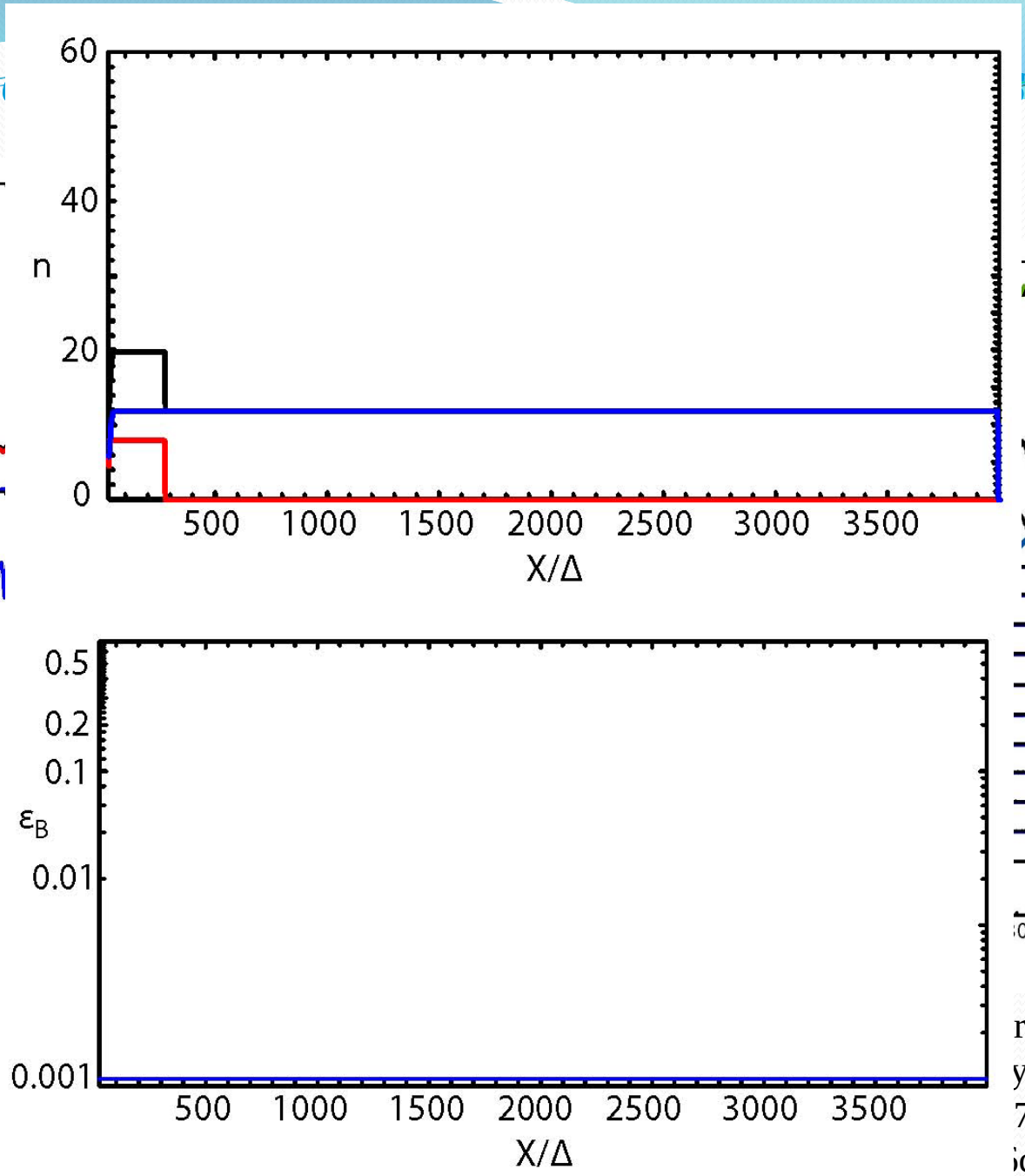

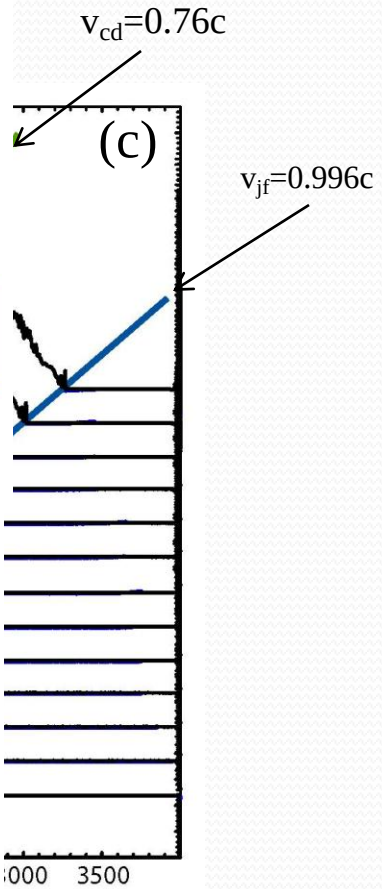

(a) electron de
field energy ($\varepsilon_$
kinetic energy

ron density.
y c, the predicted
76c, and the
c.

(Nishikawa e

Shock velocity and structure based on 1-D HD analysis

moving contact discontinuity (CD)

trailing shock
(reverse shock)

leading shock
(forward shock)

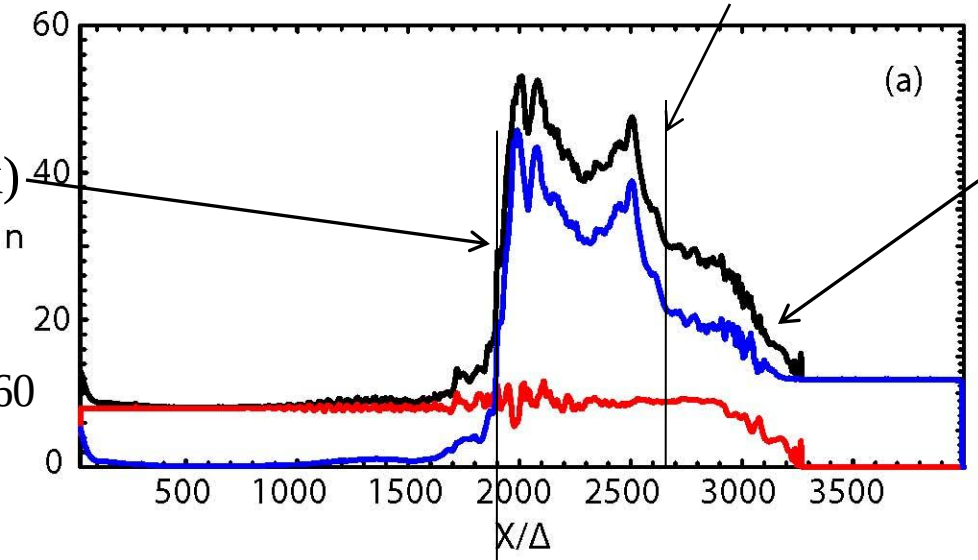

(Nishikawa et al. 2009)

in CD frame

$n_{sj}/\gamma_{cd} n_j = 3.36$

$b_s = 0.417$ $\gamma_{cd} = 5.60$

$4/3 < G = 3/2 < 5/3$

fixed CD

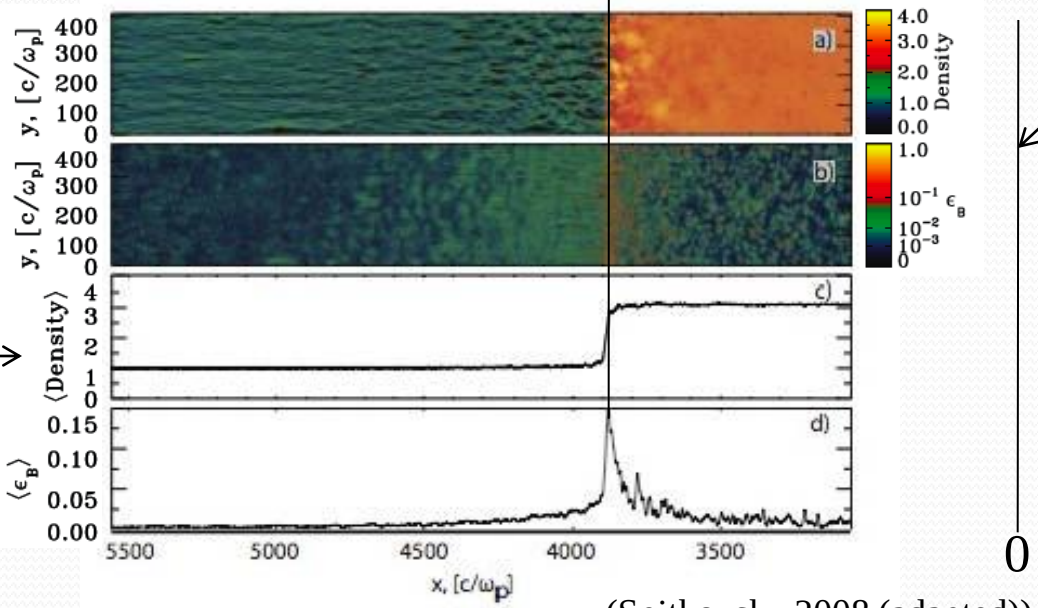

Density →

$n_2/\gamma_0 n_1 = 3.13$

$b_c = 0.47$

$\gamma_0 = 15$

0

(Spitkovsky 2008 (adapted))

Comparison with different mass ratio (electron-positron and electron-ion)

electron-positron

electron-ion (m_i/m_e = 20)

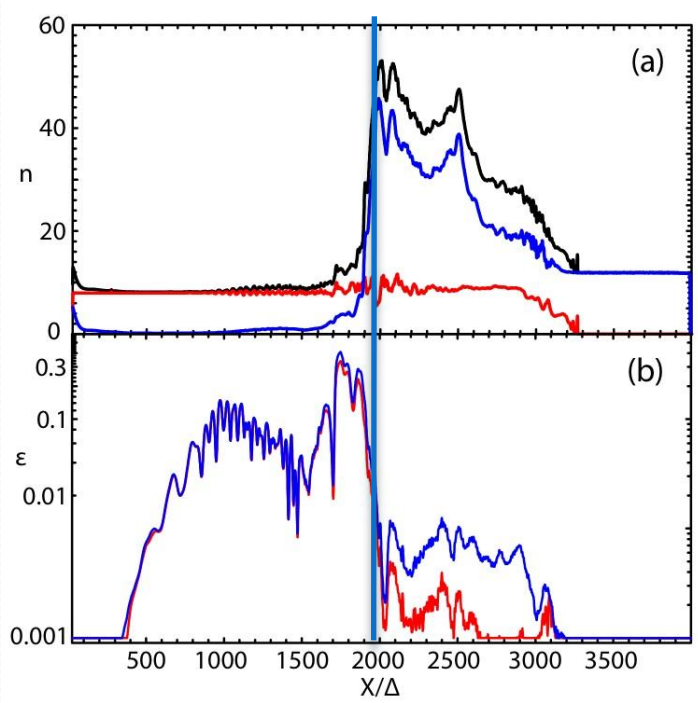

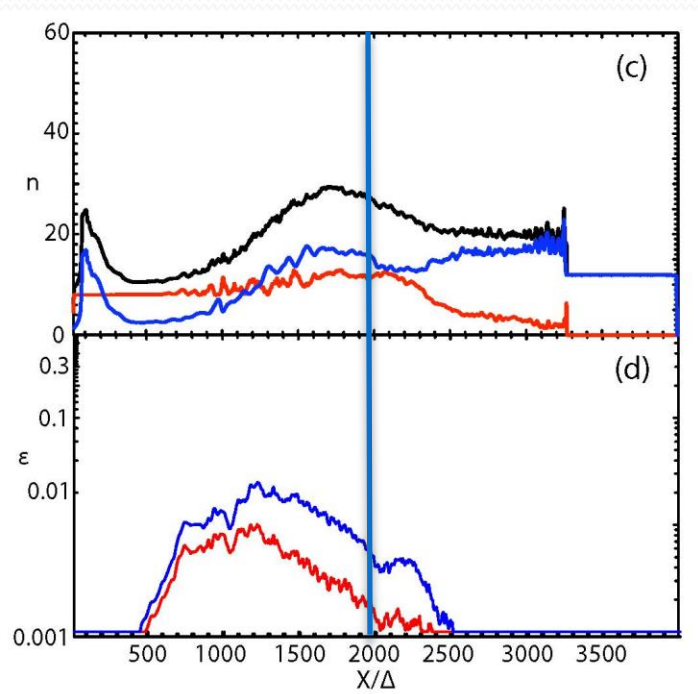

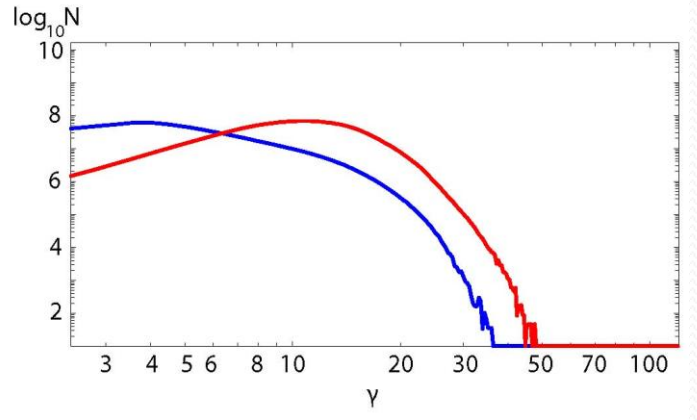

X/Δ>2000

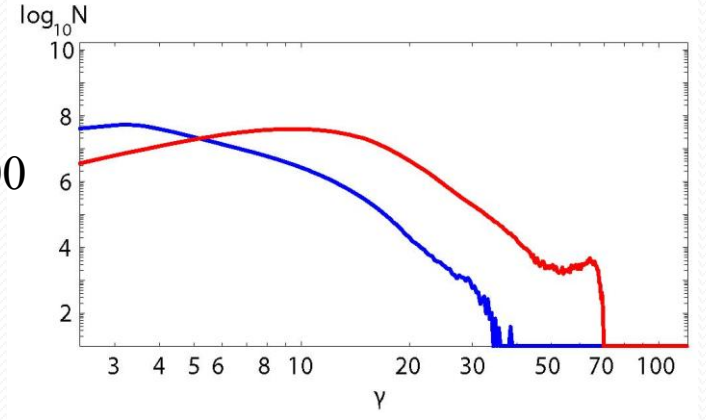

Reconnection in jet

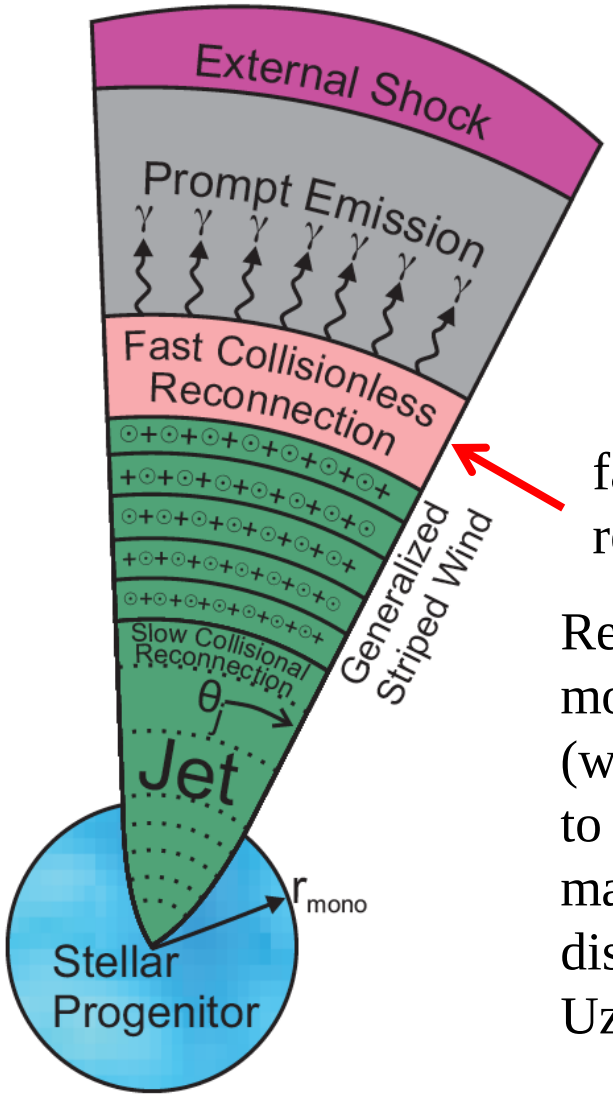

fast collisionless reconnection

Reconnection switch concept: Collapsar model or some other system produces a jet (with opening half-angle θ_j) corresponding to a generalized stripped wind containing many field reversals that develop into dissipative current sheets. (McKinney & Uzdensky, MNRAS, 2011)

3-D kink instability with helical magnetic field

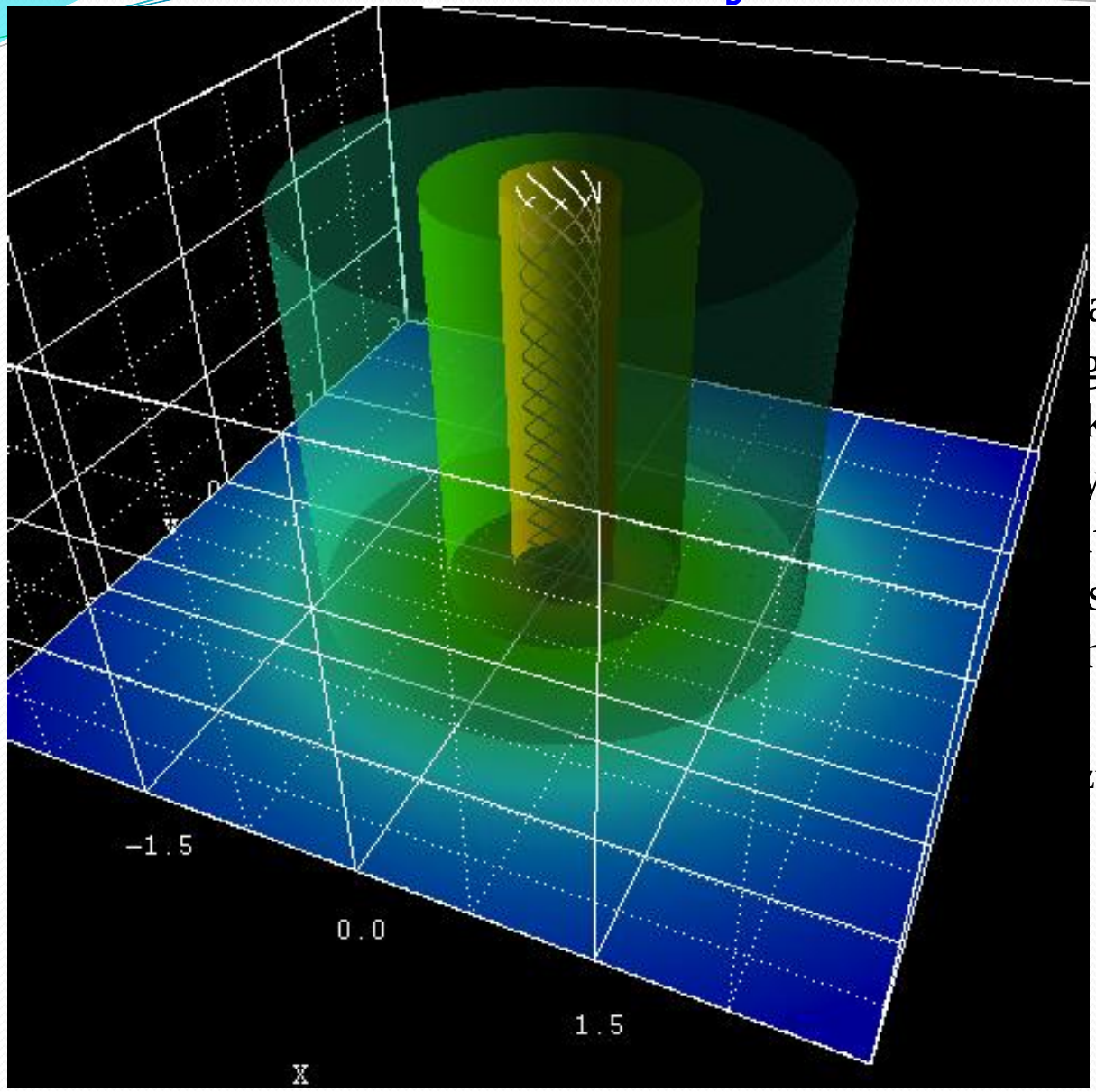

ativistic jet with helical
gnetic field leads
k instability and reconnection
y take place using resistive
tivistic MHD simulations
s simulation was performed
n RMHD code).

zuno et al. ApJ, 734:19 (18pp), 2011)

Electron shock surfing acceleration

$\theta = 90$

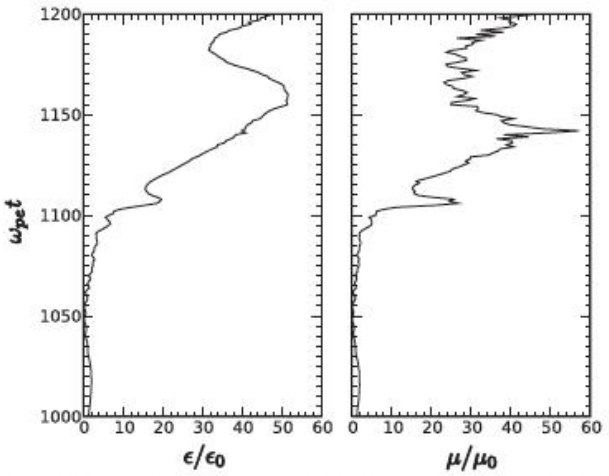

Figure 5. Time history of an accelerated electron: energy (left) and the first adiabatic invariant (right).

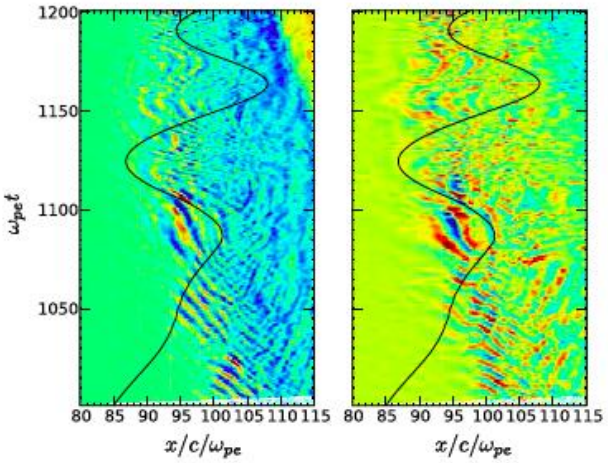

Figure 6. Electron trajectory and electric fields E_x (left) and E_y (right), respectively.

(Sironi & Spitkovsky, 2009, 2011,ApJ)

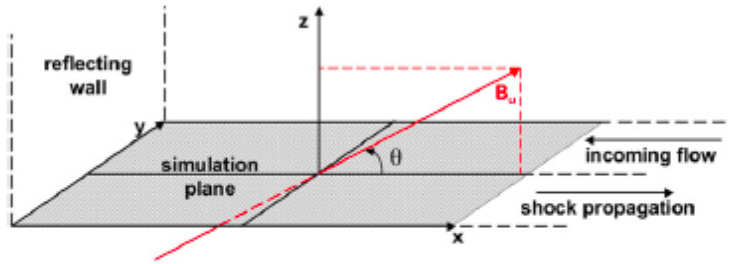

Figure 1. Simulation geometry and configuration of the upstream magnetic field.

(A color version of this figure is available in the online journal.)

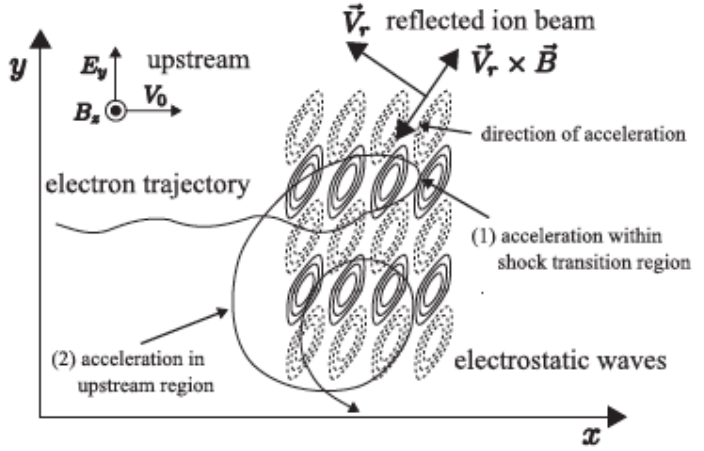

Figure 8. Schematic illustration of acceleration mechanism. Electrons are accelerated in two steps: (1) they are accelerated by the stochastic electron shock surfing in the shock transition region and preferentially transported to the upstream region. (2) The accelerated electrons escaping into the upstream suffer further acceleration by the constant motional electric field.

(Amano & Hoshino, 2009, ApJ)

The importance of the magnetic-field angle

- A SNR blast waves moves into a ***B*** with a preferred direction
  - The angle between B and shock normal varies from 90 deg to 0 deg.

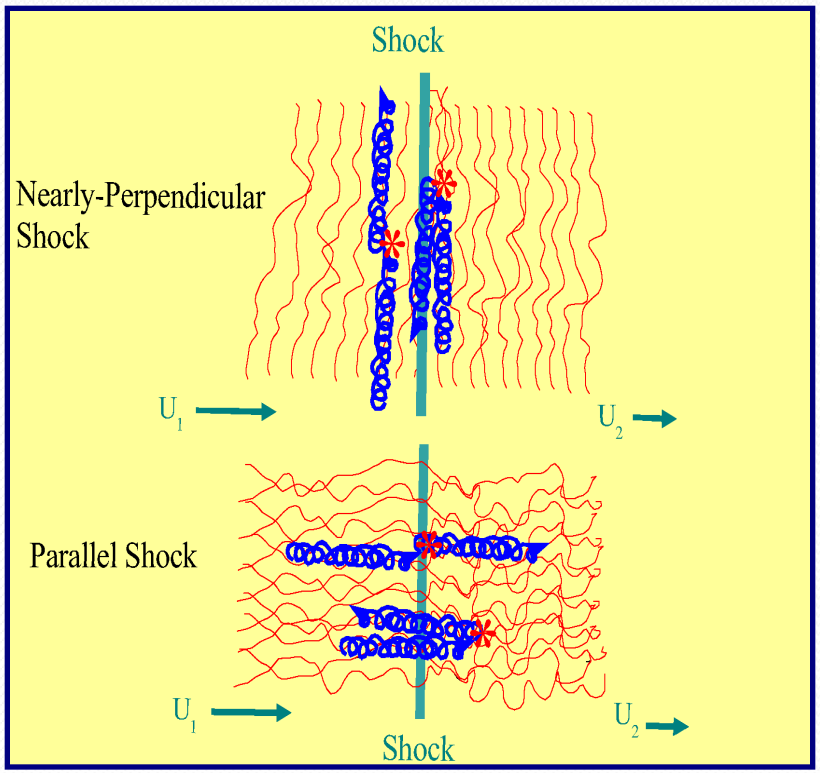

- The physics of acceleration at parallel and perpendicular shocks is different

$$\tau_{acc} \propto \frac{\kappa_{nn}}{V_{shock}^2}$$

Parallel shocks → slow

Perpendicular shocks → fast

($K_\perp < K_\parallel$)

- for a given time interval or size of shock, a perpendicular shock will yield a larger maximum energy than a parallel shock.

Jokippi and Giacalone, Isradynamic 2008

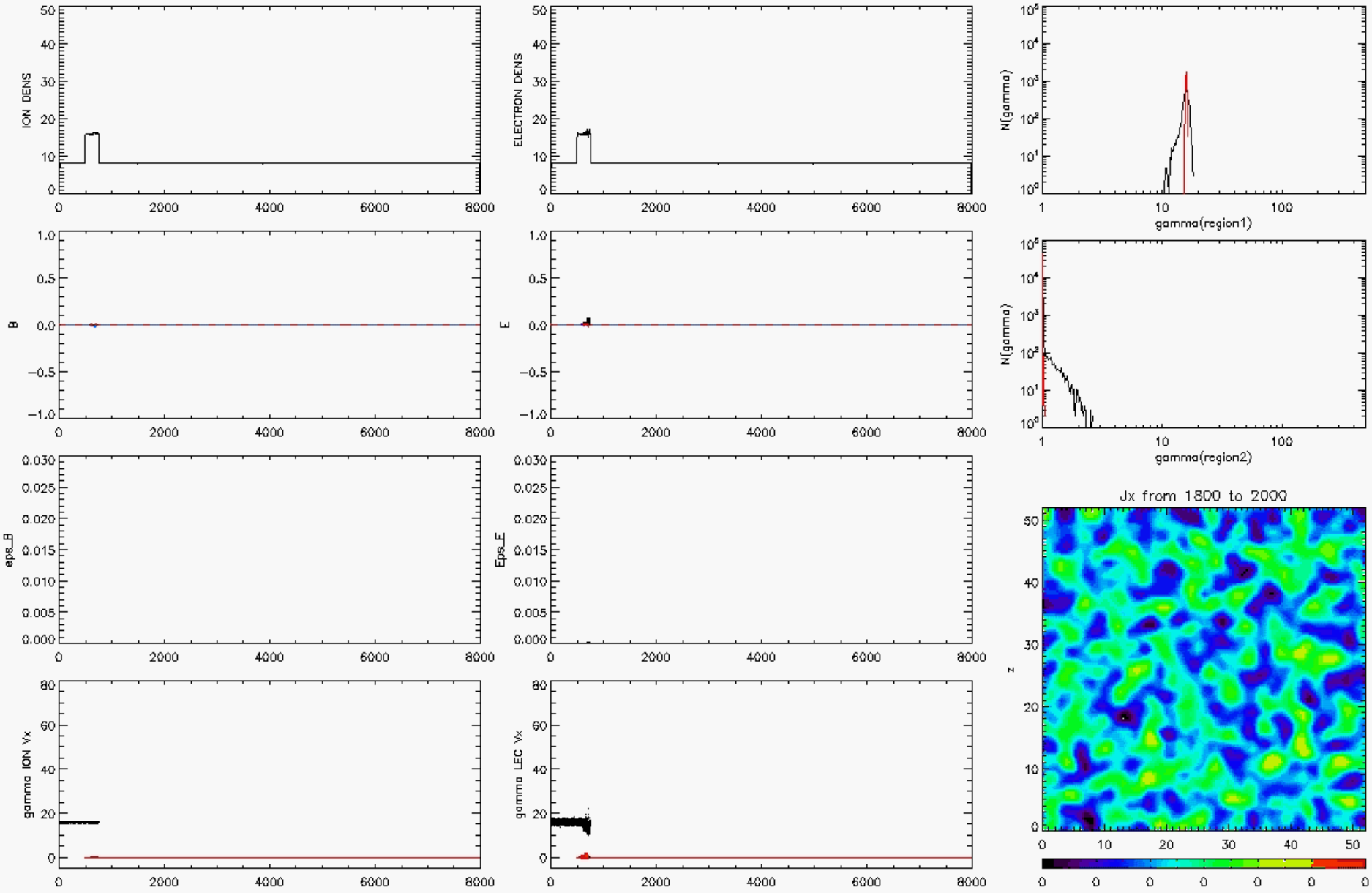
ION DENS
ELECTRON DENS
N(gamma)
gamma(region1)
gamma(region2)
B
E
eps_B
Eps_E
gamma ION Vx
gamma LEC Vx
Jx from 1800 to 2000
z

Perpendicular magnetic field

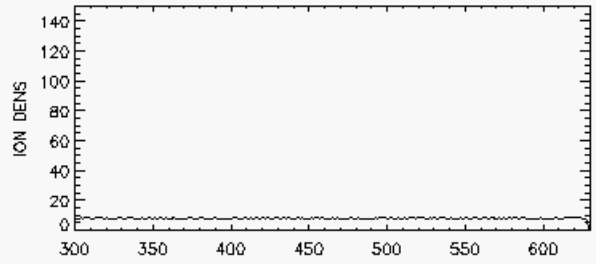

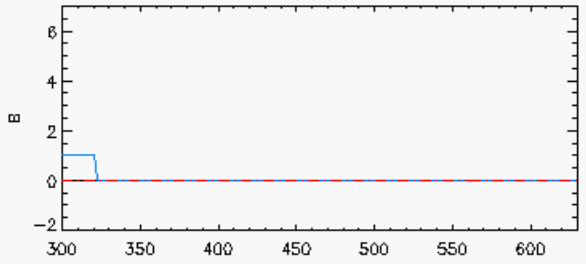

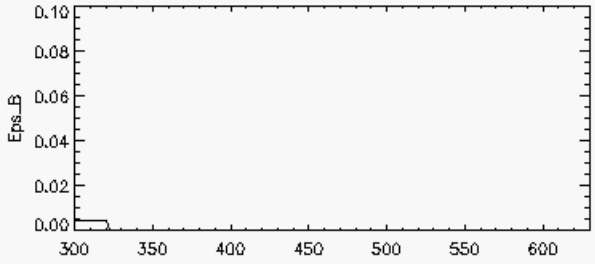

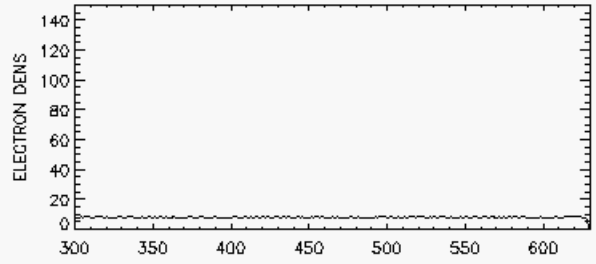

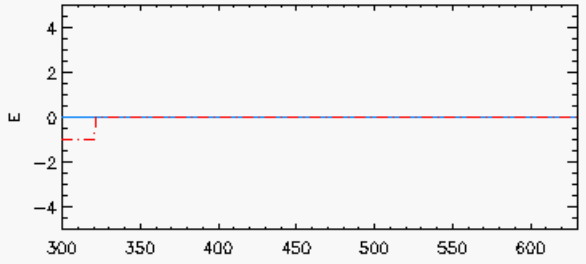

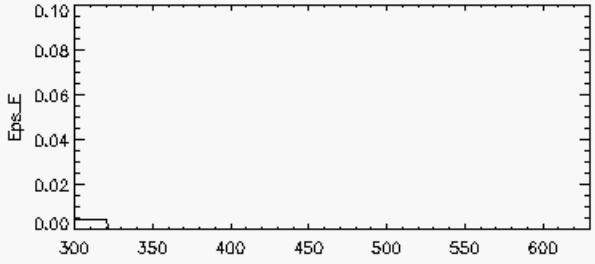

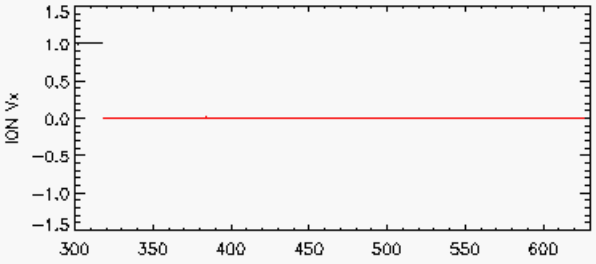

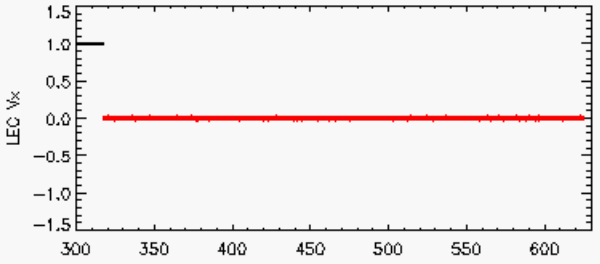

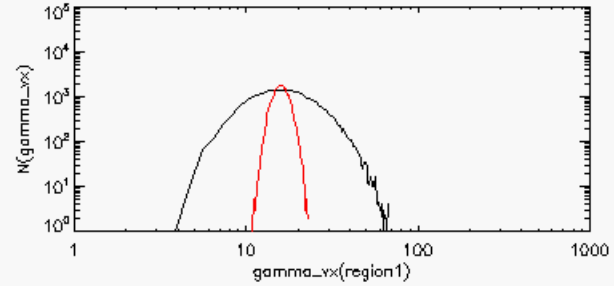

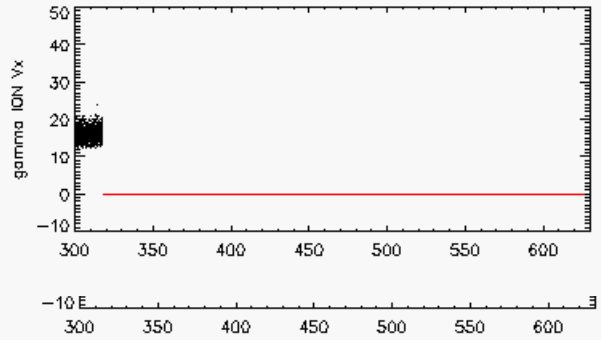

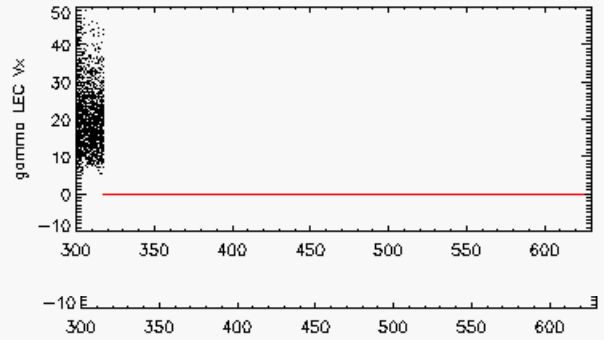

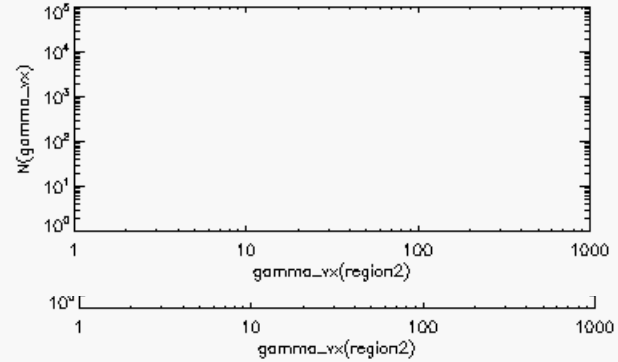

Synchrotron Emission: radiation from accelerated

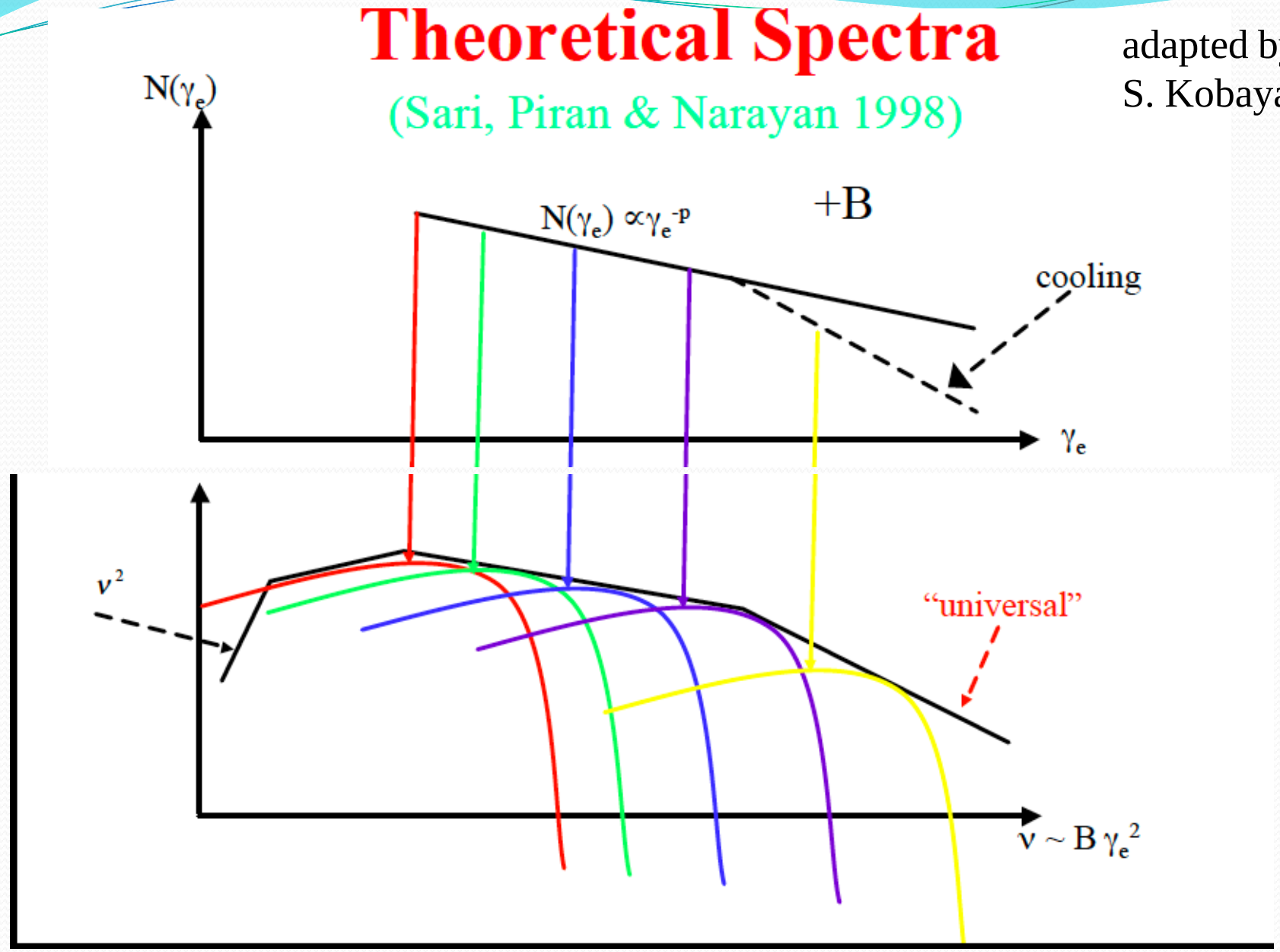

Standard radiation model by E. Waxman (2006)

- the luminosity and spectrum of synchrotron radiation, the strength of the magnetic field and the energy distribution of the electrons
- Due to the lack of a first principles theory of collisionless shocks, we present in this section a purely phenomenological approach to the model of afterglow radiation emission
- we simply assume that a fraction ε_B of the post-shock thermal energy density is carried by the magnetic field, that a fraction ε_e is carried by electrons, and that the energy distribution of the electrons is a power-law, $\mathbf{d}\log n_e/\mathbf{d}\log \boldsymbol{\varepsilon} = \mathbf{p}$ (above some minimum energy $\boldsymbol{\varepsilon}_0$ which is determined by ε_e and **p**)
- $\boldsymbol{\varepsilon}_B$, $\boldsymbol{\varepsilon}_e$ and **p** are treated as free parameters, to be determined by observations
- the constraints implied on these parameters by observations are independent of any assumptions regarding the nature of the afterglow shock and the processes responsible for particle acceleration or magnetic field generation
- The parameters ε_B, $\boldsymbol{\varepsilon}_e$ and **p**, together with the parameters **E** and **n** which determine the shock dynamics, completely determine the magnetic field strength and electron distribution (including their temporal and spatial dependence).

Radiated power from Hededal thesis (astro-ph/0506559)

To skip a trivial, but rather long derivation, we adopt the expression from Jackson (1999) for the retarded electric field from a charged particle moving with instant velocity $\boldsymbol{\beta}$ under acceleration $\dot{\boldsymbol{\beta}}$,

$$\mathbf{E} = \underbrace{\frac{q}{4\pi\epsilon_0}\left[\frac{\mathbf{n}-\boldsymbol{\beta}}{\gamma^2\left(1-\mathbf{n}\cdot\boldsymbol{\beta}\right)^3 R^2}\right]_{\text{ret}}}_{\text{velocity field}} + \underbrace{\frac{q}{4\pi\epsilon_0 c}\left[\frac{\mathbf{n}\times\{(\mathbf{n}-\boldsymbol{\beta})\times\dot{\boldsymbol{\beta}}\}}{\left(1-\mathbf{n}\cdot\boldsymbol{\beta}\right)^3 R}\right]_{\text{ret}}}_{\text{acceleration field}}. \quad (2.4)$$

Here, $\mathbf{n} \equiv \mathbf{R}(t')/|\mathbf{R}(t')|$ is a unit vector that points from the particles retarded position towards the observer. The first term on the right hand side, containing the velocity field, is the Coulomb field from a charge moving without influence from external forces. The second term is a correction term that arises if the charge is subject to acceleration. Since the velocity-dependent field is falling of as R^{-2} while the acceleration-dependent field falls off as R^{-1}, the latter becomes dominant when observing the charge at large distances ($R \gg 1$). This term is therefore often referred to as the radiation term. The corresponding magnetic field is given by

$$\mathbf{B} = \left[\frac{\mathbf{n}\times\mathbf{E}}{c}\right]_{\text{ret}} \quad (2.5)$$

.

The energy W per unit area dA per unit time dt that is radiated from the accelerated particle is given by the Poynting flux $\mathbf{S}$

$$\mathbf{S} \equiv \frac{d^2W}{dtdA} = \frac{\mathbf{E}\times\mathbf{B}}{\mu_0} = \frac{|E|^2}{\mu_0 c}\mathbf{n} \quad (2.6)$$

from which we define the energy per unit time, received through a unit solid angle element $d\Omega$ about $\mathbf{n}$

$$\frac{dP(t)}{d\Omega} = R^2\left[\mathbf{S}\cdot\mathbf{n}\right]_{\text{ret}}. \quad (2.7)$$

A note of caution must be added here. The Poynting vector is related to the observer time t but we are interested in the radiated power measured at the particle's retarded time t'. Thus, to get the total *emitted* power we multiply with the correction term dt/dt' (see Chapter 7 for details)

$$\begin{aligned}\frac{dP_{rad}}{d\Omega} &= R^2\left(\mathbf{S}\cdot\mathbf{n}\right)\frac{dt}{dt'} = R^2\mathbf{S}\cdot\mathbf{n}\left(1-\mathbf{n}\cdot\boldsymbol{\beta}\right)\\ &= \frac{\mu_0 q^2 c}{16\pi^2}\frac{\left[\mathbf{n}\times\left\{(\mathbf{n}-\boldsymbol{\beta})\times\dot{\boldsymbol{\beta}}\right\}\right]^2}{\left(1-\mathbf{n}\cdot\boldsymbol{\beta}\right)^5}. \quad (2.8)\end{aligned}$$

Numerical simulations (PIC)

The 3-dimensional simulations have provided compelling evidence that transverse electromagnetic (Weibel- like) instabilities can mediate relativistic collisionless shocks, and that the upstream magnetic field is unimportant if the upstream is not highly magnetized. As expected, the width of the shock transition region is found to be a few $\times$ 10 c/ω_p. These simulations also indicate that near-equipartition magnetic fields are generated in the downstream of relativistic shocks propagating in pair (e^+e^-) plasmas, and $\varepsilon_B \geq m_e/m_p$ magnetic fields are generated in the downstream of shocks in electron-proton plasmas. Simulations of electron-proton plasmas are forced to employ an effective small proton to electron mass ratio, $\tilde{m}_p / m_e \pounds 20$with present computational resources, and the preliminary results thus obtained are not easily extrapolated to more realistic mass ratios.
Obviously, the question of field survival and correlation length evolution on length scales $\gg c/\omega_p$, which is the main challenge to our theoretical understanding, are not yet answered. Similarly, highly energetic particles cannot be contained in the small simulation boxes used, so Fermi-like acceleration processes are suppressed.
It appears, therefore, that the numerical resources required to answer some of the main open questions by direct 3-dimensional numerical simulations will not be available in the near future. (E. Waxman 2006)

Radiation from particles in collisionless shock

To obtain a spectrum, "just" integrate:

$$\frac{d^2W}{d\Omega d\omega} = \frac{\mu_0 c q^2}{16\pi^3}\left|\int_{-\infty}^{\infty}\frac{\mathbf{n}\times[(\mathbf{n}-\boldsymbol{\beta})\times\dot{\boldsymbol{\beta}}]}{(1-\boldsymbol{\beta}\cdot\mathbf{n})^2}\, e^{i\omega(t'-\mathbf{n}\cdot\mathbf{r}_0(t')/c)}dt'\right|^2$$

where $\mathbf{r}_0$ is the position, $\boldsymbol{\beta}$ the velocity and $\dot{\boldsymbol{\beta}}$ the acceleration

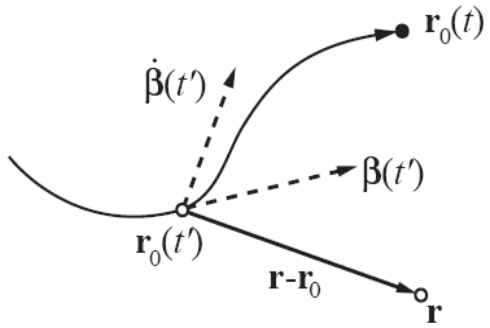

New approach: Calculate radiation from integrating position, velocity, and acceleration of ensemble of particles (electrons and positrons)

Hededal, Thesis 2005 (astro-ph/0506559)
Nishikawa et al. 2008 (astro-ph/0802.2558)
Sironi & Spitkovsky, 2009, ApJ
Martins et al. 2009, Proc. of SPIE Vol. 7359
Frederiksen et al. 2010, ApJL

Radiation from collisionless shock

Spectrum obtained directly from shock simulations

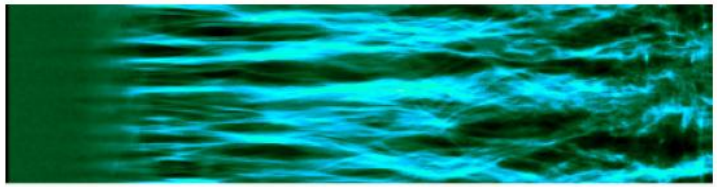

+

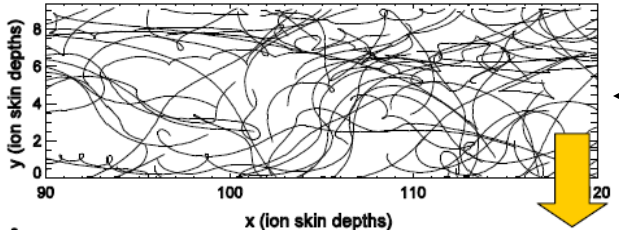

☺ observer

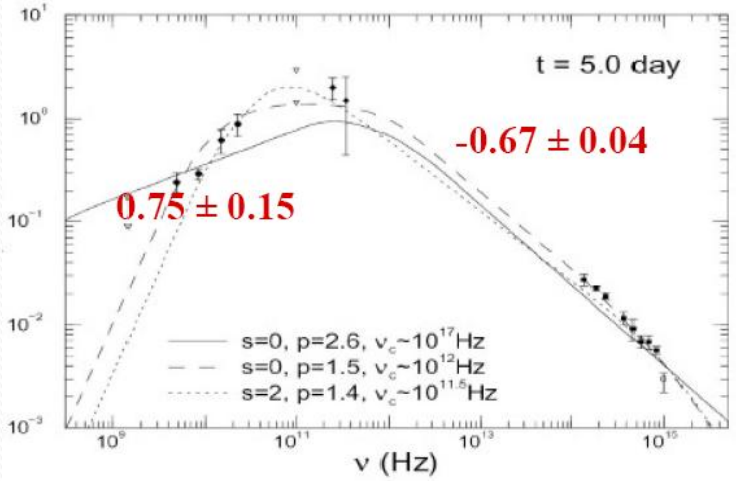

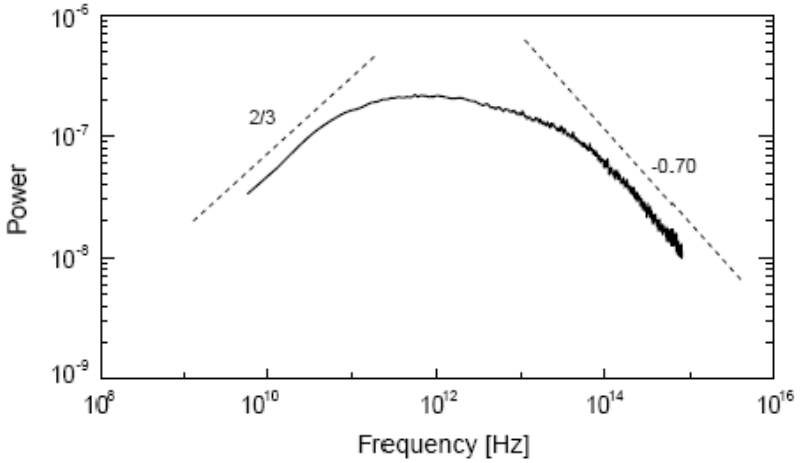

GRB 000301c (Panaitescu 2001)

Shock simulations

Hededal Thesis: http://www.astro.ku.dk/~hededal

Synchrotron radiation from gyrating electrons in a uniform magnetic field

electron trajectories

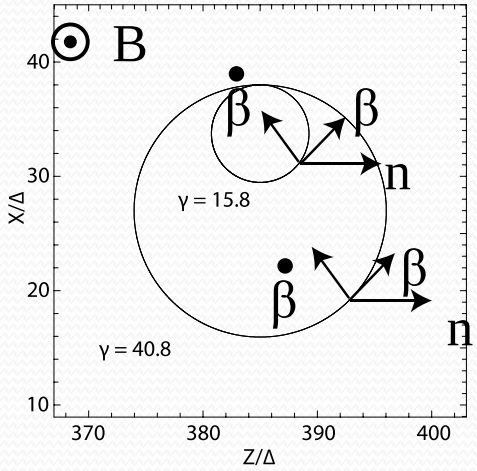

radiation electric field observed at long distance

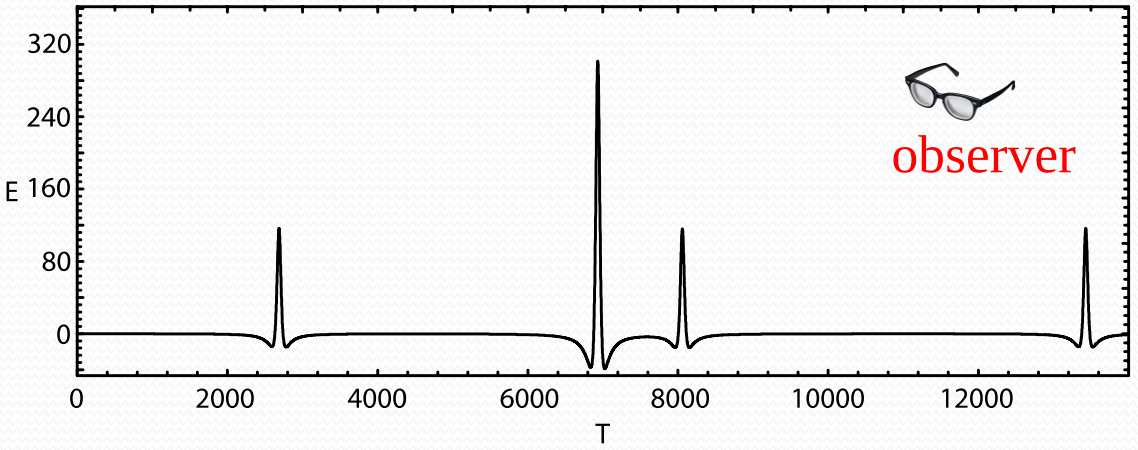

spectra with different viewing angles

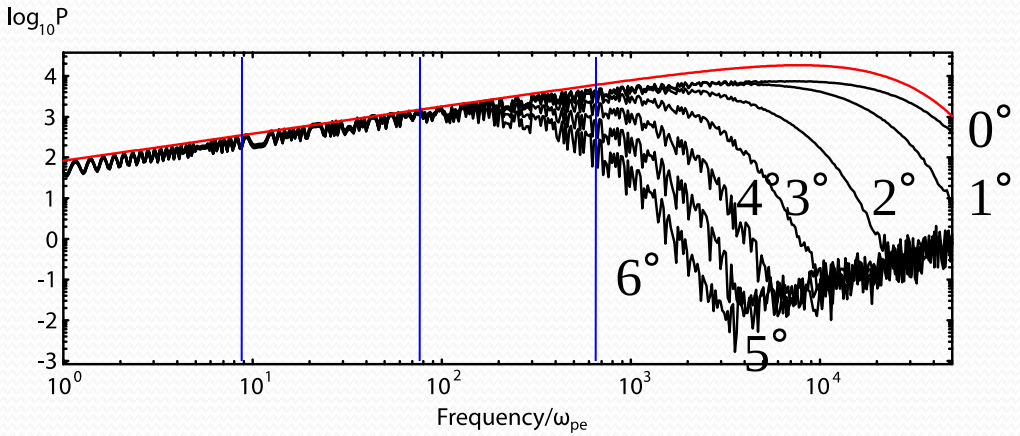

time evolution of three frequencies

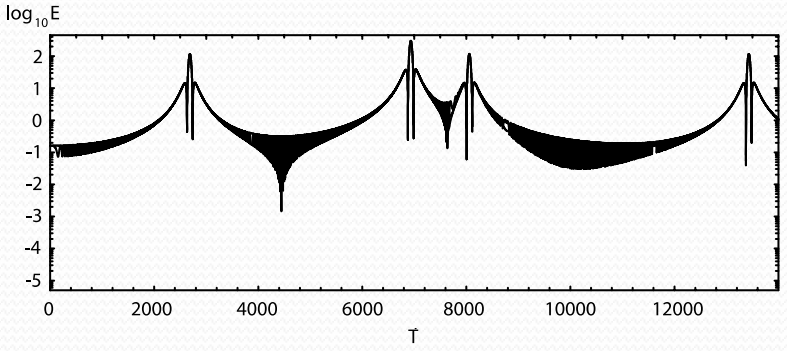

theoretical synchrotron spectrum

$f/\omega_{pe} = 8.5,\ 74.8,\ 654.$

Synchrotron radiation from propagating electrons in a uniform magnetic field

electron trajectories

radiation electric field observed at long distance

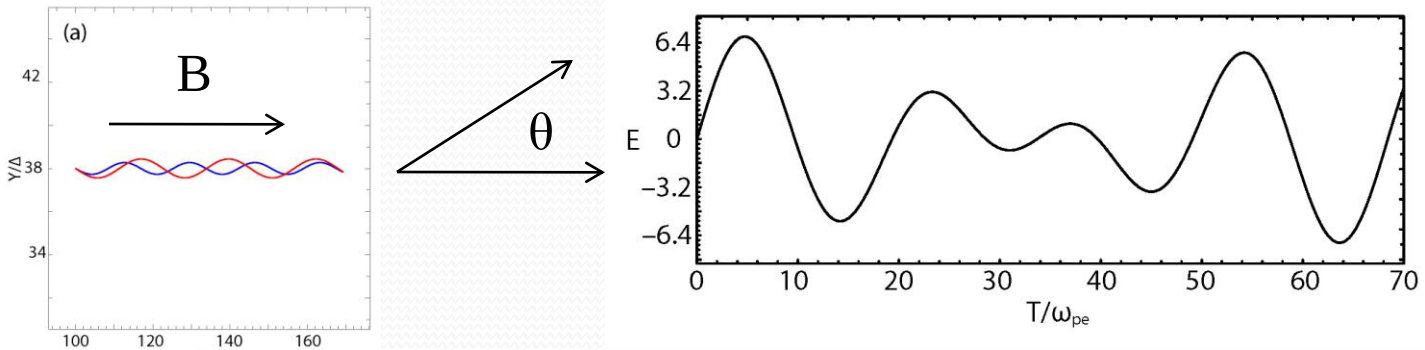

spectra with different viewing angles (helical)

$\theta_\gamma = 4.25^\circ$

gyrating

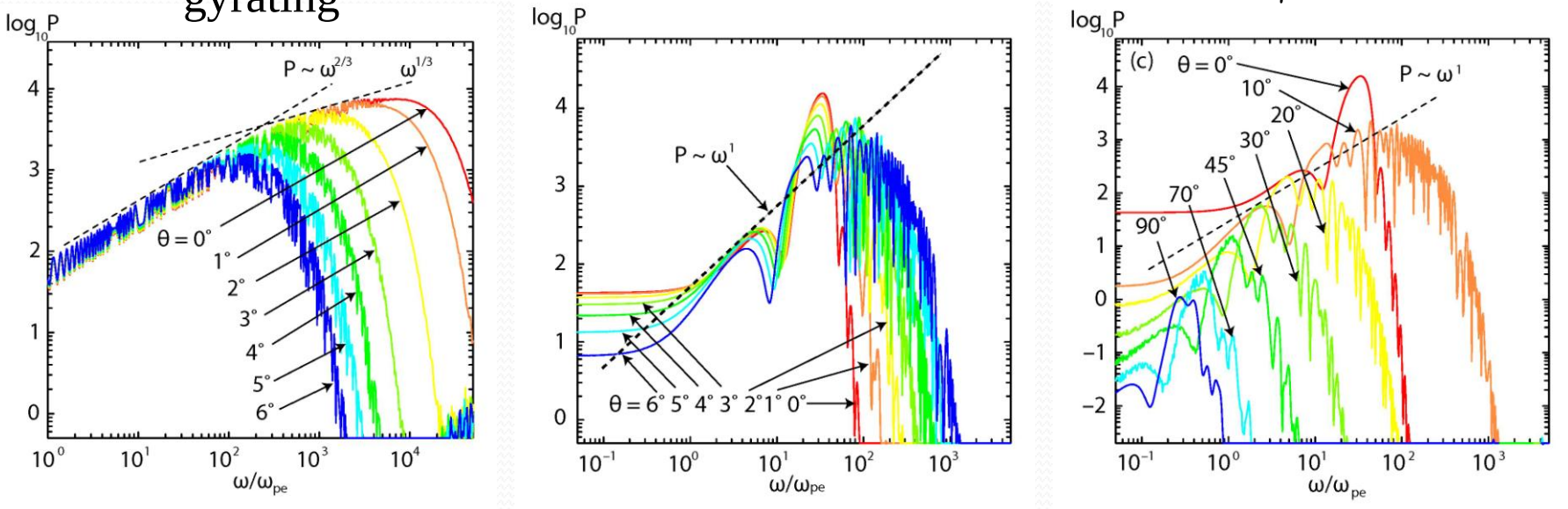

Nishikawa et al. astro-ph/0809.5067

Synchrotron vs. `Jitter'

- (a) Synchrotron emission assumes large-scale homogeneous magnetic fields
- (b) `Jitter' radiation (Medvedev 2000) occurs where the gyro-radius is larger than the randomness of turbulent magnetic fields

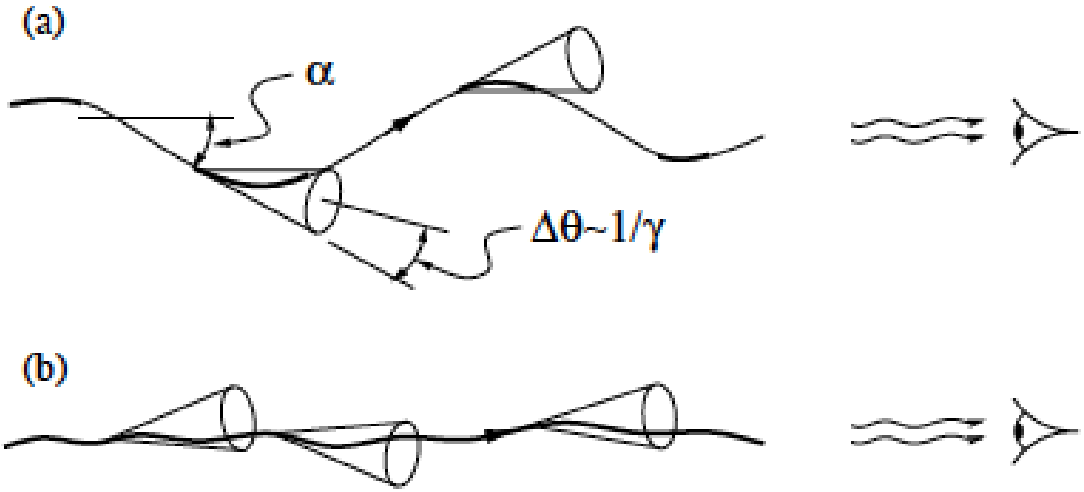

FIG. 1.—Emission from various points along the particle's trajectory. (*a*) $\alpha \gg \Delta\theta$; emission from selected parts (*bold portions*) of the trajectory is seen by an observer. (*b*) $\alpha \ll \Delta\theta$; emission from the entire trajectory is observed.

TABLE 1. Seven cases of radiation

	B_x	$V_{j1,2}$	$V_{\perp,1}$	$V_{\perp,2}$	γ_{max}	θ_T	**Remarks**
P	3.70 (B_z)	0.0c	0.998c	0.9997c	40.08	4.491	gyrating
A	3.70	0.99c	0.1c	0.12c	13.48	13.35	jet
B	3.70	0.9924c	0.1c	0.12c	36.70	4.905	jet
C	3.70	0.99c	0.01c	0.012c	7.114	25.30	jet
D	0.370	0.99c	0.01c	0.012c	7.114	25.30	jet
E	0.370	0.99c	0.1c	0.12c	13.48	13.35	$\Delta t = 0.005$
F	0.370	0.99c	0.1c	0.12c	13.48	13.35	$\Delta t = 0.025$

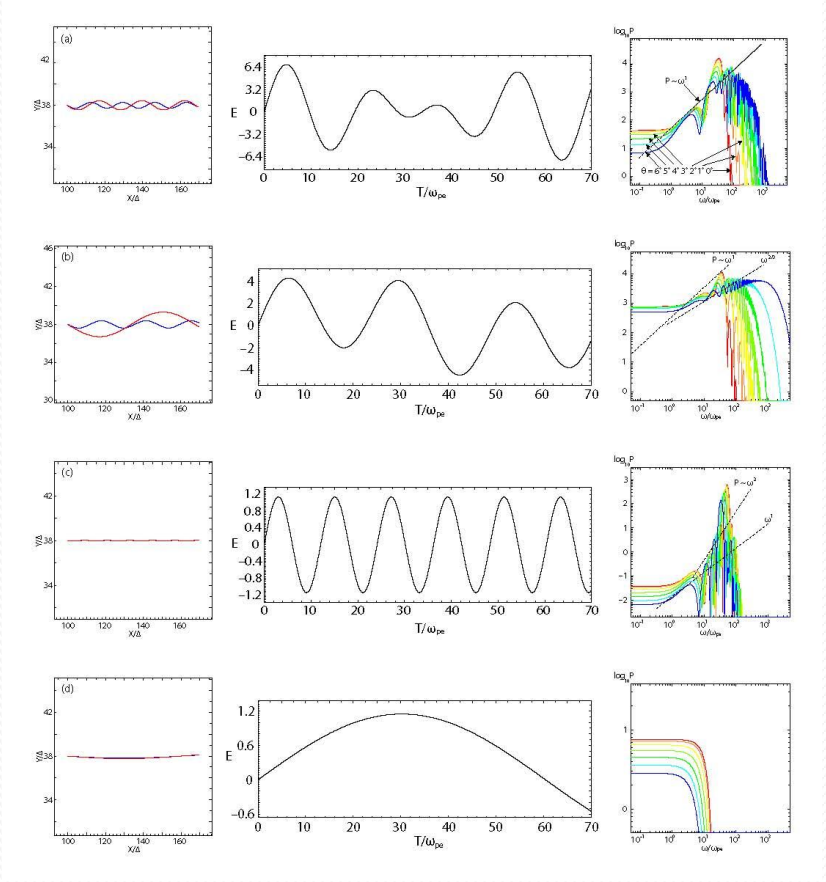

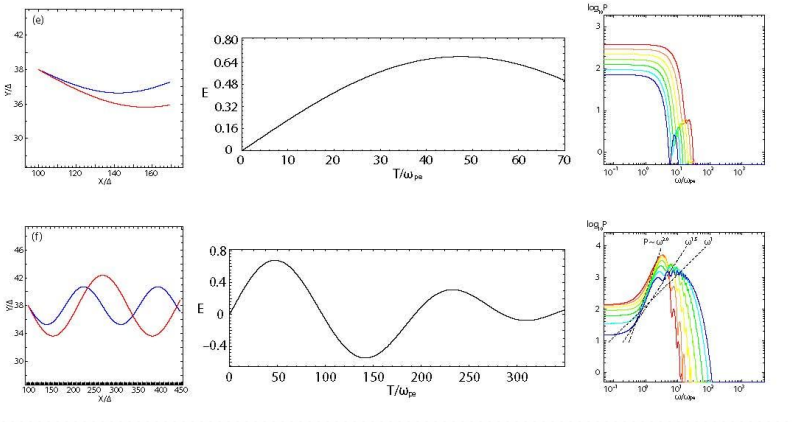

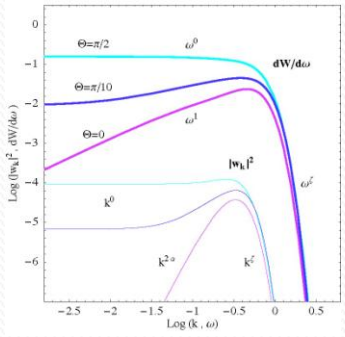

(Nishikawa et al. astro-ph/0809.5067)

TABLE 1. Seven cases of radiation

	B_x	$V_{j1,2}$	$V_{\perp,1}$	$V_{\perp,2}$	γ_{max}	θ_Γ	**Remarks**
P	3.70 (B_z)	0.0c	0.998c	0.9997c	40.08	4.491	gyrating
A	3.70	0.99c	0.1c	0.12c	13.48	13.35	jet
B	3.70	0.9924c	0.1c	0.12c	36.70	4.905	jet
C	3.70	0.99c	0.01c	0.012c	7.114	25.30	jet
D	0.370	0.99c	0.01c	0.012c	7.114	25.30	jet
E	0.370	0.99c	0.1c	0.12c	13.48	13.35	$\Delta t = 0.005$
F	0.370	0.99c	0.1c	0.12c	13.48	13.35	$\Delta t = 0.025$

Case A

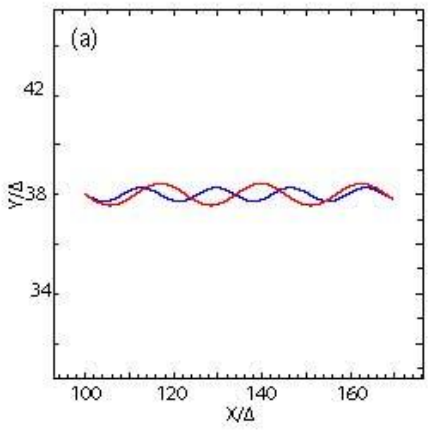

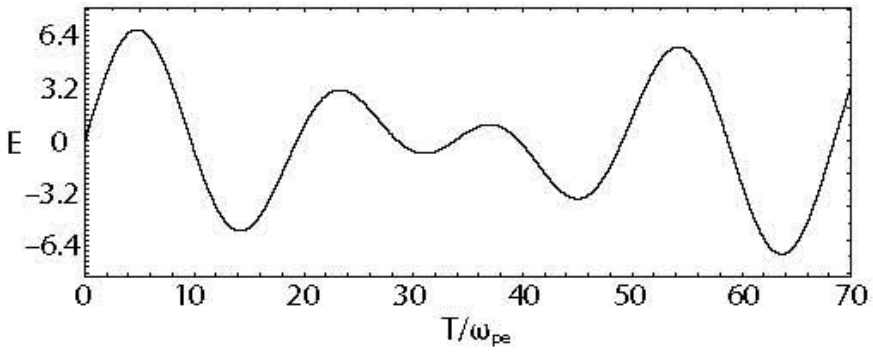

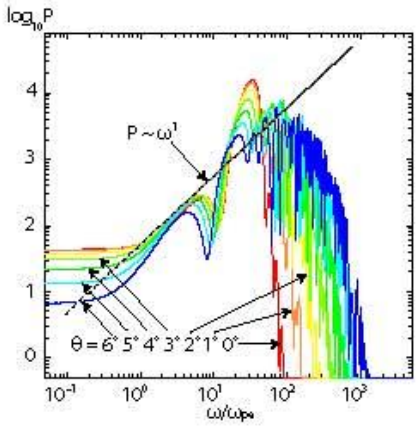

(Nishikawa et al. astro-ph/0809.5067)

TABLE 1. Seven cases of radiation

	B_x	$V_{j1,2}$	$V_{\perp,1}$	$V_{\perp,2}$	γ_{max}	θ_Γ	**Remarks**
P	3.70 (B_z)	0.0c	0.998c	0.9997c	40.08	4.491	gyrating
A	3.70	0.99c	0.1c	0.12c	13.48	13.35	jet
B	3.70	0.9924c	0.1c	0.12c	36.70	4.905	jet
C	3.70	0.99c	0.01c	0.012c	7.114	25.30	jet
D	0.370	0.99c	0.01c	0.012c	7.114	25.30	jet
E	0.370	0.99c	0.1c	0.12c	13.48	13.35	$\Delta t = 0.005$
F	0.370	0.99c	0.1c	0.12c	13.48	13.35	$\Delta t = 0.025$

Case B

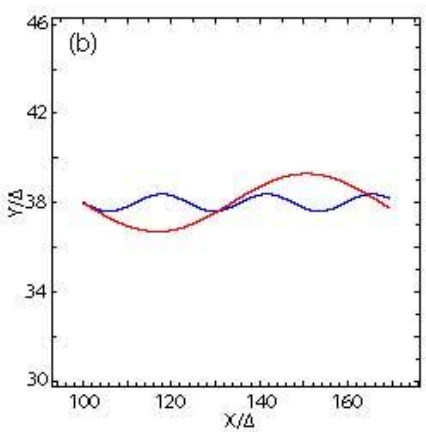

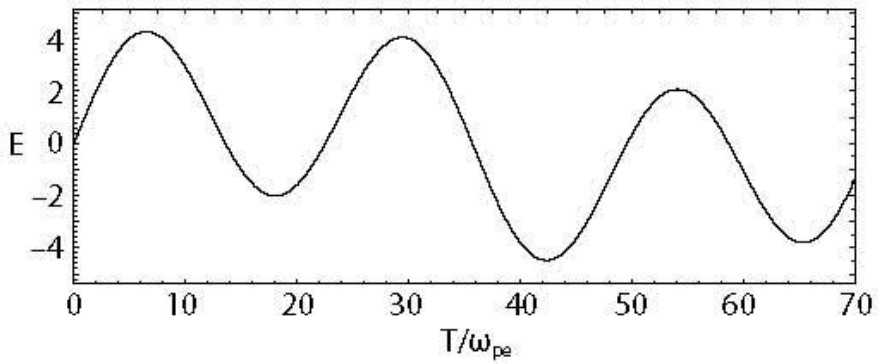

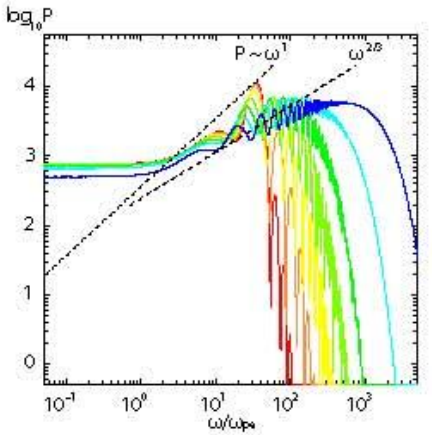

(Nishikawa et al. astro-ph/0809.5067)

TABLE 1. Seven cases of radiation

	B_x	$V_{j1,2}$	$V_{\perp,1}$	$V_{\perp,2}$	γ_{max}	θ_Γ	**Remarks**
P	3.70 (B_z)	0.0c	0.998c	0.9997c	40.08	4.491	gyrating
A	3.70	0.99c	0.1c	0.12c	13.48	13.35	jet
B	3.70	0.9924c	0.1c	0.12c	36.70	4.905	jet
C	3.70	0.99c	0.01c	0.012c	7.114	25.30	jet
D	0.370	0.99c	0.01c	0.012c	7.114	25.30	jet
E	0.370	0.99c	0.1c	0.12c	13.48	13.35	$\Delta t = 0.005$
F	0.370	0.99c	0.1c	0.12c	13.48	13.35	$\Delta t = 0.025$

Case C

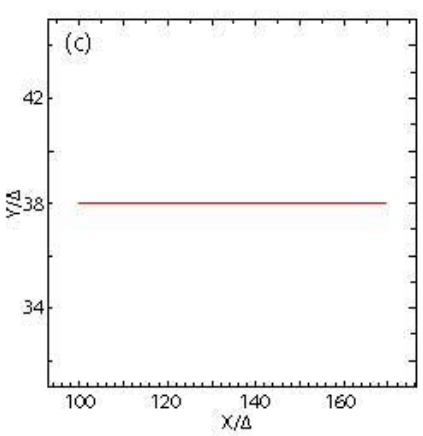

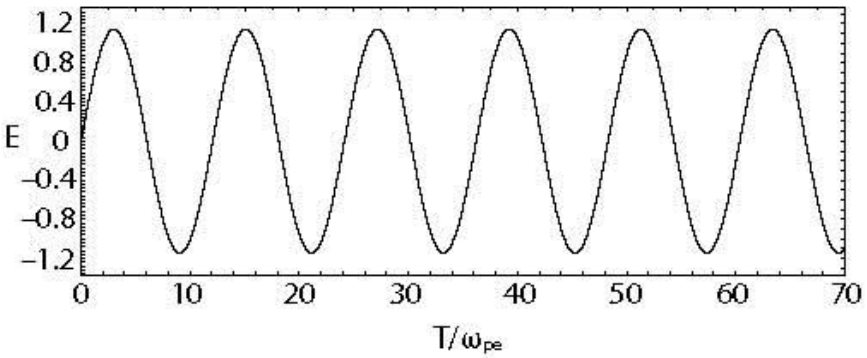

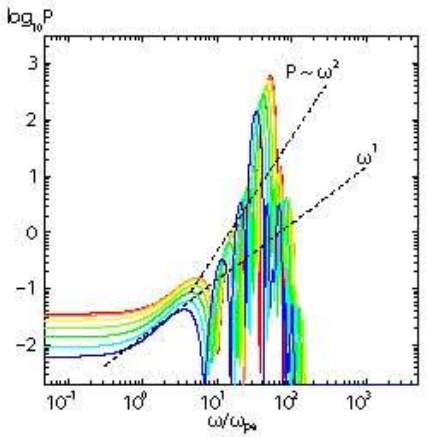

(Nishikawa et al. astro-ph/0809.5067)

TABLE 1. Seven cases of radiation

	B_x	$V_{j1,2}$	$V_{\perp,1}$	$V_{\perp,2}$	γ_{max}	θ_Γ	**Remarks**
P	3.70 (B_z)	0.0c	0.998c	0.9997c	40.08	4.491	gyrating
A	3.70	0.99c	0.1c	0.12c	13.48	13.35	jet
B	3.70	0.9924c	0.1c	0.12c	36.70	4.905	jet
C	3.70	0.99c	0.01c	0.012c	7.114	25.30	jet
D	0.370	0.99c	0.01c	0.012c	7.114	25.30	jet
E	0.370	0.99c	0.1c	0.12c	13.48	13.35	$\Delta t = 0.005$
F	0.370	0.99c	0.1c	0.12c	13.48	13.35	$\Delta t = 0.025$

Case D

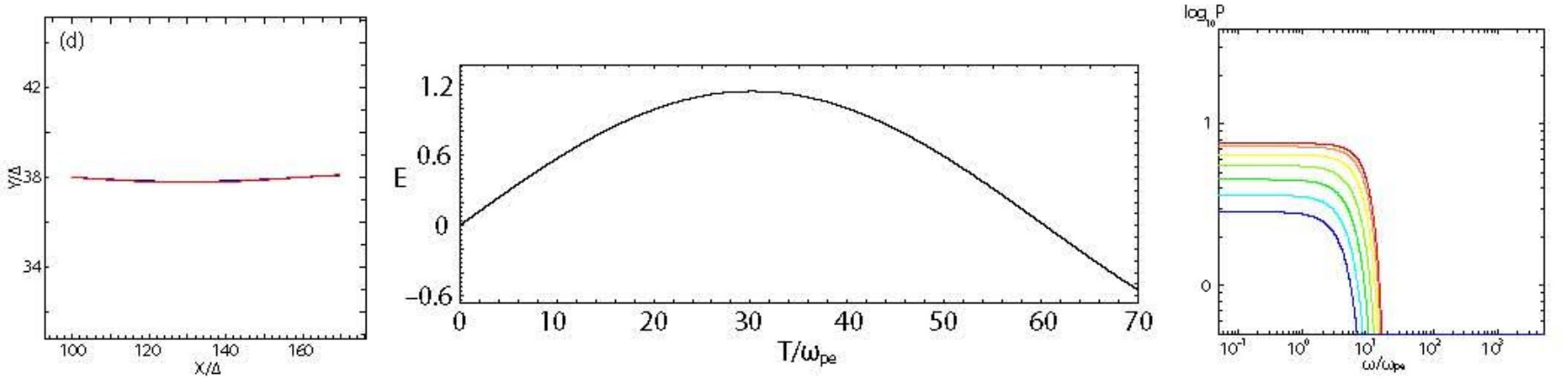

(Nishikawa et al. astro-ph/0809.5067)

TABLE 1. Seven cases of radiation

	B_x	$V_{j1,2}$	$V_{\perp,1}$	$V_{\perp,2}$	γ_{max}	θ_Γ	**Remarks**
P	3.70 (B_z)	0.0c	0.998c	0.9997c	40.08	4.491	gyrating
A	3.70	0.99c	0.1c	0.12c	13.48	13.35	jet
B	3.70	0.9924c	0.1c	0.12c	36.70	4.905	jet
C	3.70	0.99c	0.01c	0.012c	7.114	25.30	jet
D	0.370	0.99c	0.01c	0.012c	7.114	25.30	jet
E	0.370	0.99c	0.1c	0.12c	13.48	13.35	$\Delta t = 0.005$
F	0.370	0.99c	0.1c	0.12c	13.48	13.35	$\Delta t = 0.025$

Case E

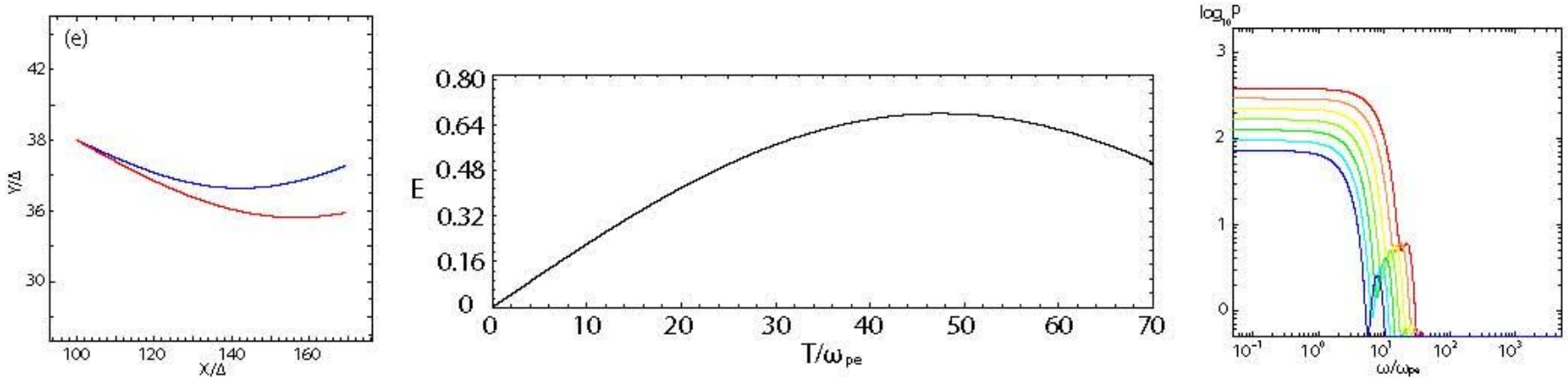

(Nishikawa et al. astro-ph/0809.5067)

TABLE 1. Seven cases of radiation

	B_x	$V_{j1,2}$	$V_{\perp,1}$	$V_{\perp,2}$	γ_{max}	θ_Γ	**Remarks**
P	3.70 (B_z)	0.0c	0.998c	0.9997c	40.08	4.491	gyrating
A	3.70	0.99c	0.1c	0.12c	13.48	13.35	jet
B	3.70	0.9924c	0.1c	0.12c	36.70	4.905	jet
C	3.70	0.99c	0.01c	0.012c	7.114	25.30	jet
D	0.370	0.99c	0.01c	0.012c	7.114	25.30	jet
E	0.370	0.99c	0.1c	0.12c	13.48	13.35	$\Delta t = 0.005$
F	0.370	0.99c	0.1c	0.12c	13.48	13.35	$\Delta t = 0.025$

Case F

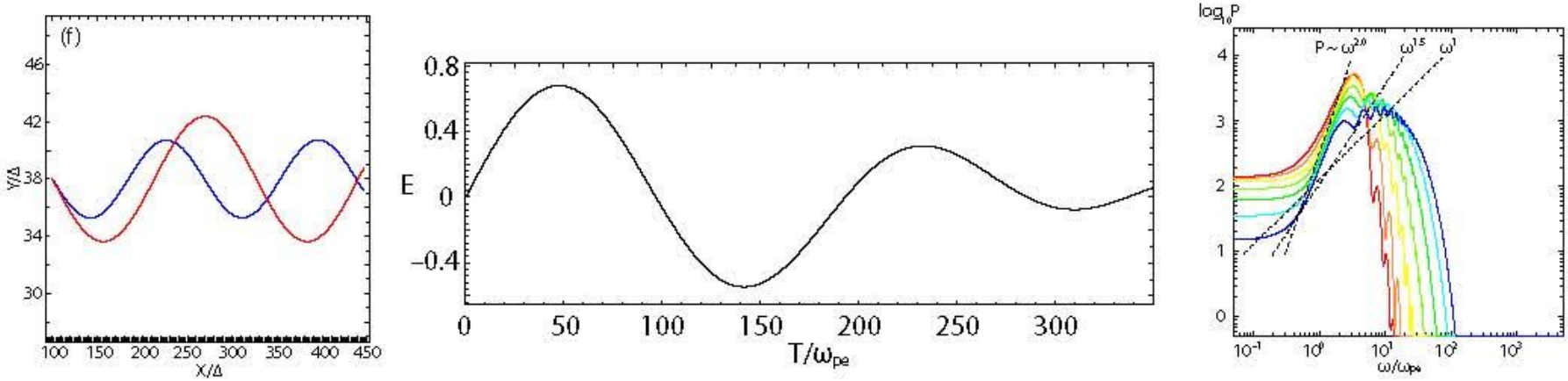

(Nishikawa et al. astro-ph/0809.5067)

Synchrotron vs. `Jitter'

- (a) Synchrotron emission assumes large-scale homogeneous magnetic fields
- (b) `Jitter' radiation (Medvedev 2000) occurs where the gyro-radius is larger than the randomness of turbulent magnetic fields

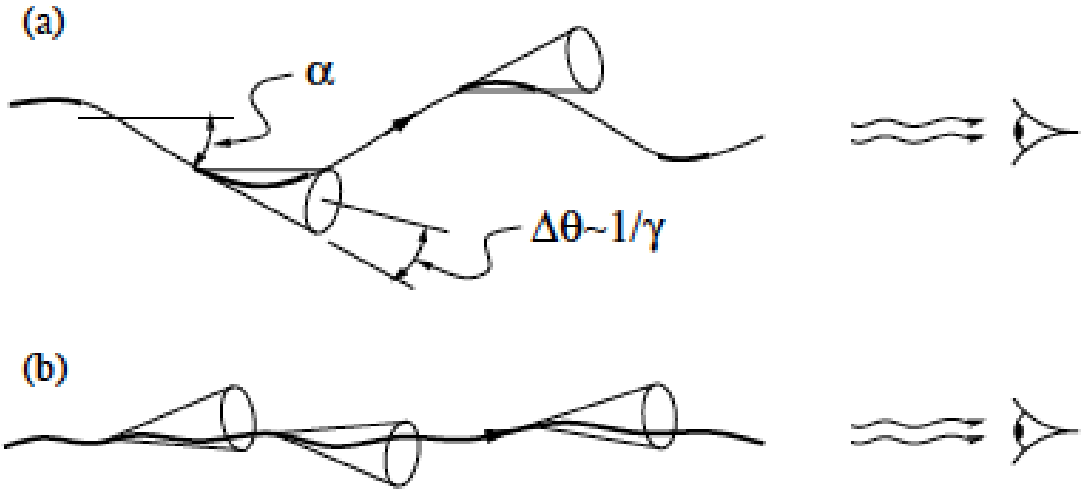

FIG. 1.—Emission from various points along the particle's trajectory. (*a*) $\alpha \gg \Delta\theta$; emission from selected parts (*bold portions*) of the trajectory is seen by an observer. (*b*) $\alpha \ll \Delta\theta$; emission from the entire trajectory is observed.

Radiation from test (accelerated) particles in static turbulent magnetic fields generated by the Weibel instability in 2D PIC simulation

$t = 2250\,\omega_{pe}^{-1}$ number density

$t_s = 3000\,\Delta t = 135\,\omega_p^{-1}$ $\Delta t = 0.045\,\omega_p^{-1}$

$N_s \sim 10{,}000$

test particle simulation in a
fixed snapshot of electromagnetic filed

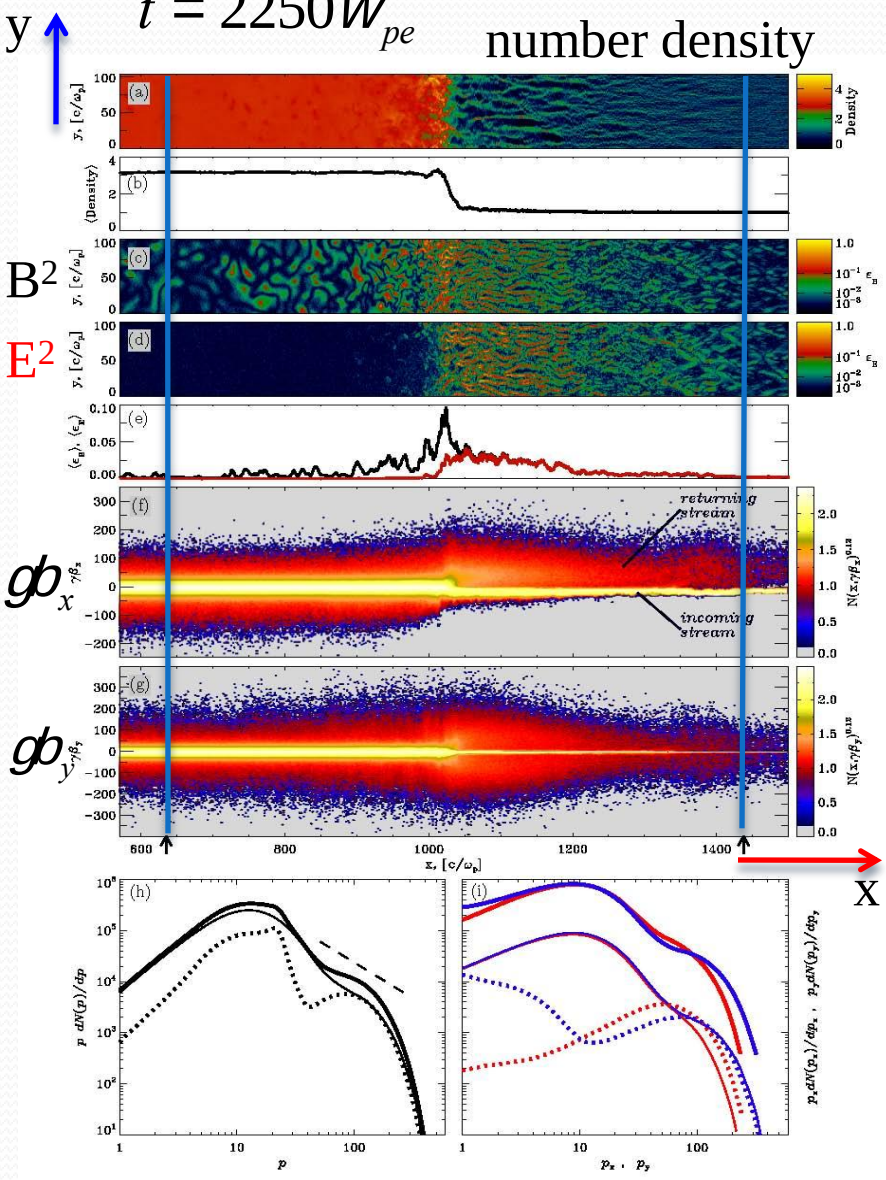

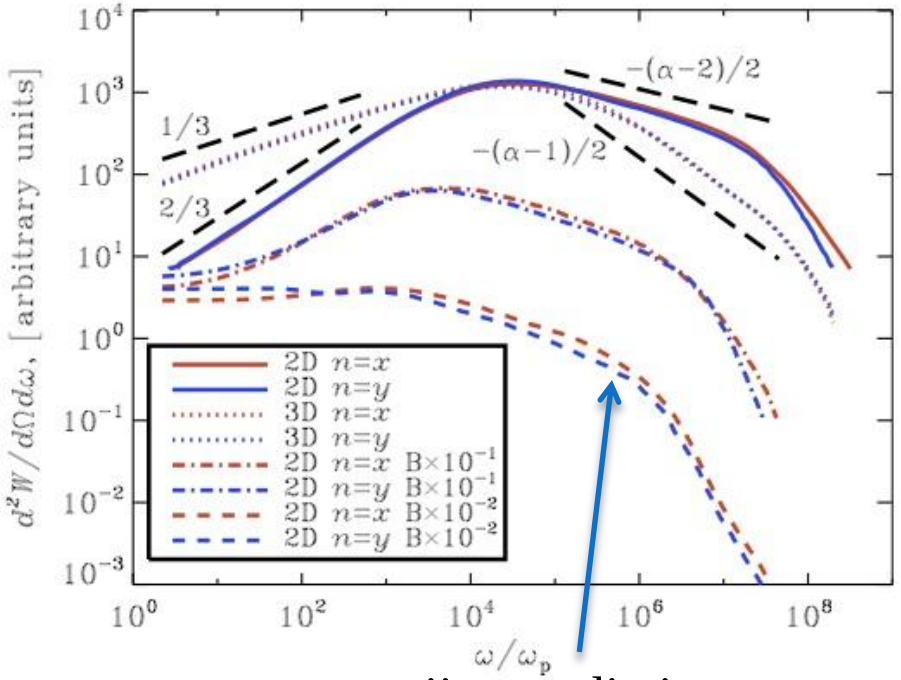

jitter radiation

(Sironi & Spitkovsky 2009)

Radiation from electrons in self-consistent electromagnetic field from a 2D PIC simulation

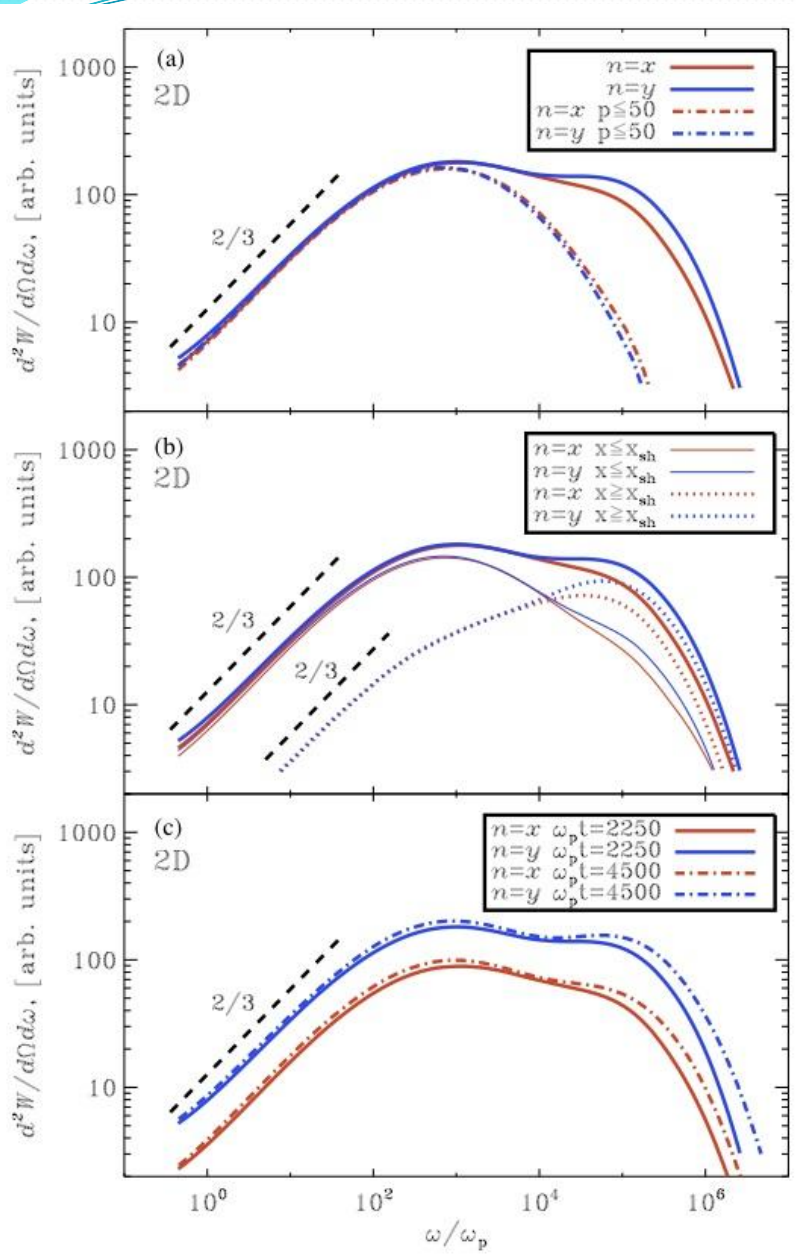

Due to the radiation is calculated in downstream frame the radiation is isotropic. An additional Lorentz transformation is required, if the down-stream medium is moving with respect to the observer (no beaming effect is taken account and they are different from the observed radiation).

They conclude that jitter regime is obtained only if with artificially reduced the strength of the electromagnetic filed?
($K \propto qBl / mc^2$)

This conclusion is due to that radiation is calculated in downstream frame?

(Sironi & Spitkovsky 2009)

Importance of Synchrotron radiation calculated in 3-D system

$\gamma = 6$, P^+ e^- counter-streaming jet, no shock generated

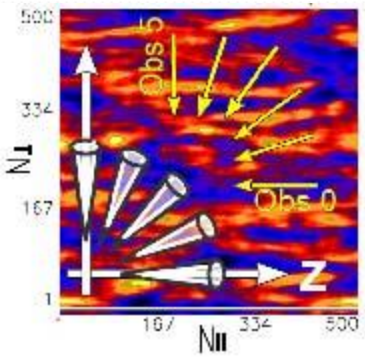

3D

2D

6<t<16

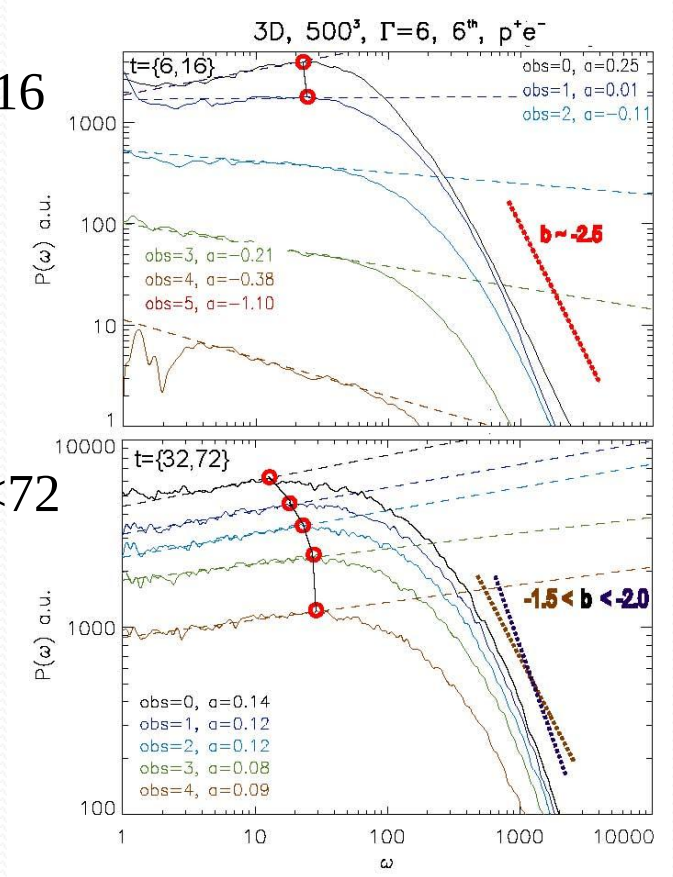

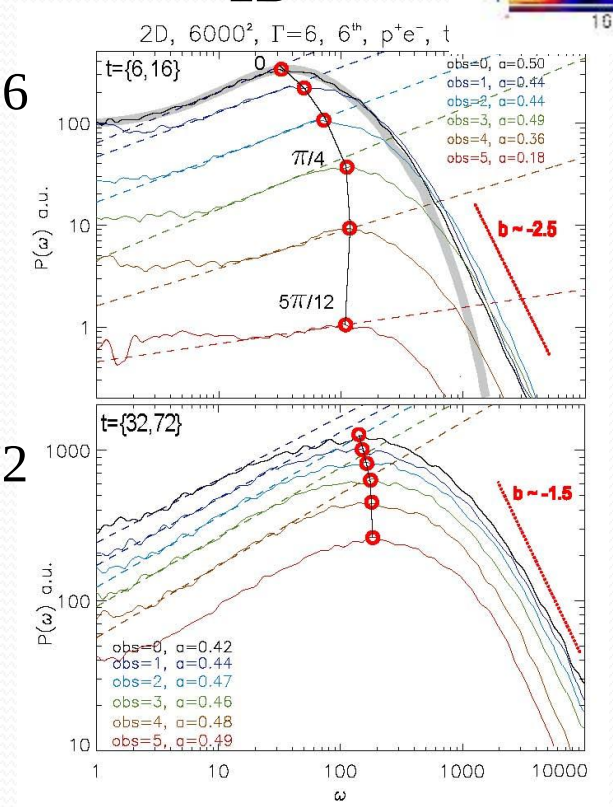

32<t<72

32<t<72

Frederiksen et al. ApJL, accepted, (arXiv:1003.1140)

Radiation from electrons by tracing trajectories self-consistently

using a small simulation system

initial setup for jitter radiation

select electrons randomly (12,150) in jet and ambient

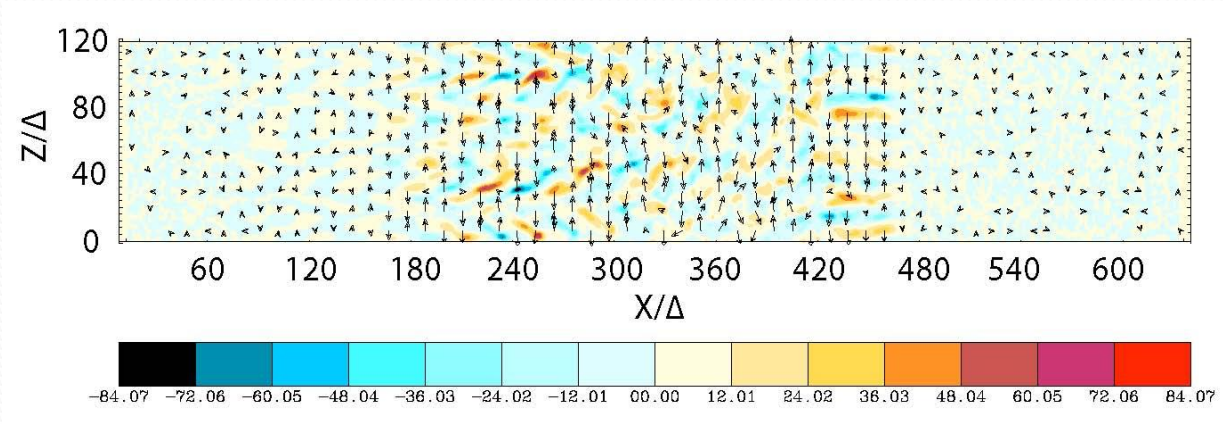

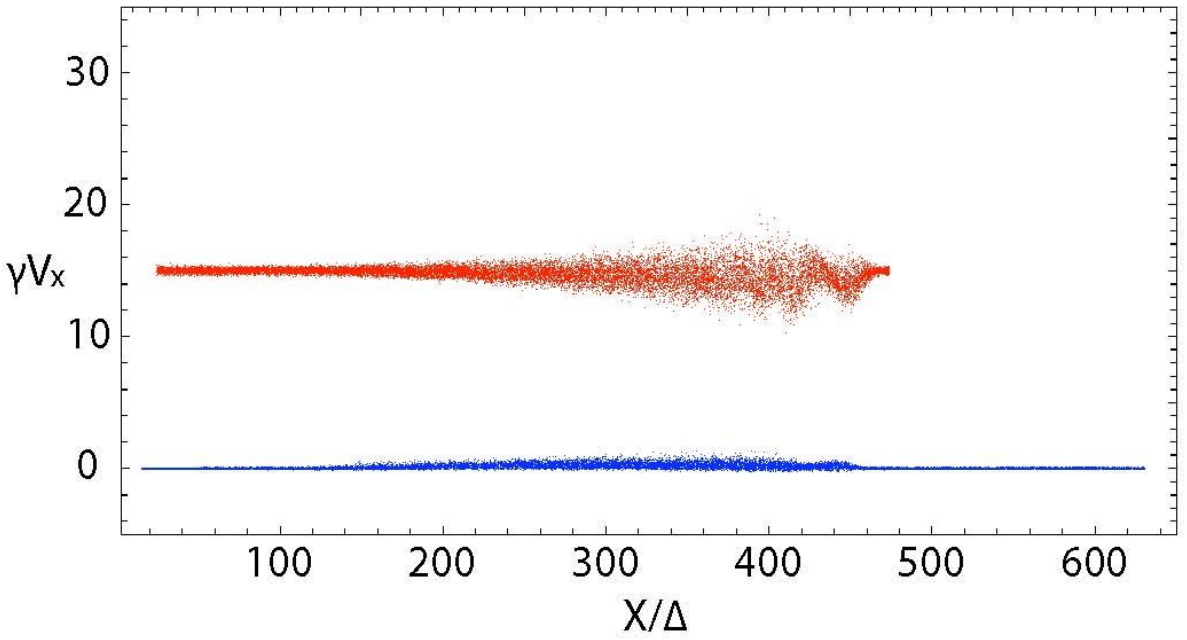

final condition for radiation

15,000 steps

dt = 0.005 ω_{pe}^{-1}

$n_\omega = 100$

$n_\theta = 2$

$\Delta x_{jet} = 75\Delta$

$t_r = 75\ \omega_{pe}^{-1}$

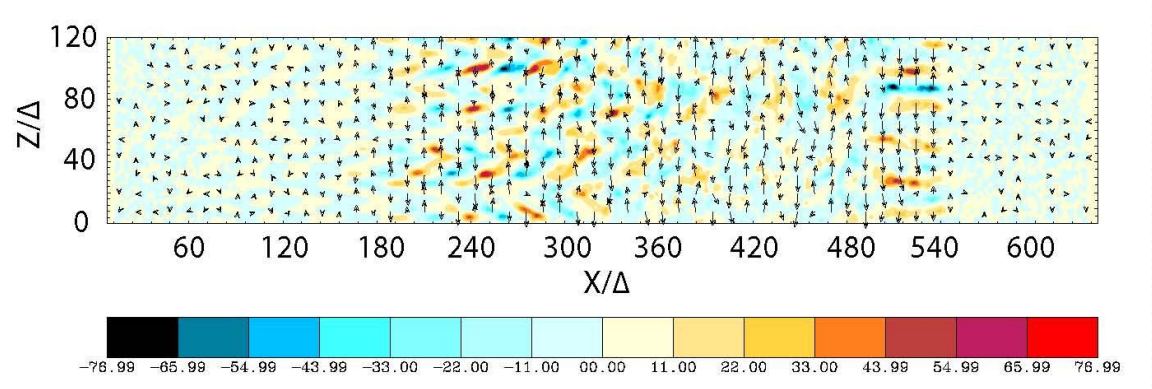

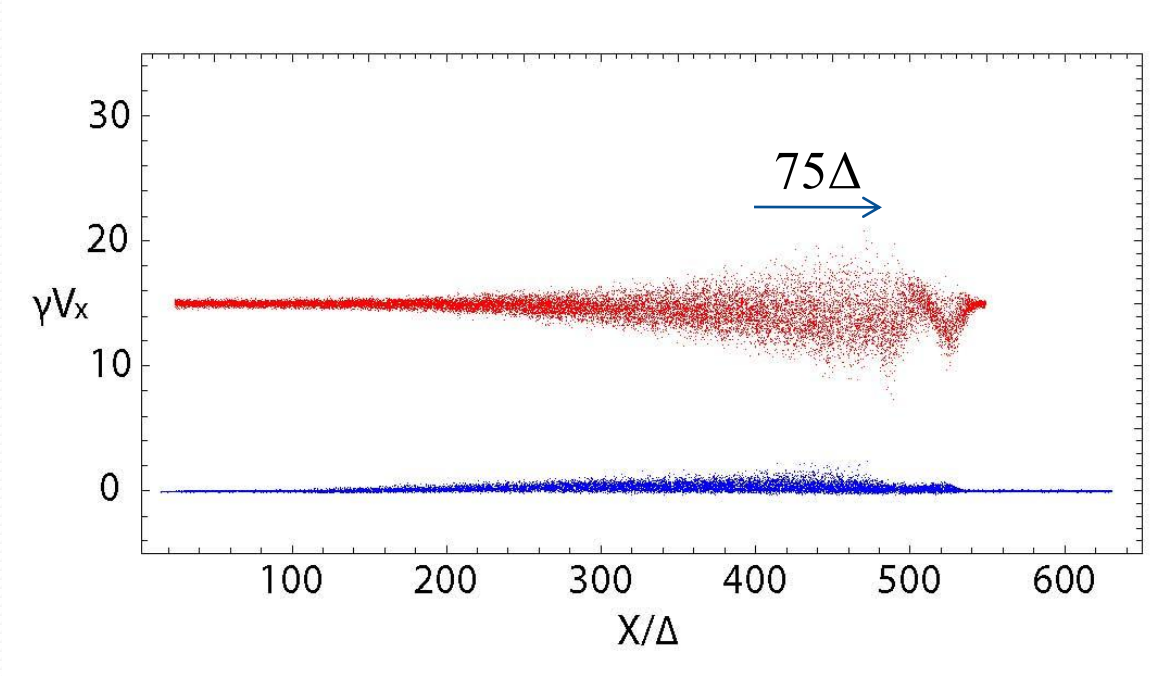

Calculated spectra for jet electrons and ambient electrons

$a = \lambda e|\delta B|/mc^2 < 1$ (λ: the length scale and $|\delta B|$ is the magnitude of the fluctuations)

$\gamma = 15$

$\theta = 0^\circ$ and 5° $q_g = 3.81^\circ$

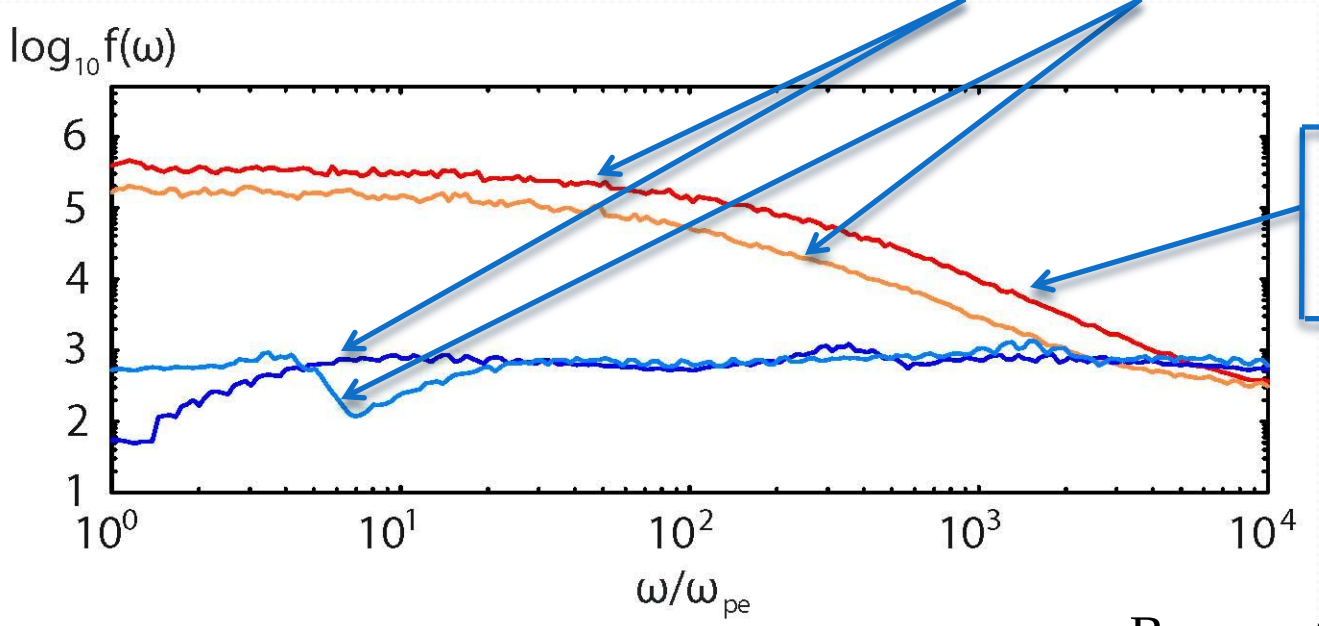

high frequency due to turbulent magnetic field

Bremesstrahlung (ballistic)

Case D

$\gamma = 7.11$

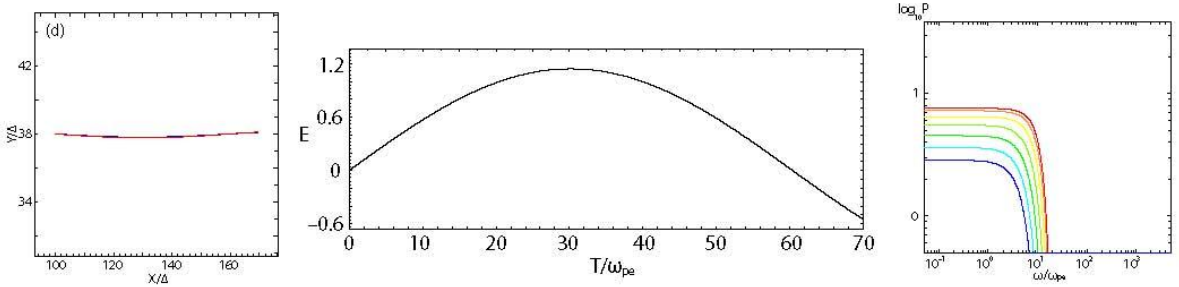

Nishikawa et al. 2009 (arXiv:0906.5018)

3D jitter radiation (diffusive synchrotron radiation) with a ensemble of mono-energetic electrons (γ = 3) in turbulent magnetic fields (Medvedev 2000; 2006, Fleishman 2006) (ballistic)

$$P_B(k) \propto k^{\mu}$$

2d slice of magnetic field

3D jitter radiation with γ = 3 electrons

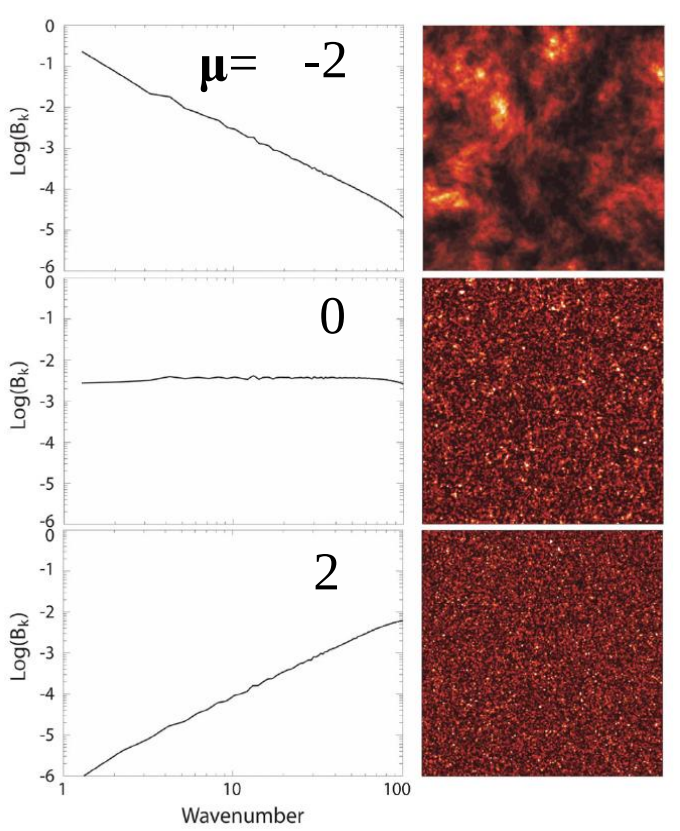

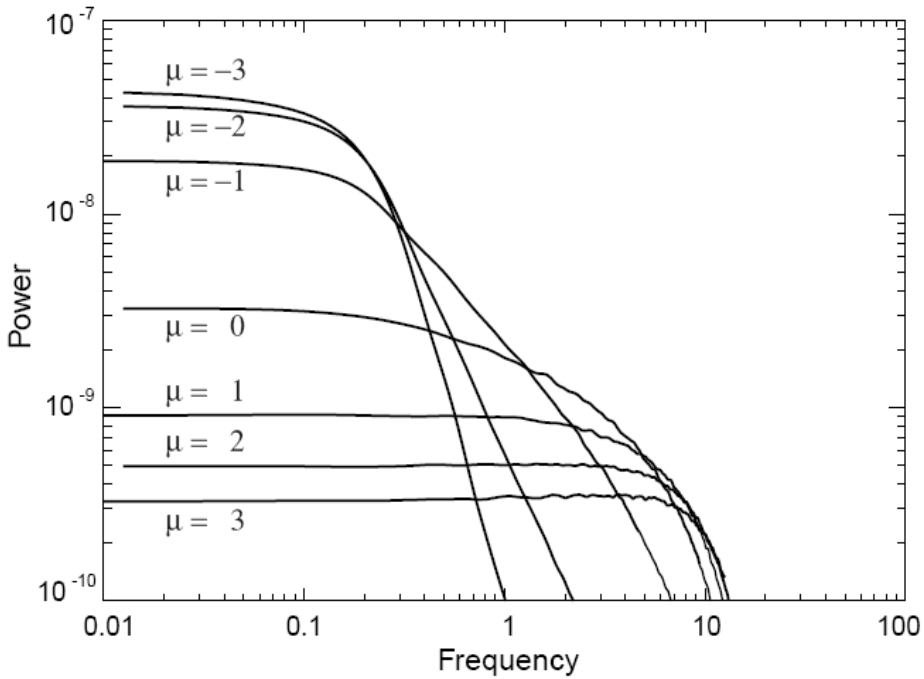

Hededal & Nordlund (astro-ph/0511662)

Dependence on Lorentz factors of jets

$\gamma = 15$

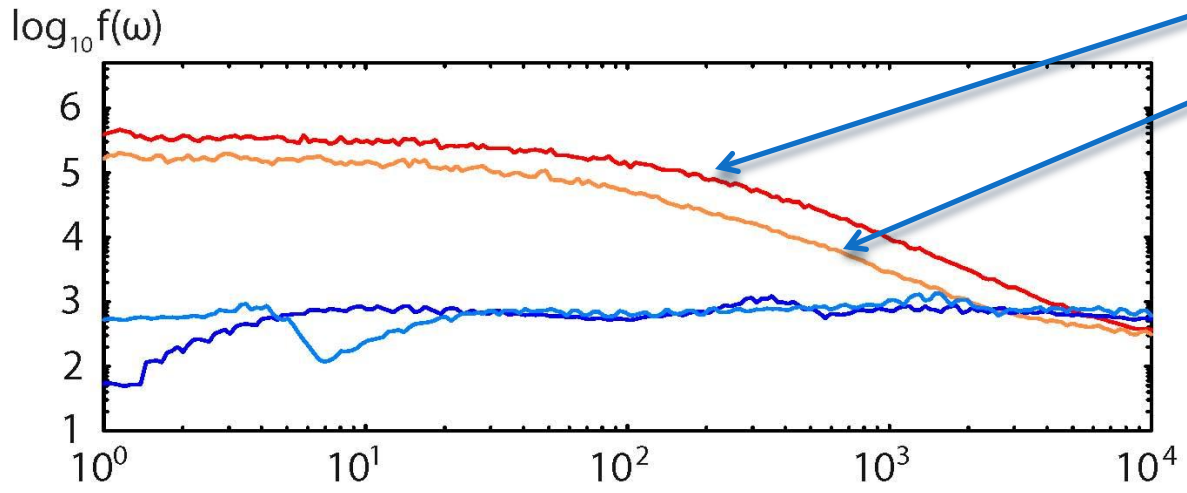

$\theta = 0^\circ$

5° $q_g = 3.81^\circ$

$\gamma = 100$

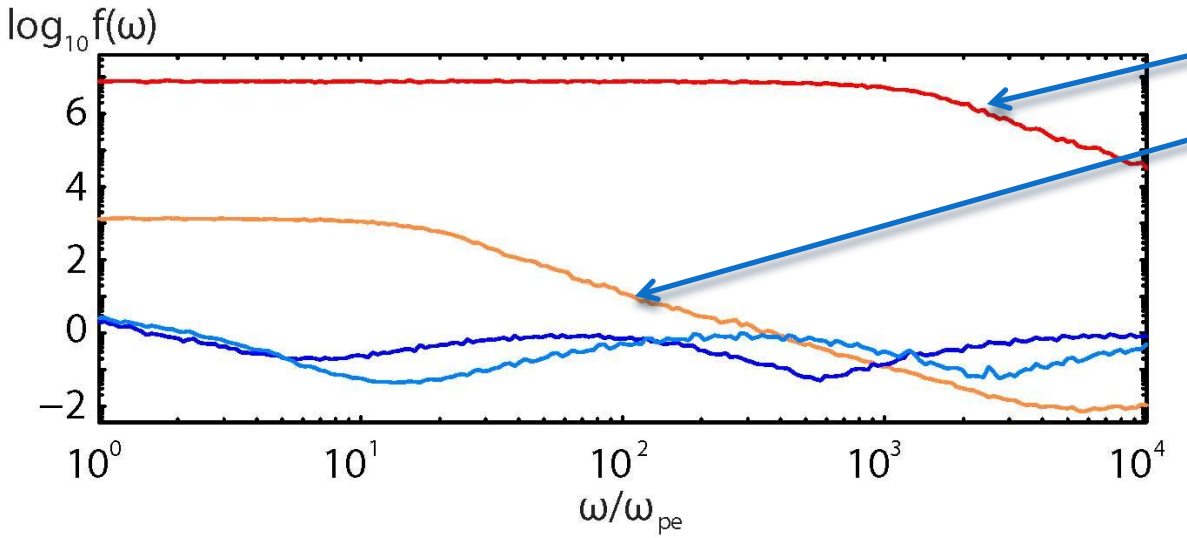

$\theta = 0^\circ$

5° $q_g = 0.57^\circ$

Narrow beaming angle

Observations and numerical spectrum

GRB 080916C

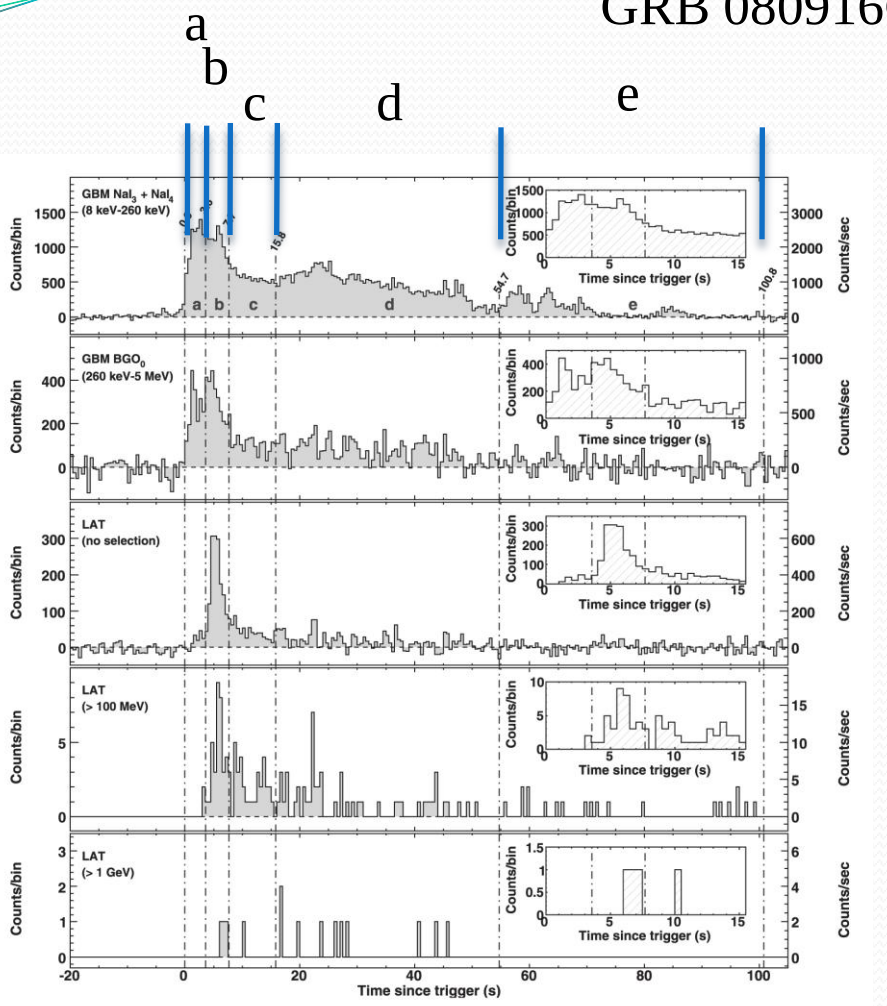

Abdo et al. 2009, Science

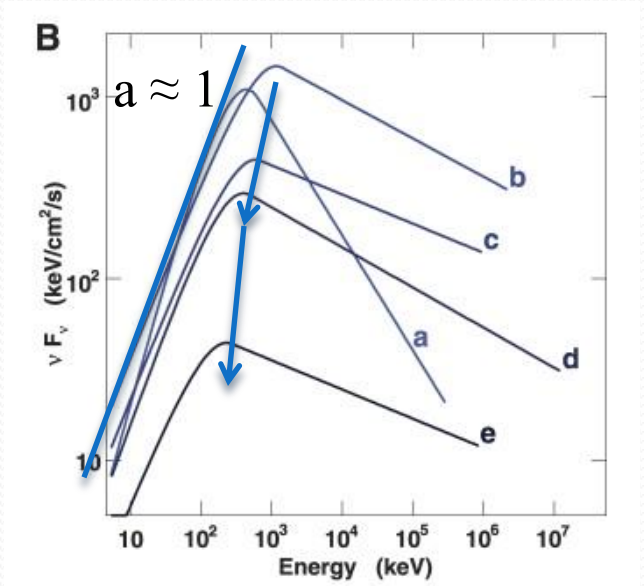

a ≈ 1

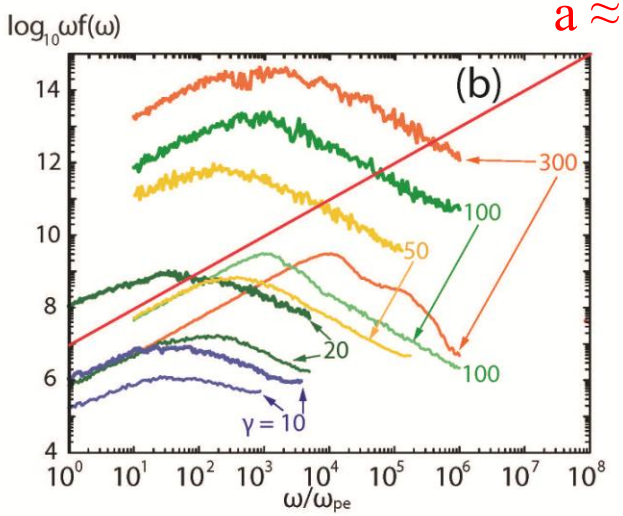

Nishikawa et al. 2010

Radiation in a small system

without iteration

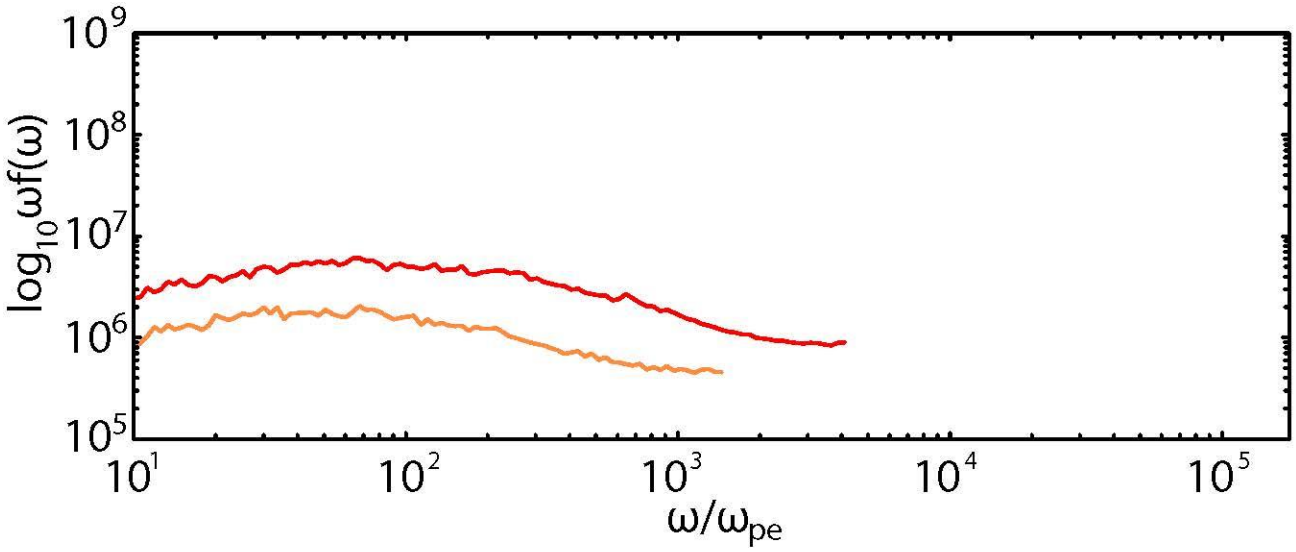

with iteration

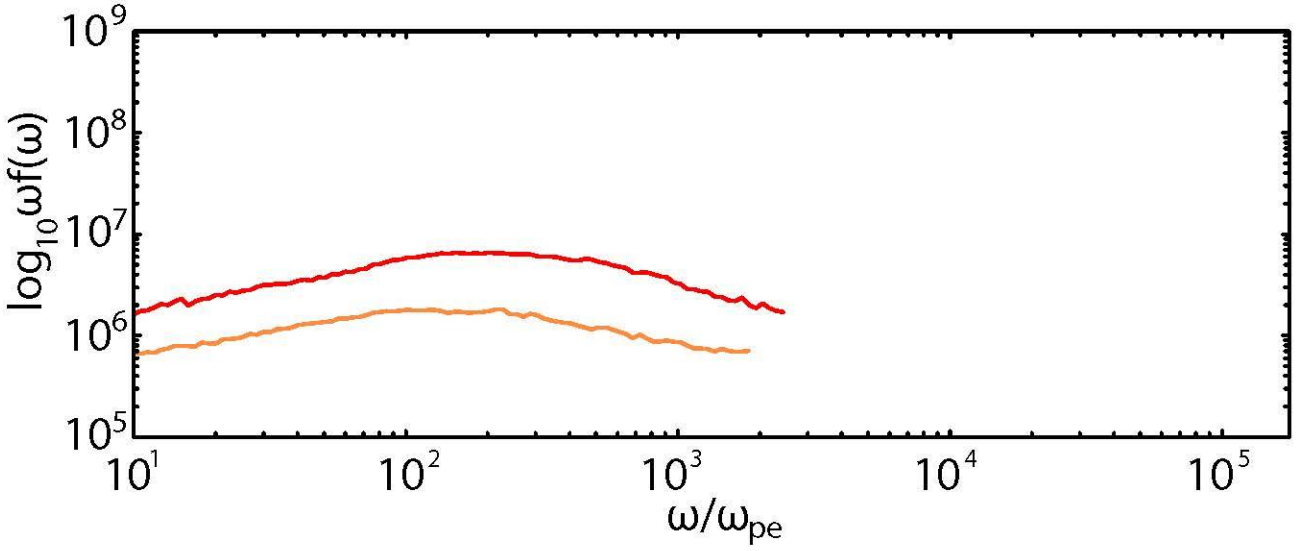

Radiation in a larger system

System size: 8000 × 240 × 240
Electron-positron , $\gamma = 15$

Sampled particles 115,200

(a)$150\,w_{pe}^{-1} \le t \le 225\,w_{pe}^{-1}$

(b) $200\,w_{pe}^{-1} \le t \le 275\,w_{pe}^{-1}$

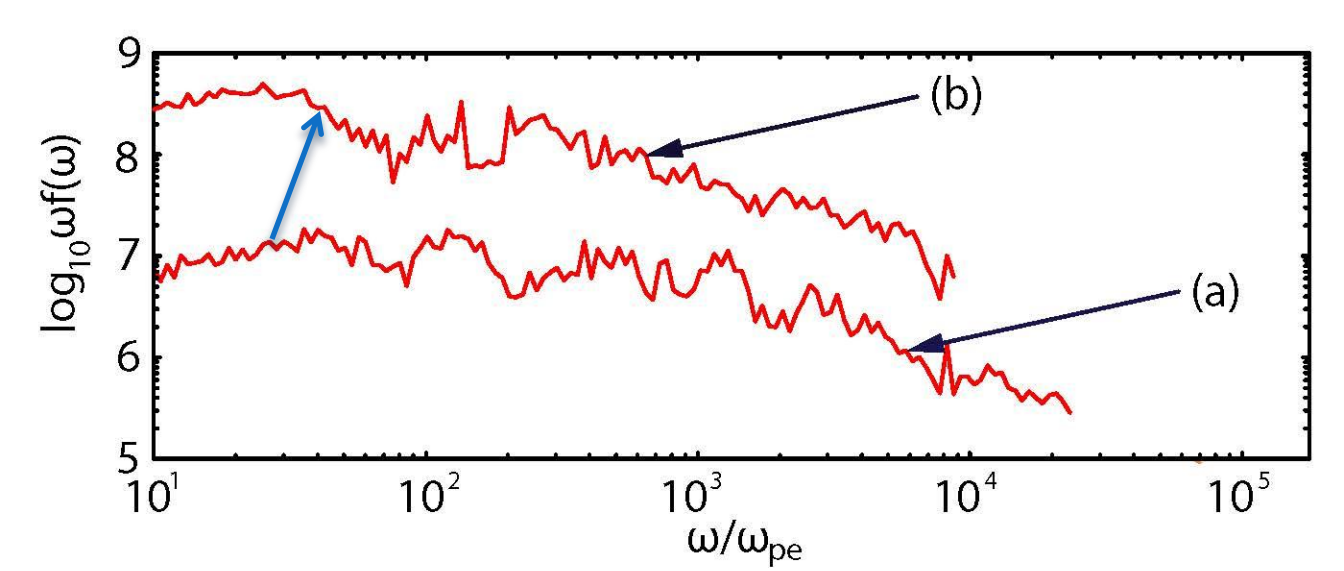

Emission Lines from Tori

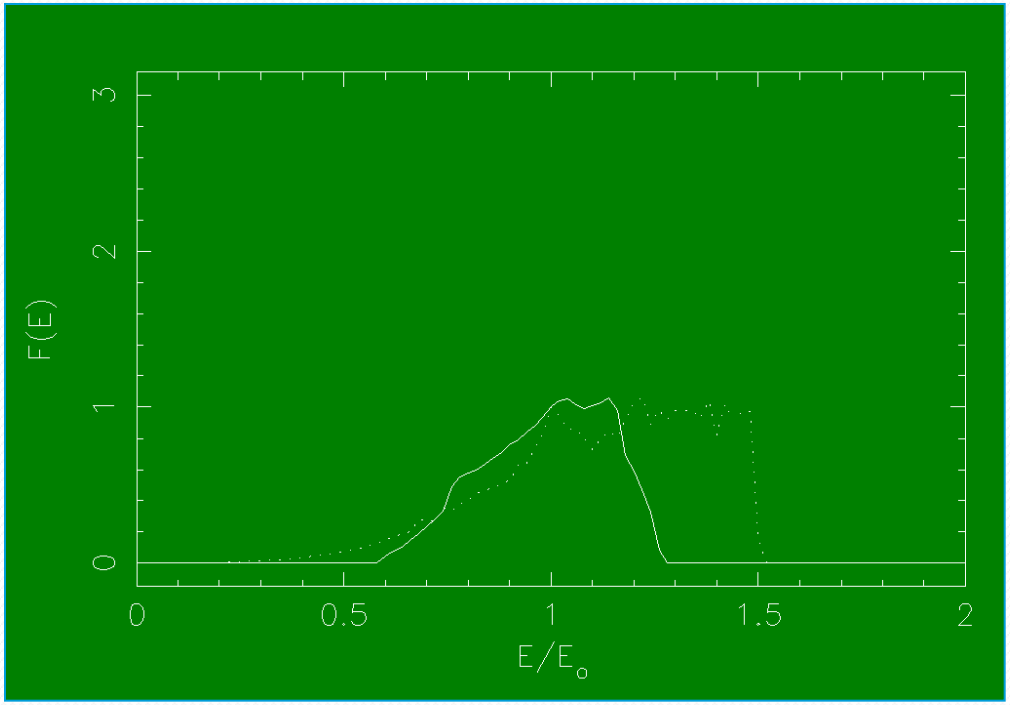

Comparison of emission line between accretion torus (solid) and disk (dotted) inclined at 85^o.

- Inner most region is obscured – weakening the red and blue wings.
- A broad emission line centered at 6.4keV results.
- This may explain why not many sources with asymmetric lines like MCG-6-30-15 are observed.

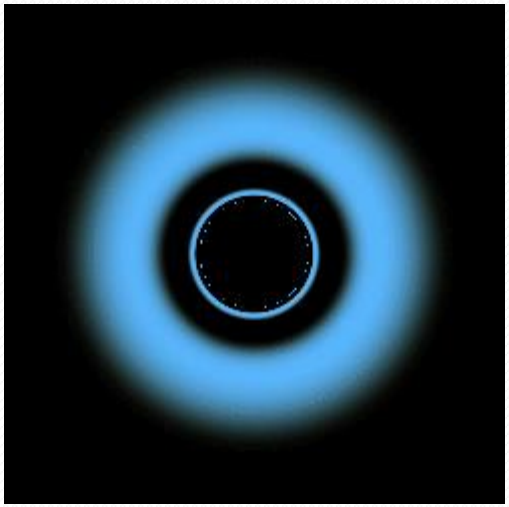

Partially transparent torus around a Kerr Black Hole.

(Fuerst & Wu 2004, A&A, 424, 733)

Magnetic field lines

(Alves et al. ApJL, 2012)

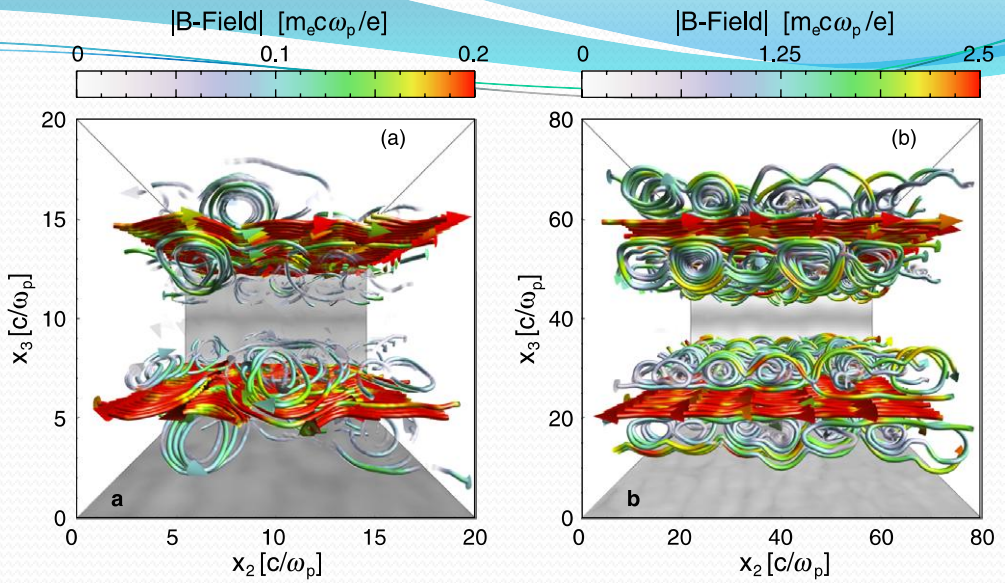

Figure 3. Magnetic field lines generated in (a) the subrelativisitc scenario, and (b) the relativistic scenario, at time $t = 100/\omega_p$.
(A color version of this figure is available in the online journal.)

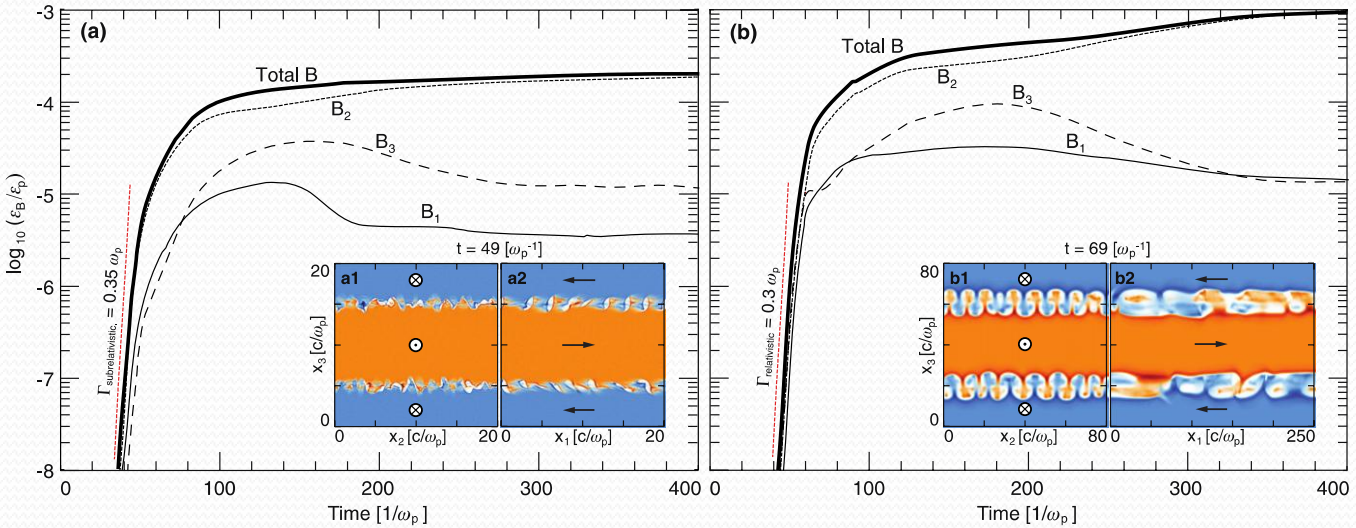

Figure 4. Evolution of the equipartition energy ϵ_B/ϵ_p for a (a) subrelativistic and (b) relativistic shear scenarios. The contribution of each magnetic field component is also depicted. The insets in each frame represent two-dimensional slices of the electron density at $t = 49/\omega_p$ and $t = 69/\omega_p$ for the respective case. The red (blue) color represents the electron density of the plasma that flows in the positive (negative) x_1 direction. Darker regions in the color map indicate high electron density, whereas lighter regions indicate low electron density. Slices for insets (a1), (a2), (b1), and (b2) were taken at the center of the simulation box; (a1) and (b1) are transverse to the flow direction, and slices (a2) and (b2) are longitudinal to the flow direction.

(A color version of this figure is available in the online journal.)

Simulation set up

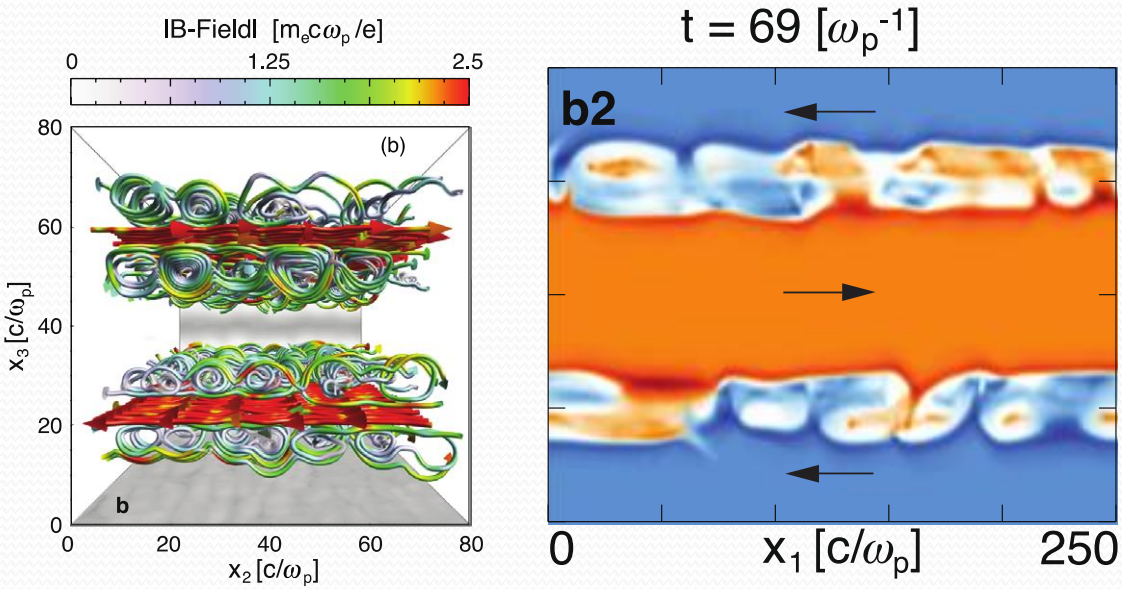

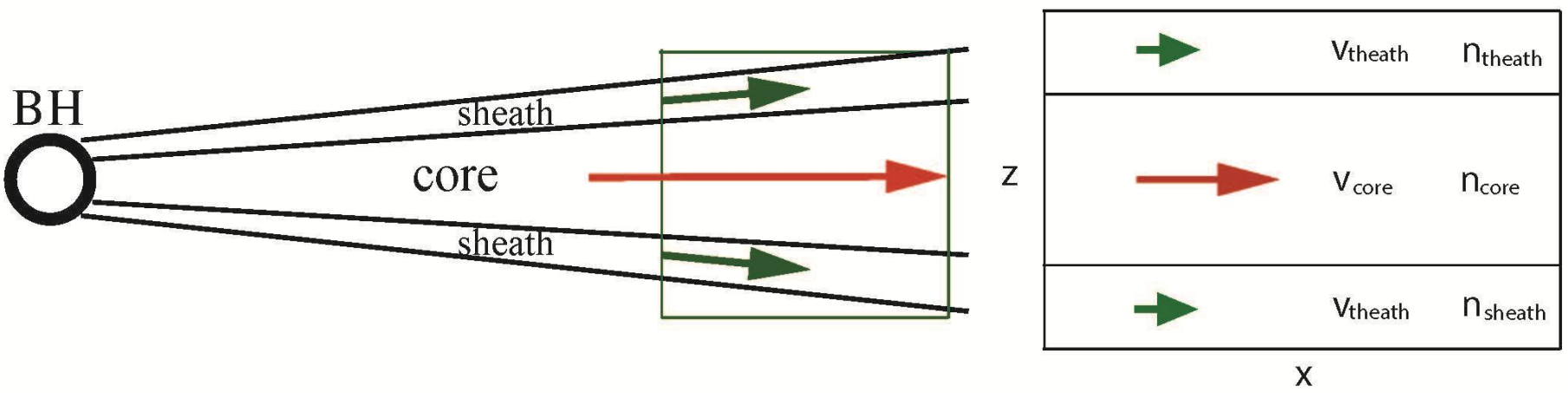

Relativistic Radiation Transfer

Fuerst, Mizuno, Nishikawa, & Wu, 2007, ApJL, submitted

- **We have calculated the thermal free-free emission and thermal synchrotron emission from a relativistic flows in black hole systems based on the results of our 2D GRMHD simulations (rotating BH cases).**
- **We consider a general relativistic radiation transfer formulation (Fuerst & Wu 2004, A&A, 424, 733) and solve the transfer equation using a ray-tracing algorithm.**
- **In this algorithm, we treat general relativistic effect (light bending, gravitational lensing, gravitational redshift, frame-dragging effect etc.).**

Image of Emission, absorption & scattering

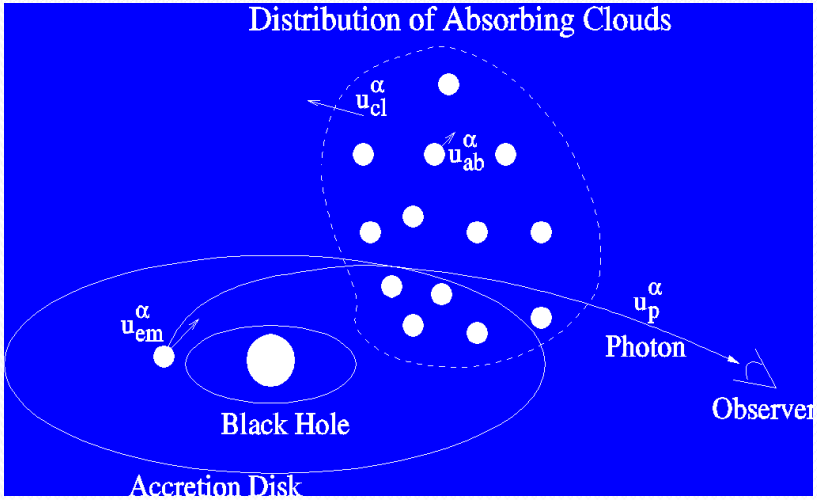

Relativistic Radiation Transfer

Project image of thermal emission (<20 rs)

2D GRMHD simulations (*old version)* (a = 0.95, B = 0.1 $(\rho c^2)^{-2}$)

- **The radiation image shows the front side of the accretion disk and the other side of the disk at the top and bottom regions.**
- **It is because the general relativistic effects.**

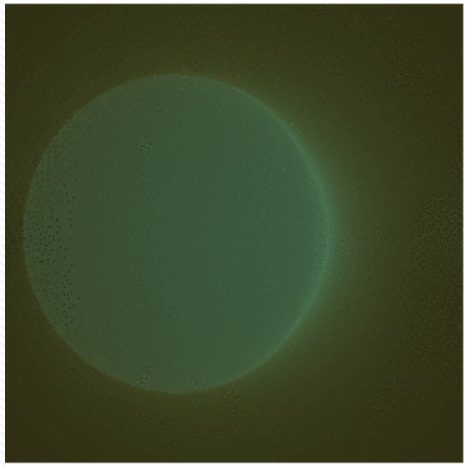

$\theta=85^\circ$

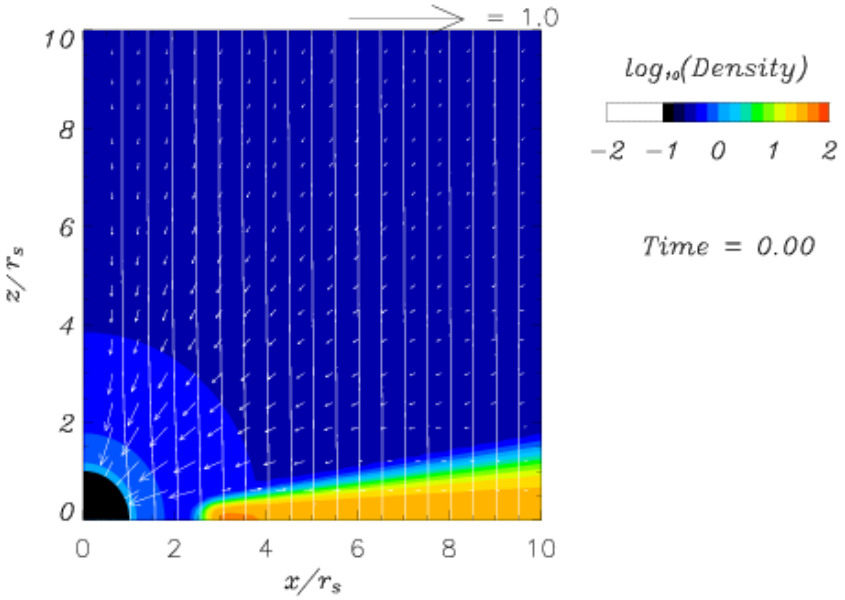

- **We can see the propagation of waves and the strong radiation from geometrically thick disk near the BHs.**
- **The jet generated in GRMHD simulation is not visible in the radiation image.**
- **This is because we assume the thermal free-free emission. It has a strong density dependence and the jet is less dense than the disk.**
- **If we calculate the emission with weaker dependence on the density, such as non-thermal process or Compton scattering, the jet would be visible.**

(Wu et al. 2008)

Radiation images of black hole-disk system

- **The radiation image shows the front side of the accretion disk and the other side of the disk at the top and bottom regions because the general relativistic effects.**
- **We can see the formation of two-component jet based on synchrotron emission and the strong thermal radiation from hot dense gas near the BHs.**
- **A beaming synchrotron emission (green-spark) is seen the surface of the disk (time-dependent). It would be a origin of QPOs?**

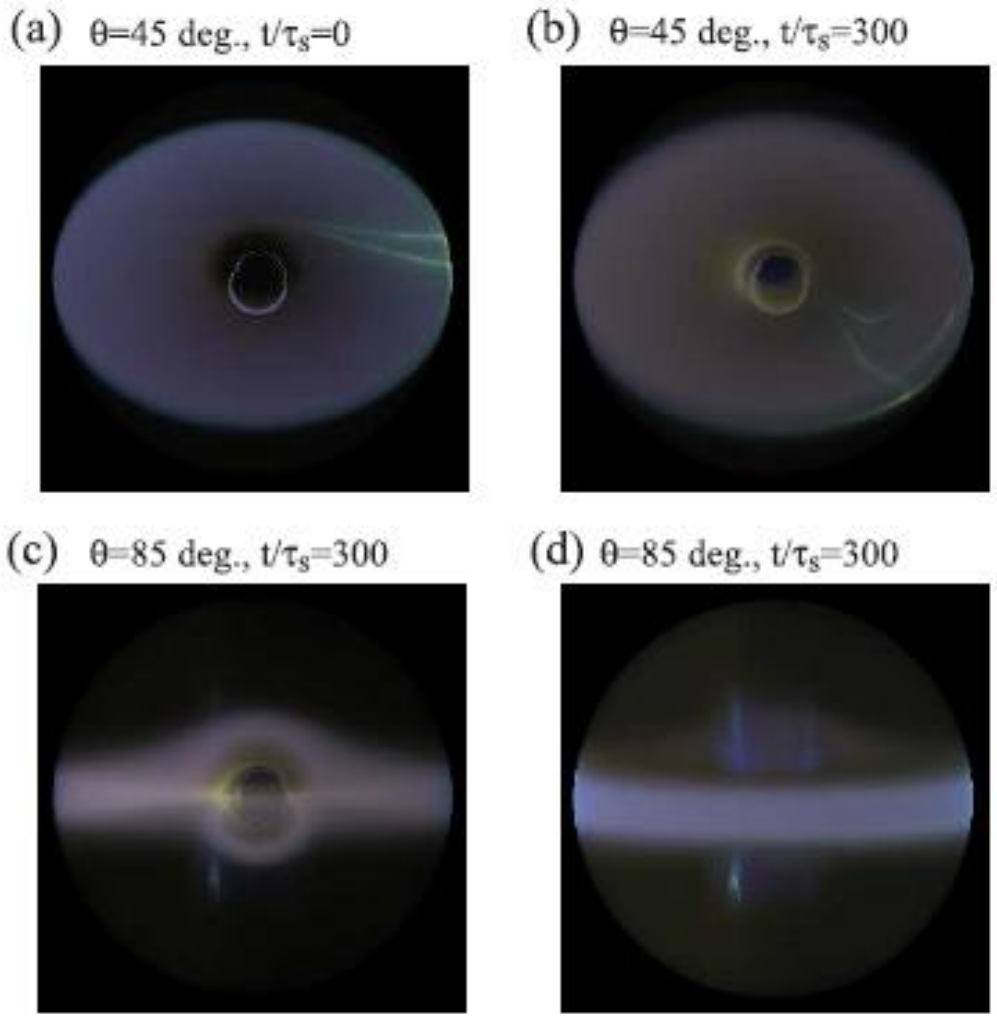

Fuerst, Mizuno, Nishikawa, & Wu, 2007, ApJL, submitted

Summary

- **Simulation results show electromagnetic stream instability driven by streaming $e^{\pm}$ pairs are responsible for the excitation of near-equipartition, turbulent magnetic fields and a structure with leading and trailing shocks.**
- **Shock is similar to the shock in simulations with the constant contact discontinuity.**
- **The spectrum from jet electrons in a weak magnetic field in a small system shows a Bremsstrahlung like spectrum with higher frequency enhancement with turbulent magnetic field.**
- **The magnetic fields created by Weibel instability generate highly inhomogeneous magnetic fields, which is responsible for jitter radiation (Medvedev, 2000, 2006; Fleishman 2006).**

Future plans of our simulations of relativistic jets

- **Calculate radiation with larger 3-D systems for different parameters including magnetic fields in order to compare with observational data**
- **Include inverse Compton emission beside synchrotron radiation to obtain high frequency radiation**
- **Simulations with magnetic fields including turbulent magnetic fields with pair plasma and electron-ion plasma**
- **Reconnection simulations for additional acceleration mechanism including magnetic reconnection**
- **Non-relativistic jet simulations for understanding SNRs**

GRB progenitor (collapsar, merger, magnetar)

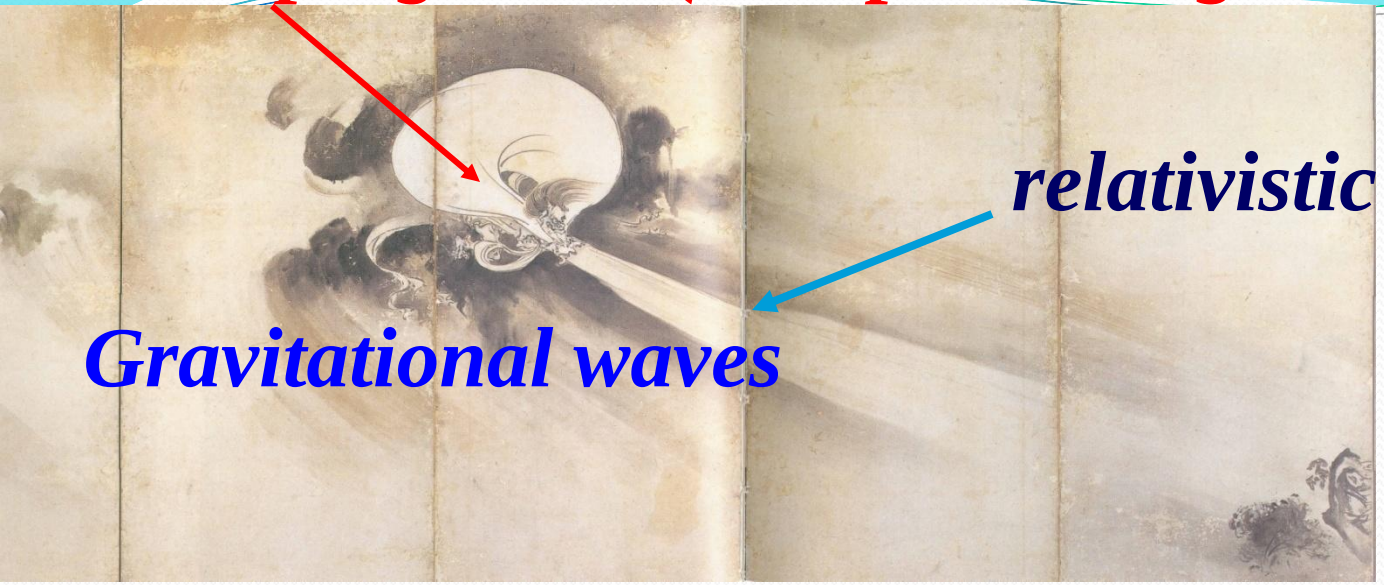

relativistic jet

Fushin

(god of wind)

Gravitational waves

EM emission

(shocks, acceleration)

Raishin

(god of lightning)

(Tanyu Kano 1657)

Gamma-Ray Large Area Space Telescope (FERMI)

(launched on June 11, 2008) http://www-glast.stanford.edu/

Compton Gamma-Ray Observatory (CGRO)

Burst And Transient Source Experiment

(BATSE) (1991-2000)

PI: Jerry Fishman

Fermi (GLAST)

All sky monitor

- **Large Area Telescope (LAT) PI: Peter Michaelson: gamma-ray energies between 20 MeV to about 300 GeV**
- **Fermi Gamma-ray Burst Monitor (GBM) PI: Bill Paciaas (UAH) (Chip Meegan (Retired;USRA)): X-rays and gamma rays with energies between 8 keV and 25 MeV (http://gammaray.nsstc.nasa.gov/gbm/)**

The combination of the GBM and the LAT provides a powerful tool for studying radiation from relativistic jets and gamma-ray bursts, particularly for time-resolved spectral studies over very large energy band.

Jet formation in general relativistic PIC simulation

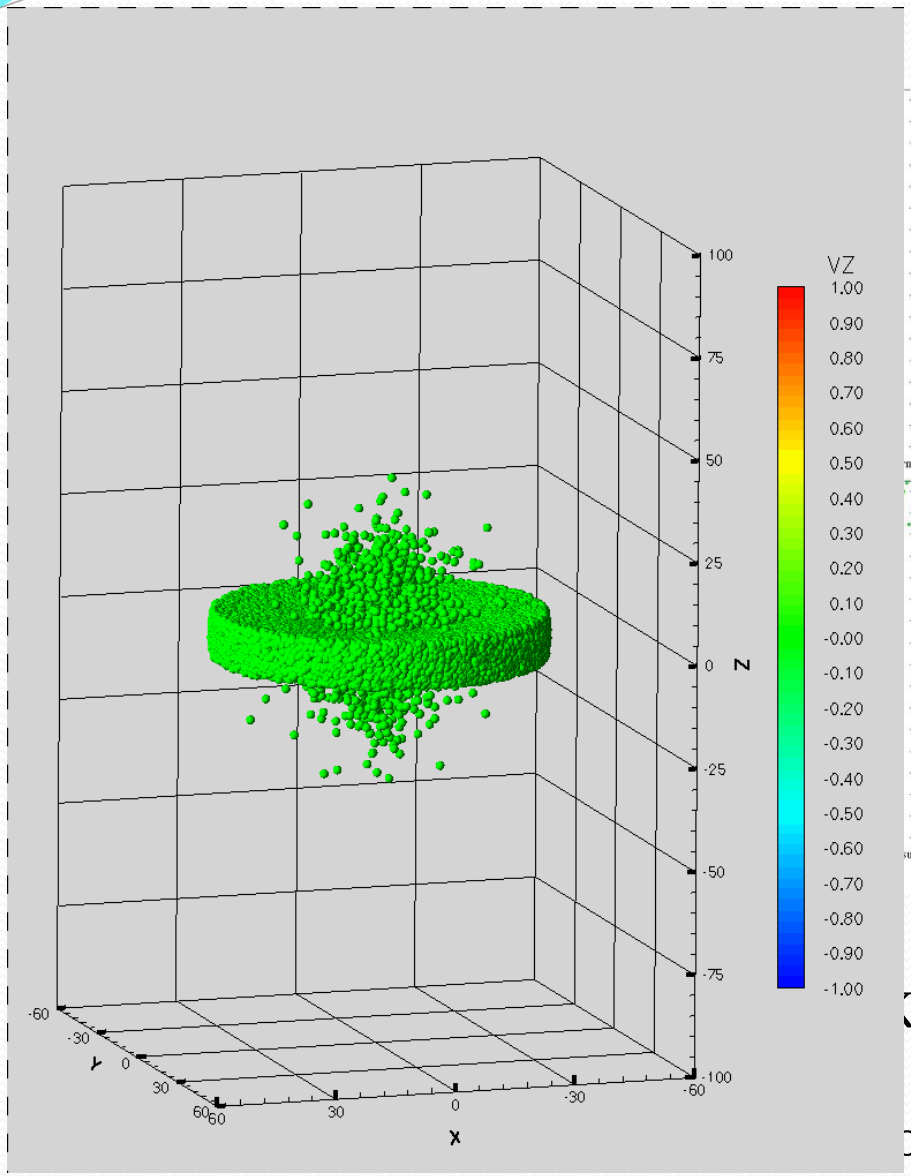

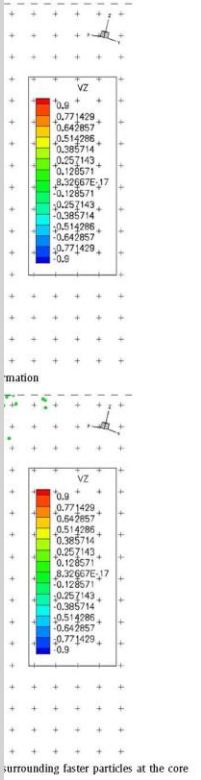

Keplerian motion of electrons and positrons may excite charge separation instability, then generate jet

Kerr–Schild metric in electromagnetic
& K.-I. Nishikawa,
ons 181 (2010) 1750–1757

Effects of ambient magnetic field and jet Lorentz factor

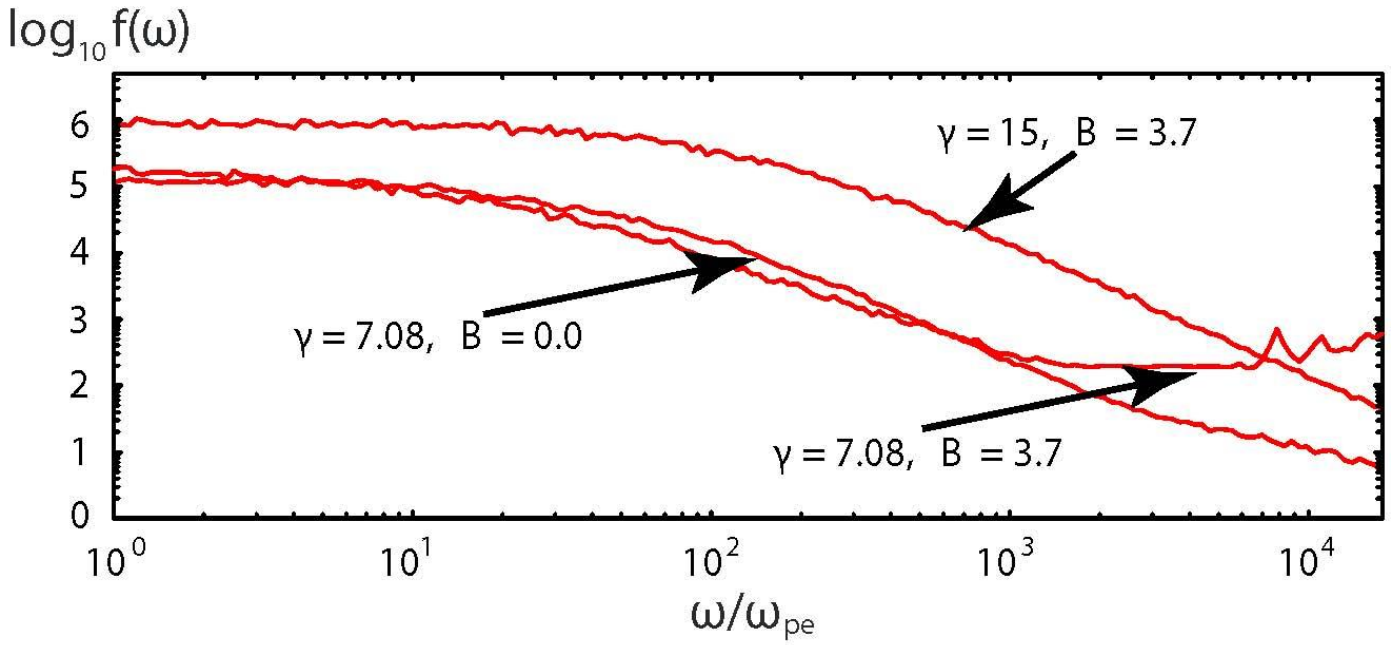

Energetic jet electrons produce higher frequency waves

Turbulent magnetic fields creates higher frequency waves

Summary

- **We have developed a new three-dimensional general relativistic magnetohydrodynamic (GRMHD) code ``RAISHIN" (RelAtivIStic magnetoHydrodynamic sImulatioN, RAISHIN is the Japanese ancient god of lightning) by using a conservative, high-resolution shock-capturing scheme.**
- **The flux-interpolated, constrained transport scheme is used to maintain a divergence-free magnetic field.**
- **We have performed simulations of jet formation from a geometrically thin accretion disk near both non-rotating and rotating black holes. Similar to previous results (Koide et al. 2000, Nishikawa et al. 2005a) we find magnetically driven jets.**
- **It appears that the rotating black hole creates a second, faster, and more collimated inner outflow. Kinematic jet structure could be a sensitive function of the black hole spin parameter and magnetic field strength.**
- **GRPIC simulations will be complementary to GRMHD simulations.**